for CR-72005
10/1-10

OFFICIAL RECORD COPY

[redacted]

[redacted]

GIIIIIIIID

GENERAL DYNAMICS
ASTRONAUTICS

GPO PRICE $ _____

CFSTI PRICE(S) $ _____

Hard copy (HC) 4.00

Microfiche (MF) 1.00

ff 653 July 65

[redacted]

A2136-1 (REV. 6-61)

OFFICIAL RECORD COPY

ERR-AN-051
Aerophysics

ENVIRONMENTAL CONTROL STUDY

OF SPACE VEHICLES

(Part III)

Thermal Control Techniques and Systems

J. C. Ballinger
E. H. Christensen

31 December 1960

Engineering Department

This work was supported under Convair sponsored research program number 111-9121

TABLE OF CONTENTS

TABLE OF CONTENTS (CONTINUED)

FIGURES

FIGURES

FIGURES

FIGURES

TABLES

NOMENCLATURE

English

a	albedo, dimensionless
A	area, ft^2
b	half thickness of fin, ft.
B	width of land for rectangular fin, ft
c	perimeter, ft.
C	concentrated loss coefficient dimensionless
c_p	constant pressure specific heat, Btu/lb-°R
c_p^*	specific heat ratio, dimensionless
COP	coefficient of performance, dimensionless
d	term defined by equation (50)
D	diameter, ft.
e	energy conversion efficiency dimensionless
f	basic parameter multiplying factor, dimensionless
F	view factor, dimensionless
ζ	friction factor
g	gravitational acceleration, 32.2 ft/sec ^{2}
h	convective heat transfer coefficient, Btu/hr-ft^2-°R
H	height, ft.
I_t	thermal energy rate emitted by planet, Btu/hr-ft^2
J	transmittance factor, dimensionless
k	thermal conductivity Btu/hr-ft°R
K	radiation interchange factor between parallel infinite flat plates, dimensionless
L	length, ft.
L*	dimensionless distance
$\dot{m}$	mass flow rate, lb sec.
n	denotes number or quantity of n
N	denotes normal
p	pressure psf or psi
P	power Btu/hr

P*	power ratio, dimensionless
Pr	Prandtl Number, dimensionless
q	heat flux, Btu/hr-ft^2
Q	heat rate, Btu/hr, watts, or tons of refrigeration
r	radius, ft.
R	planet radius, ft.
Re	Reynolds Number, dimensionless
S	solar constant, Btu/hr-ft^2
T	temperature, °R
T*	dimensionless temperature
V	velocity, ft/sec.
w	weight, lb.
x	length or thickness, ft.
x*	dimensionless length
y	length on rectangular fin, ft.
y*	dimensionless length
∞	denotes infinity

Greek

α	solar absorptivity, dimensionless
γ	orientation angle with respect to sun, degrees
δ	fraction or percent, dimensionless
Δ	denotes increment or finite difference
ϵ	emissivity, dimensionless
η	efficiency or effectiveness, dimensionless
θ	time, hrs.
θ*	dimensionless time
λ	radiation modulus, dimensionless
μ	viscosity, lb/ft-hr
μ*	viscosity ratio, dimensionless
ρ	density, lb/ft^3
ρ*	density ratio, dimensionless
σ	Stefan Boltzmann s Constant = 1713 x 10^{-12}Btu/hr-ft^2-°R^4
Σ	denotes summation
ϕ	cut-off angles for rectangular fins, degrees

Subscripts

a	albedo
A	actual
abs	absorbed
ac	adiabatic compressor
avg	average
c	cross sectional
℄	centerline on tube
cone	cone
cyl	cylinder
d	drive
e	equilibrium
eq	equivalent
ex	external
f	fin
fp	flat plate
fl	fluid
G	generated or dissipated
h	hydraulic
hemis	hemisphere
i	denotes i th item
I	ideal
init	initial
in	in or inner
l	land of rectangular fin
L	longitudinal
late	later or final
m	mechanical
n	denotes nth item or number
o	outer
oa	overall
out	out
p	projected with reference to sun
r	radiator
R	root

Subscripts (Cont.)

re	reference
rr	re-radiated
s	lateral surface
S	solar
sp	space
st	stored
t	thermal or long wave radiation
T	total
trans	transmitted
tc	time constant
x	at distance x from a reference

1, 2, 3 etc. = denotes items of the same type.

29291

ABSTRACT

The type of thermal control system or systems required for a given space vehicle depends not only on the external space environment and consequently the mission, but also upon the internal heat dissipation, the size and shape of the vehicle, the length of operation time, the allowable temperature range, and the nature of the payload and equipment on board. A general analysis of thermal control systems is required. A conventional as well as the more revolutionary thermal control systems are discussed with respect to the external thermal environments which may be encountered. Equations are developed to define the systems within the scope of a general report. Particular thermal control systems are analyzed for application on representative present and future missions, with an attempt to arrive at systems which will optimally accomplish the thermal control aspects of particular missions. Conclusions are drawn with respect to the type of thermal control system for use on particular missions.

This work represents a portion of the study being performed under Convair Astronautics REA 111-9121.

INTRODUCTION

The thermal control of a space vehicle depends ultimately on the energy interchange between the vehicle and its environment. The external potential heating loads on such a vehicle were discussed in detail in Reference 1, calculated and presented graphically in References 1 and 2 and tabulated in Reference 3. This present discussion treats the control of this incident environmental heating as well as control of the induced (internal) thermal environment of the vehicle, with the ultimate objective being the maintenance of all components and systems of the vehicle within their allowable operating temperature range. The external thermal loads on a vehicle above the earth's atmosphere, as pointed out in Reference 1, consist essentially of the radiant thermal energy incident on the vehicle due to direct solar heating, planetary reflected solar energy (albedo) and planetary thermal radiation from a near planet by virtue of its effective temperature. If the vehicle is more than three planet diameters distant from the planet the contributions due to albedo and planetary radiation are negligible leaving direct solar radiation as the only external source of heating. This condition has been referred to as the free space environment with only solar heating being the external source of heating. If the vehicle is close enough to the planet to consider planetary heating effects the condition has been referred to as near-planetary environment.

The internal heat dissipation will be dictated by the type of vehicle and mission and will to a large extent dictate the type of thermal control system or systems for the vehicle. The range of internal heat dissipation levels for various missions were predicted in Reference 1 and are shown in Table 4. The "first generation" vehicles now operating, for the most part, have internal dissipation levels low enough to permit the use of passive control techniques exclusively. Passive control techniques as the name

implies require no moving parts and no vehicle power for operation. As more enthusiastic missions are attempted internal power levels as well as size are expected to increase in which case active thermal control systems will not only be required to reduce thermal gradients within the vehicle but also to achieve the ultimate dissipation of thermal energy from the vehicle.

The purpose of this document is to establish the type of thermal control systems for use during particular missions and to provide handbook type solutions for design and optimization of the thermal control systems. The approach in the presentation is to first establish equations adequate for describing the systems and then to optimize the system design as much as is possible in a general treatment.

GENERAL DISCUSSION

I PASSIVE THERMAL CONTROL

Passive thermal control is basically the utilization of missile configuration, structure and vehicle primary surface to achieve the necessary regulation of temperature within the vehicle and on the skin. The passive control of energy intake from the surroundings and dissipation of heat from the vehicle is accomplished by fixed surfaces with specific finish preparations which thus causes the degree of control to become fixed during the fabrication of the vehicle. The methods and techniques are discussed generally in the order of increasing complexity.

A. Fixed Coatings

Fixed passive coatings have been and will continue to be used extensively for the thermal control of small satellites with moderate dissipation and for components on larger vehicles, and to assist in the thermal control on all vehicles. A simplified approach to the problem will show the effect of the thermal radiation properties of surface materials and distance from the sun on temperature control in free space. If a flat plate normal to the sun's rays and insulated on the side away from the sun is assumed somewhere in the solar system, its equilibrium temperature will be given approximately by the following energy balance.

$$T = \left(\frac{\alpha}{\epsilon}\right)^{1/4}\left(\frac{S}{\sigma}\right)^{1/4} \qquad (1)$$

where α = solar absorptivity

ϵ = emissivity

σ = Stefan Boltzman's constant=1713 x 10^{-12} Btu/hr-ft^2-°R^4

S = incident heat flux rate from the sun at the assumed location in the solar system, Btu/hr-ft^2

The heat flux rate S varies as the inverse of the distance from the sun squared and is 442 Btu/hr-ft^2 at the earth. Figure 1 shows the adiabatic plate equilibrium temperature as a function of α/ϵ ratio of the surface and distance from the sun.

The essentials of passive thermal control of a vehicle with internal heat dissipation are demonstrated by a steady state energy balance on the vehicle in free space assuming a spinning or tumbling vehicle and one with infinite thermal conductivity skin.

$$Q_{in} = Q_{out}$$

$$\alpha S A_p + Q_G = \epsilon \sigma A_T T^4 \qquad (2)$$

$$T = \left[\left(\frac{\alpha}{\epsilon}\right)\left(\frac{A_p}{A_T}\right)\left(\frac{S}{\sigma}\right) + \frac{Q_G}{\epsilon A_T \sigma}\right]^{1/4}$$

The effect of the parameters on the satellite temperature is readily apparent. Figure 2 shows the variation of average temperature of a spherical vehicle in cis-lunar free space (S may be considered a constant of 442 Btu/hr-ft^2), as a function of an internal heat dissipation density parameter $Q_G/\epsilon A_T$ and the surface characteristics parameter α/ϵ. This figure shows that as the internal heat dissipation density becomes higher the variation of α/ϵ has less effect, i.e. internal dissipation becomes more important than the solar heating of the vehicle. For moderate and low internal dissipation densities the α/ϵ ratio exhibits wide control over the temperature. Also from the parameter $Q_G/\epsilon A_T$ it is seen that the temperature decreases for higher emissivity. It is therefore concluded that to minimize satellite temperature where internal dissipation is a problem the α/ϵ ratio should be minimized and the emissivity should be maximized. Since the A_p/A_T ratio for random tumbling or spinning vehicles is lowest for a sphere, Figure 2 provides an indication of the practical maximum internal generation that may be dissipated passively from the primary surface of a space vehicle in cis-lunar space more than three planet diameters

from the earth with a given maximum temperature. Coatings are readily available with α/ϵ = .25 and ϵ = .90. If the skin temperature is limited to 100°F which is near a maximum allowable for a satellite containing electronic equipment the maximum Q_G/A_T that may be dissipated is 38 watts/ft^2 surface and places a practical limit on passive control.

Engineering surfaces are readily available which can vary the α/ϵ value from .25 to 5 and some experimental surface coatings are being devised which may increase the range of α/ϵ to .05 to 10. Table 2 shows samples of some of the more common engineering surfaces with their α, ϵ and α/ϵ values as measured in Reference (4). Although the paints exhibit α and ϵ values that are desirable for thermal control it should be remembered that most paints are relatively unstable and vulnerable with respect to ultraviolet light and meteoric dust erosion and are not suitable for long term missions, i.e., those longer than a few days, and even then the change of thermal radiation parameters with ultraviolet radiation for exposures of even a few hours must be considered. (References 5, 6). The ceramic and metallic materials are somewhat more stable than the paints and less affected by ultraviolet radiation.

Since a full range of emissivities and absorptivities cannot be obtained with a few surfaces, it is desirable to combine surface finishes to give almost any thermal parameters desired. By finely striped or spotted patterns with two coatings having dissimilar emissivities and solar absorptivities, average surface emissivities may be derived according to the expression

$$\epsilon_{avg} = \delta\epsilon_1 + (1-\delta)\epsilon_2 \qquad (3)$$

where δ denotes the fraction of area covered by one of the coatings. The solar absorptivity is given similarly by

$$\alpha_{avg} = \delta \alpha_1 + (1-\delta)\alpha_2 \qquad (4)$$

B. Variation of Geometry and Orientation

Equation 2 also indicates the importance of the ratio of projected area in the sun direction to the total vehicle area especially in the case of vehicles with low internal generation density and/or vehicles requiring cryogenic propellant storage in space. The A_P/A_T ratio may be controlled by configuration and orientation. For purposes of computation and thermal prediction it is advantageous to have curves showing the ratio, A_P/A_T for common vehicle geometries and general orientation with respect to the sun. For a sphere the ratio $A_P/A_T = .25$ (constant). It is especially of interest to have plotted the A_P/A_T for lateral areas of geometric figures only as these may be used to determine A_P/A_T ratios for vehicles formed of composite simple geometries. The A_P/A_T for lateral areas will be referred to as A_P/A_S .

For a cylinder A_P/A_S is given by

$$\left(\frac{A_P}{A_S}\right)_{cyl} = \frac{1}{\pi}\sin\gamma \qquad (5)$$

where γ is the orientation angle between the axis of the cylinder and the vehicle-sun vector. This area ratio is shown plotted in Figure 3 as a function of the orientation angle, γ .

For a hemisphere A_p/A_S is given by

$$\left(\frac{A_p}{A_s}\right)_{hemis} = \frac{1}{4}(1+\cos\gamma) \qquad (6)$$

Figure 4 shows this area ratio as a function of the orientation angle. Since this geometry is lacking in the end-for-end symmetry present in the case of the cylinder, values of γ from 0-180° must be considered.

The expression for a cone is somewhat more complex in that a new parameter (H/D) must be introduced. H is the height and D is the diameter of the base. Limiting conditions must be considered in the calculations of A_p/A_S of a cone. When

$$\gamma \leq \tan^{-1}\frac{1}{2(H/D)}$$

$$\left(\frac{A_p}{A_s}\right)_{cone} = \frac{\cos\gamma}{\left[1+4(H/D)^2\right]^{1/2}} \qquad (7)$$

when $\tan^{-1}\frac{1}{2(H/D)} < \gamma < 180 - \tan^{-1}\frac{1}{2(H/D)}$

$$\left(\frac{A_p}{A_s}\right)_{cone} = \frac{\left[\frac{180 - 2\tan^{-1}\left\{\left[4(H/D)^2 - \frac{1}{\tan^2\gamma}\right]^{1/2}\tan\gamma\right\}}{360}\right]\cos\gamma + \frac{1}{\pi}\left[4(H/D)^2 - \frac{1}{\tan^2\gamma}\right]^{1/2}\sin\gamma}{\left[1+4\left(\frac{H}{D}\right)^2\right]^{1/2}} \qquad (8)$$

when $\gamma \geq 180 - \tan^{-1}\frac{1}{2(H/D)}$, $\left(\frac{A_p}{A_s}\right)_{cone} = 0$

$(A_p/A_s)_{cone}$ is shown graphically in Figure 5 as a function of orientation angle, γ, with H/D ratio as parameter.

The expression (A_p/A_s) for a flat plate is given simply for one side for $\gamma < 90°$ as

$$\left(\frac{A_p}{A_s}\right)_{fp} = \cos\gamma \qquad (9)$$

where γ is the angle between the normal and the vector to the sun. For $\gamma > 90$, $(A_p/A_s)_{fp} = 0$, the function is shown plotted in Figure 6.

By a combination of the functions shown in Figures 3 through 6 it is possible to build an A_p/A_T for most vehicle geometries. This solution may be accomplished as follows for a generally convex vehicle.

$$\frac{A_p}{A_T} = \left(\frac{A_p}{A_s}\right)_1 \frac{A_{s_1}}{A_{s_1}+A_{s_2}+\cdots+A_{s_n}} + \left(\frac{A_p}{A_s}\right)_2 \frac{A_{s_2}}{A_{s_1}+A_{s_2}+\cdots+A_{s_n}} + \cdots \qquad (10)$$

$$+\left(\frac{A_p}{A_s}\right)_n \frac{A_{s_n}}{A_{s_1}+A_{s_2}+\cdots+A_{s_n}}$$

The A_p/A_T for some common composite vehicle geometries have been computed and included in this document. Figure 7 shows (A_p/A_T) for a cylinder with flat ends as a function of orientation angle, γ, with the length-diameter ration (L/D) as parameter.

The $(A_p/A_T)_{cyl-fp}$ was computed by the following equation.

$$\left(\frac{A_p}{A_T}\right)_{cyl-fp} = \frac{\pi/4 \cos\gamma + \frac{L}{D}\sin\gamma}{\pi/2\left(1+2\frac{L}{D}\right)} \qquad (11)$$

Also included as an indication of time average $(A_p/A_T)_{avg}$ for a tumbling cylinder, Figure 14 shows A_p/A_T for a cylinder tumbling end-over-end in a plane containing the vehicle-sun vector.

Figure 8 shows (A_p/A_T) for a cylinder with hemispherical end closures, as a function of γ with (H/D) as parameter and was computed from

$$\left(\frac{A_p}{A_T}\right)_{hemis-cyl} = \frac{\pi/4 + \frac{L}{D}\sin\gamma}{\pi(1+L/D)} \qquad (12)$$

Figure 14 shows the time average $(A_p/A_T)_{avg}$ for a cylinder with hemispherical end closures tumbling at a constant rate in a plane containing the vehicle-sun vector.

Figure 9 shows (A_p/A_T) for a hemispherical surface including the flat plate base and was computed from the equations

when $\gamma \leq 90$

$$\left(\frac{A_p}{A_T}\right)_{hemis-fp} = \frac{1}{6}(1+\cos\gamma) \qquad (13)$$

when $\gamma > 90$

$$\left(\frac{A_p}{A_T}\right)_{hemis\text{-}fp} = \frac{1}{6}(1-\cos\gamma) \qquad (14)$$

The value for $(A_p/A_T)_{avg}$ is independent of the size of the hemisphere and is shown in Figure 14.

Figure 10 shows (A_p/A_T) for a conical surface including the base as a function of γ with (H/D) as parameter and was computed by the following equations. When $\gamma \leq \tan^{-1}\frac{1}{2(H/D)}$

$$\left(\frac{A_p}{A_T}\right)_{cone\text{-}fp} = \frac{\cos\gamma}{\left[1+4\left(\frac{H}{D}\right)^2\right]^{1/2}+1} \qquad (15)$$

when $\tan^{-1}\frac{1}{2(H/D)} < \gamma \leq \pi/2$

$$\left(\frac{A_p}{A_T}\right)_{cone\text{-}fp} = \frac{\left[\frac{180+2\tan^{-1}\left\{\frac{1}{\left[4\left(\frac{H}{D}\right)^2-\frac{1}{\tan^2\gamma}\right]^{1/2}\tan\gamma}\right\}}{360}\right]\cos\gamma+\frac{1}{\pi}\left[4\left(\frac{H}{D}\right)^2-\frac{1}{\tan^2\gamma}\right]^{1/2}\sin\gamma}{\left[1+4\left(\frac{H}{D}\right)^2\right]^{1/2}+1} \qquad (16)$$

when $\pi/2 < \gamma < 180-\tan^{-1}\frac{1}{2(H/D)}$

$$\left(\frac{A_p}{A_T}\right)_{cone\text{-}fp} = \frac{-\cos\gamma+\left[\frac{180+2\tan^{-1}\left\{\frac{1}{\left[4\left(\frac{H}{D}\right)^2-\frac{1}{\tan^2\gamma}\right]^{1/2}\tan\gamma}\right\}}{360}\right]\cos\gamma+\frac{1}{\pi}\left[4\left(\frac{H}{D}\right)^2-\frac{1}{\tan^2\gamma}\right]^{1/2}\sin\gamma}{\left[1+4\left(\frac{H}{D}\right)^2\right]^{1/2}+1} \qquad (17)$$

when $180-\tan^{-1}\frac{1}{2(H/D)} \leq \gamma < 180$

$$\left(\frac{A_P}{A_T}\right)_{cone\text{-}fp} = \frac{-\cos\gamma}{\left[1+4(H/D)^2\right]^{1/2}+1} \qquad (18)$$

Figure 14 shows $(A_P/A_T)_{avg}$ for tumble in a plane containing the vehicle sun vector.

The area ratio was calculated by equation (10) using data from Figures (3), (5) & (6) for a cone-cylinder with a flat plate end closure, as this geometry approximates the shape of many vehicles. The results are indicated parametrically in Figures 11, 12 and 13.

C. Rectangular Finned Surfaces

Sometimes passive thermal control surfaces, expecially of small components, are finned for reasons other than space thermal control. This is true, for instance, of electronic packages which see space directly but require fins for ground cooling prior to launch. It is necessary in these cases to predict an equivalent emissivity and solar absorptivity of an isothermal finned surface. An approximation of the effective emissivities and absorptivities of finned surfaces may be obtained by an examination of the three dimensional view of space from various points on the finned surface as well as a consideration of interreflections within

the fin structure. The assumption is made that the fins are infinite in length. For ease of analysis the fin and land will be analyzed separately. The fin geometry is shown in the following figure.

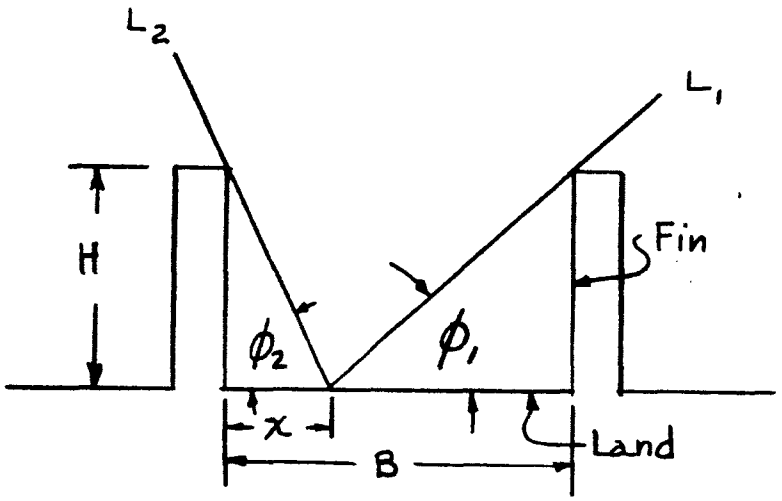

Geometry for View Factors on Land

The local view factor on the land and fin may be computed from fundamental considerations and calculus or by the mathematical application of the radiation hemisphere graphical method (Reference 26) assuming diffusely radiating surfaces. The local view factor on the land is given by the following equation

$$F_1 = \frac{1}{2}\left[\cos\phi_1 + \cos\phi_2\right] \qquad (19)$$

which has the expected extremes $F_1\ (\phi_1 = \phi_2 = 0) = 1.0$, $F_1\ (\phi_1 = \phi_2 = \pi/2) = 0$. The cut off angles ϕ_1 and ϕ_2 may be computed for a given $x^* = x/B$ from

$$\tan\phi_1 = \frac{H/B}{1-x^*}\ ,\ \tan\phi_2 = \frac{H/B}{x^*} \qquad (20)$$

The local land view factors are plotted in Figure 15 as a function of x^* with H/B as parameter. Integration of these curves is accomplished analytically and permitted plotting an average land view factor as a function of H/B and is shown in Figure 17.

The local view factors on the fin may be computed similarly. The parameters are indicated in the following figure.

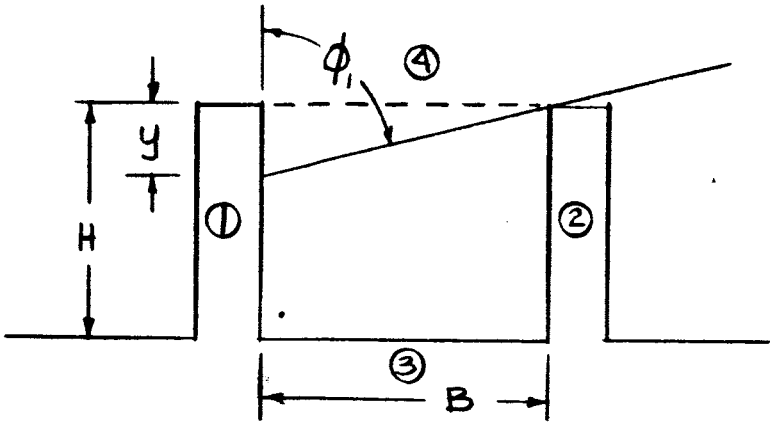

Geometry for View Factors on Fin

The local fin view factor can be shown to be

$$F_f = \frac{1}{2}(1 - \cos\phi_1) \tag{21}$$

where ϕ_1 is defined by

$$\tan\phi_1 = \frac{B/H}{y^*} \quad \text{where } y^* = y/H \tag{22}$$

The local fin view factors were plotted as functions of y* with B/H as parameter and are shown in Figure 16. Analytical integration of these curves permitted plotting an average fin view factor as a function of H/B and is shown in Figure 17.

To convert surface emissivities and solar absorptivities to effective values for finned surface envelopes, a multiplying factor was defined and describes the apparent increase in finned surface emissivity and absorptivity due to inter reflections within the fin structure.

$$\epsilon_{eq} = f\epsilon \;,\; \alpha_{eq} = f\alpha \tag{23}$$

f was estimated from a weighted consideration of the apparent increase in emissivity due to individual effects of inter reflections for the fin and land surfaces. For estimation purposes three inter reflections on all surfaces were considered. Average view factors were assumed between surfaces and were computed as follows.

The subscript numbers refer to the previous figure.

$$F_{1-4} = F_{2-4} = F_{1-3} = F_{2-3} = \frac{1}{2}\left[1 + \frac{B}{H} - \left\{\left(\frac{B}{H}\right)^2 + 1\right\}^{1/2}\right]$$

$$F_{3-4} = \left[\left(H/B\right)^2 + 1\right]^{1/2} - H/B$$

$$F_{1-2} = F_{2-1} = \left[\left(\frac{B}{H}\right)^2 + 1\right]^{1/2} - \frac{B}{H} \qquad (24)$$

$$F_{3-1} = F_{3-2} = \frac{1}{2}\left[1 + H/B - \left\{\left(\frac{H}{B}\right)^2 + 1\right\}^{1/2}\right]$$

f is then given approximately by

$$f = 1 + 2\left(\frac{H}{B}\right)\Big[\Big(F_{1-2}F_{2-4} + F_{1-3}F_{3-4}\Big)(1-\epsilon) + \Big(F_{1-2}F_{2-1}F_{1-4} + F_{1-2}F_{2-3}F_{3-4} + 2F_{1-3}F_{3-2}F_{2-4}\Big)(1-\epsilon)^2 + \Big(F_{1-2}F_{2-1}F_{1-2}F_{2-4} + F_{1-3}F_{31}F_{1-3}F_{3-4} + F_{1-2}F_{2-3}F_{3-1}F_{1-4} + F_{1-3}F_{3-2}F_{2-1}F_{1-4} + F_{1-2}F_{2-3}F_{3-2}F_{2-4} + F_{1-3}F_{3-1}F_{1-2}F_{2-4} + F_{1-3}F_{3-2}F_{2-3}F_{3-4} + F_{1-2}F_{2-1}F_{1-3}F_{3-4}\Big)(1-\epsilon)^3\Big] + \Big[2F_{3-1}F_{1-4}(1-\epsilon) + 2\left(F_{3-1}F_{1-2}F_{2-4} + F_{3-1}F_{1-3}F_{3-4}\right)(1-\epsilon)^2 + 2\left(F_{3-1}F_{1-2}F_{2-3}F_{3-4} + F_{3-1}F_{1-2}F_{2-1}F_{1-4} + F_{3-1}F_{1-3}F_{3-2}F_{2-4}\right)(1-\epsilon)^3\Big] \qquad (25)$$

f is shown as a function of H/B in Figure 18. In view of the approximations used, f as computed above is assumed to apply equally well to the absorptivity. ϵ eq and α eq must approach 1 as $\rightarrow\infty$. The area used with ϵ eq and α eq should be the finned surface envelope area.

D. Insulations

Insulation of a vehicle surface is an example of passive control and is somewhat more complex mathematically and practically than simple surface coating. It has been demonstrated (Reference 8) that from a weight standpoint multiple film radiation shielding is a better space insulation than conventional insulations especially since the vacuum is ready made. The advantage in favor of radiation shielding is less, the higher the outer skin temperature rises. However, for high surface temperatures, i.e., close to the sun, metallic shielding is again of advantage from a thermal integrity standpoint. Radiation shielding is especially important in the protection of cryogenic fluids contained in space vehicles. General equations for studying the conventional insulations and radiation shield insulations are readily developed for the steady state condition (Reference 8).

A steady state energy balance at the outer surface of the insulation or radiation shielding yeilds

$$q_{abs} = q_{rr} + q_{trans} \tag{26}$$

The absorbed energy may be divided into two components, absorbed energy of solar wave lengths and absorbed energy of long wave length.

$$q_{abs} = \alpha_o q_s + \epsilon_o q_t \tag{27}$$

where, since the temperature of the outer surface will correspond to long wave radiation the following "grey body" relation may be assumed

ϵ_o = absorptivity for long wave lengths (28)

Then the absorbed energy on a vehicle surface may be written generally as

$$\alpha_o q_s + \alpha_o q_a + \epsilon_o q_t = q_{abs} \tag{29}$$

The re-radiated thermal energy from the outer surface is determined by

$$q_{rr} = \sigma \epsilon_o T_o^4 \tag{30}$$

The transmitted energy in the conventional insulation is given by

$$q_{trans} = \frac{k}{x} (T_o - T_{in}) \tag{31}$$

The transmitted energy in radiation shield insulations is given by

$$q_{trans} = \sigma J (T_o^4 - T_{in}^4) \tag{32}$$

From energy balance considerations on n successive shields the transmittance factor is found to be

$$J = \frac{1}{1/K_{1,2} + 1/K_{2,3} + \cdots + 1/K_{n,n+1}} \tag{33}$$

or in summation notation

$$J = 1 \Big/ \sum_{i=1}^{n} \frac{1}{K_{i,i+1}} \tag{34}$$

The radiation interchange factor between two shields is

$$K_{i,i+1} = \frac{1}{1/\epsilon_i + 1/\epsilon_{i+1} - 1} \tag{35}$$

For shields with equal emissivities equation (34) simplifies to

$$J = \frac{K}{n} \tag{36}$$

Substitution of equations (27) (28) (29) (30) and (31) in energy balance (26) yeilds the conventional insulation equation

$$\alpha_o q_s + \alpha_o q_a + \epsilon_o q_t - \sigma \epsilon_o T_o^4 = \frac{k}{x}(T_o - T_{in}) \tag{37}$$

Substitution of equations (27) (28) (29) (30) and (32) in energy balance (26) yields a similar equation for radiation shield insulation.

$$\alpha_o q_s + \alpha_o q_a + \epsilon_o q_t - \sigma \epsilon_o T_o^4 = \sigma J (T_o^4 - T_{in}^4) \tag{38}$$

The quantities q_s, q_a, and q_t are computed by the methods of References 1, 2 & 3. It is difficult to solve the conventional insulation equation (37) analytically since T_o occurs in both the first and fourth powers. However, the radiation shield insulation equation (38) may be solved for the outer shield temperature

$$T_o = \left[\frac{\alpha_o q_s + \alpha_o q_a + \epsilon_o q_t + \sigma J T_{in}^4}{\sigma(\epsilon_o + H)} \right]^{1/4} \tag{39}$$

Substitution of (39) in (32) gives the heat transferred in the shield insulation

$$q_{trans} = \frac{\alpha_o q_s + \alpha_o q_2 + \epsilon_o q_t - \sigma \epsilon_o T_{in}^4}{\epsilon_o / J + 1} \qquad (40)$$

which may be solved knowing the insulation parameters, the rate of incident solar and longwave radiation and the inner surface temperature. The individual shield temperatures may be computed if the outer and inner surface temperature are known and the shield emissivities are the same.

$$T_i = \left[\frac{(n-i+1) T_o^4 + (i-1) T_{in}^4}{n} \right] \qquad (41)$$

where i indicates the i^{th} shield from the outside.

For purposes of estimation of the heat leak through an insulation or multiple radiation shield on a space vehicle, graphical methods of solution of the equations (37) and (38) for the q transmitted and T_o are included.

The alignment chart shown in Figure 19 may be used to solve the conventional insulation equation (37). The upper family of curves is the conducted heat rate as a function of temperature differen tial across the insulation and conductance. The lower chart shows the reradiated energy as a function of outer surface temperature, T_o, with outer surface emissivity as a parameter. The solution may be made as follows. Compute the absorbed energy at the outer surface from equation (29) and the method defined in

References 1, 2 and 3. Draw a line from the origin of the upper chart to the T_{in} on the abscissa of the lower chart. Assume a T_o on the abscissa of the lower chart and draw from this point a line parallel to the first and intersecting the abscissa of the upper chart. At the Δ T thus defined on the upper chart read the conducted heat rate and at T_o on the lower chart read the reradiated energy rate. Continue this procedure until the sum of these two heat rates equals the computed absorbed energy.

Figure 20 provides a similar solution to the radiation shield equation (38). The upper family of curves is the transmitted heat rate through the shielding as a function of the surface temperature, with the transmittance factor as parameter. The lower chart shows reradiated heat rate as a function of outer surface temperature with outer surface emissivity as parameter. As in the solution for conventional insulation the absorbed heating rate is computed by equation (29) and the method defined in References 1, 2 and 3. An outer surface temperature is assumed and the reradiated energy determined from the lower chart. The net transmitted energy is obtained from the upper chart by subtracting the value for the inner surface temperature from the value for the outer surface temperature for the given transmission factor. The procedure is repeated until the sum of the reradiated energy and net transmitted energy equals the computed absorbed energy.

For radiation shielding protection of cryogenic fluids tanks in free space the equation (38) may be greatly simplified. For liquid oxygen or a colder fluid, the term containing T_{in}^4 in equation (39) or (40) may be neglected with a maximum 2%

error. For free space, i.e. more than three planet diameters distant from a planet, the albedo and thermal radiation may be neglected. Equation (40) may then be put in the form

$$\frac{q_{trans}}{q_s} = \frac{\alpha_o}{\epsilon_o}\left[\frac{1}{1/J + 1/\epsilon_o}\right] \qquad (42)$$

This function is plotted parametrically in Figure 21 indicating the fraction of impinging solar energy flux to the outer surface that is transmitted to the cryogenic fluid. Figure 22 is a parametric plot of the function for a white painted outer surface as a function of number of shields having equal emissivities for all inner shield surfaces. The vast theoretical reduction in transmitted heat is apparent from this figure.

For the insulation of cryogenic tanks subjected to solar radiation, equation (39), after neglecting the term containing T_{in}, may be placed in the form

$$T_o = \left[\frac{1}{1 + H/\epsilon}\right]^{1/4} \left(\frac{\alpha}{\epsilon}\right)_o^{1/4} \left(\frac{1}{\sigma}\right)^{1/4} q_s^{1/4} \qquad (43)$$

This expression is similar to that of equation (1) except for the modifying term in brackets. q_s is defined as

$$q_s = S \cos\gamma \qquad (44)$$

where γ is the angle between the normal to the outer surface and the vector to the sun. If $J/\epsilon_o < .10$, the outer shield surface temperature may be estimated from Figure 1 by assuming S cos γ is the solar constant. If shield emissivities are all equal, then equation (41) gives the temperature of any intermediate shield.

The simplified radiation shield analysis presented assumes radiation transfer only, which in actuallity would be highly desirable, however practical multiple radiation shields must be supported and physically separated so that conduction in supports and separators must be considered. Much experimentation and study of fabrication techniques must be engaged upon to minimize the conduction in the separators and supports. The result of initial work in these areas has been the "super" vacuum insulations which are essentially multiple radiation shields separated by low conductivity materials. However, because of weight and lack of structural integrity these good insulators are not particularly suited to vehicle-borne applications.

E. Prediction of Satellite Temperatures

Although satellite and space vehicle skin temperature histories are normally predicted by computation on digital computers, it is desirable for estimation purposes and proposal studies to have a method for rapid temperature history prediction. A transient energy balance on the vehicle takes the following form

$$q_{ex} + q_G = q_{st} + q_{rr} \qquad (45)$$

or

$$q_{ex} + q_G = wC_p \frac{dT}{d\theta} + \epsilon\sigma A_T T^4 \qquad (46)$$

The external heating, q_{ex} consists of absorbed albedo, earth thermal radiation, and solar heating. The energy fluxes incident to the vehicle can be calculated by the methods and equations outlined in References 1, 2 and 3. The absorbed energy is found by multiplying the incident albedo and solar flux by the solar absorptivity of the surface, and the incident earth thermal radiation by the emissivity of the surface. Separating variables in equation (46) yeilds

$$d\theta = \frac{\frac{wC_p}{\epsilon\sigma A_T}\, dT}{\frac{q_{ex} + q_G}{\epsilon\sigma A_T} - T^4} \qquad (47)$$

Substituting

$$q_{in} = q_{ex} + q_G \qquad (48)$$

$$T_e = \left(\frac{q_{in}}{\epsilon\sigma A_T}\right)^{1/4} \qquad (49)$$

$$d = \frac{wC_p}{\epsilon\sigma A_T} \qquad (50)$$

in equation (47) and integrating yields

$$\theta = \frac{d}{T_e^3}\left[\frac{1}{2}\left(\tan^{-1}\frac{T_{late}}{T_e} - \tan^{-1}\frac{T_{init}}{T_e}\right) + \frac{1}{4}\ln\frac{(T_e+T_{late})(T_e-T_{init})}{(T_e+T_{init})(T_e-T_{late})}\right] \quad (51)$$

It is advantageous to non-dimensionalize the equation with the following relations

$$\theta_{tc} = d/T_e^3 \quad (52a)$$

$$\theta^* = \theta/\theta_{tc} \quad (52b)$$

$$T^*_{late} = T_{late}/T_e \quad (52c)$$

$$T^*_{init} = T_{init}/T_e \quad (52d)$$

Substitution of these non-dimensional parameters is equation (51) yields

$$\theta^* = \frac{1}{2}\left(\tan^{-1}T^*_{late} - \tan^{-1}T^*_{init}\right) + \frac{1}{4}\ln\frac{(1+T^*_{late})(1-T^*_{init})}{(1-T^*_{late})(1+T^*_{init})} \quad (53)$$

This equation has been plotted in Figure 23 with T^*_{late} on the ordinate, θ^* on the abscissa and $T_{init}{}^*$ as parameter. Then knowing the external heating and internal heating of the vehicle q_{in}, the weight and effective specific heat, and the emissivity,

the temperature at any time may be determined with equation (53) and equations (52). If q_{in} is itself a function of time a stepwise procedure may be used to predict temperature as a function of time.

II ACTIVE THERMAL CONTROL

A. Mechanical Control Surfaces

Active mechanical control surfaces may be designated in two groups. One group is pseudo-passive in that no vehicle power is required to activate the control. The other group is fully active relying on vehicle power for actuation. Mechanical thermal control surfaces generally consist of a combination of two coatings on two surfaces, one superimposing the other, that may move relative to one another. Ordinarily one surface has a high α/ϵ and the other a low α/ϵ. When the vehicle and/or the surface cools, more of the high α/ϵ surface is exposed permitting a greater absorption of solar energy than is emitted and consequently the vehicle warms. When the vehicle approaches the warm end of the temperature range more of the low α/ϵ surface is exposed reducing the solar energy intake and increasing the emitted energy permitting the vehicle to cool.

These control surfaces may be classified as to their geometry and movement, e.g. rotary surfaces, of which the maltese cross is an example, and linear surfaces such as grates and linear blinds or shutters. The linear devices are particularly adaptable to surfaces having relatively large flat areas. The rotary devices facilitate the application to single or double curvature surfaces.

The pseudo-passive drive devices ordinarily are some form of bimetallic strip or spring. Bimetallic strips may be used advantageously with linear control surfaces and coiled springs may be and have been used with rotary control surfaces (Reference 9). It is conceivable that other drive devices such as Bourdon tubes may be used.

The actively driven surfaces (those requiring vehicle power) rely on sensing of some temperature dependent quantity which controls a servo mechanism which in turn controls the thermal control surface utilizing vehicle power to produce the drive forces.

The advantages of active control surfaces over passive surfaces are:

1. Some compensation may be made for changing properties of the surface due to the space environment.

2. The control may be accomplished with narrower temperature limits.

3. Control may be accomplished when the thermal environment changes due to trajectory changes either of a short or long term nature.

4. To a certain extent thermal gradients across a non rotating satellite or space vehicle may be reduced by active surfaces.

5. Limited compensation may be made for time dependent changes in internal generation.

6. Anticipation control can be utilized.

The two major disadvantages are that the thermal control system is somewhat more complex and that the maximum allowable internal dissipation is still limited as in the case of passive control by the surface area and skin temperature of the vehicle or satellite.

B. Active Radiators

The only way to increase the amount of heat that may be dissipated from a particular vehicle at a given temperature is to increase or improve the available heat dissipating area. The use of a heat dissipating radiator implies that this is an effective surface for ultimately releasing heat to the space environment and that an efficient method is utilized to transfer the heat from the dissipating elements to the radiator. Two types of radiators will be discussed. Some detailed discussion of the conventional fin-tube fluid radiator will be included. The more revolutionary belt type radiator will only be discussed briefly.

a. Fin-Tube Fluid Radiator

The conventional fin-tube radiator may be either a vehicle primary surface radiator and radiates to space from only one side, or the radiator may be deployable and will then radiate from two sides. Advantages of the primary surface radiator are:

1. The radiator may be built into the basic wall structure of the vehicle.

2. No flexible connections are required between vehicle and radiator.

3. Somewhat greater protection against meteorite damage is afforded in that the same protection serves both the radiator and vehicle.

The advantages of the deployable radiator are:

1. Radiating surface is essentially unlimited

2. Both sides of the radiator are utilized

3. It is possible to orient the radiator to receive little or no solar load thereby improving the heat dissipating qualities of the radiator.

For reliability purposes it is advisable to use a primary surface, non-deployable radiator if such will suffice.

As in the case of isothermal rectangular fins it is desirable to know the local and average view factors for the combined fin-tube geometry. These view factors are developed by an analysis similar to that described previously for the rectangular fin. These view factors have been plotted. Figure 24 shows the local view factors for space as a function of position on the fin with tube radius to fin width ratio as the parameter. Figure 25 shows the integrated average view factors of the fin and tubes as a function of r/2L. The average view factor on the tube varies over a small range .818 to .635 as r/2L varies from 0 to ∞ .

For an adequate analysis of a light weight fin-tube radiator it is essential to establish a radiation fin effectiveness as well as a radiator effectiveness due to longitudinal temperature drop of the fin. Conventional convective fin effectiveness cannot be used to define the effectiveness of a true radiation fin. The following analysis for a rectangular fin is reported in Reference 11.

More refined analyses have been and are being made but this analysis will suffice for our purposes. The fin of half length L and constant thickness 2b is assumed to radiate to an equivalent space temperature T_{sp} defined by the equilibrium condition between the fin and its external environment with no internal dissipation.

A steady state energy balance on an element dx of the fin with x measured from the center of the fin takes the form

$$-kA_x\frac{dT}{dx}+kA_{x+dx}\left[\left(\frac{dT}{dx}\right)_x+\frac{d^2T}{dx^2}dx\right] = \sigma\epsilon\, 2\,dx\,(T^4-T_{sr}^4) \tag{54}$$

The parameter T_{sr} is defined as

$$T_{sr}^4 = T_{sp}^4(1-F)+T_R^4F \tag{55}$$

where T_{sp} is the equivalent space temperature, T_R is the fin root temperature and F is the view factor of the element surface dx for the adjacent tubes. Noting that A_x and $A_{x+dx} = 2b$, substituting equation (55) and simplifying equation (54) the energy balance becomes

$$kb\frac{d^2T}{dx^2} = \sigma\epsilon\left[T^4-T_{sp}^4(1-F)-T_R^4F\right] \tag{56}$$

The boundary conditions are

$$\text{at } x=0,\ \frac{dT}{dx}=0$$

$$\text{at } x=L,\ T=T_R \tag{57}$$

The equation (56) may be solved and the results readily displayed if the equation is non-dimensionalized to

$$\frac{d^2T^*}{dx^{*2}} = \lambda\left[T^{*4} - T_{sp}^{*4} - F\left(1 - T_{sp}^{*4}\right)\right] \qquad (58)$$

where

$$T^* = T/T_R$$
$$x^* = x/L \qquad (59)$$
$$\lambda = \sigma \epsilon L^2 T_R^3 / kb$$

The boundary equations are,

$$x^* = 0 \;,\; \frac{dT^*}{dx^*} = 0$$
$$x^* = 1 \;,\; T^* = 1 \qquad (60)$$

The fin effectiveness is defined as the ratio of actual energy dissipated from the fin to that which would be dissipated if the fin were isothermal at the root temperature T_R.

$$\eta_f = \frac{Q_A}{Q_I} \qquad (61)$$

The actual heat dissipated is that conducted at the root

$$Q_A = \left| -k2b \frac{T_R}{L} \left(\frac{dT^*}{dx^*} \right)_{x^*=1} \right| \qquad (62)$$

The ideal heat flux Q_I is given by

$$Q_I = \sigma \epsilon 2L T_R^4 \left[1 - T_{sp}^{*4} \right] \qquad (63)$$

Combining equations (62) and (63) according to (61) yields the fin effectiveness

$$\eta_f = \frac{\left(\frac{dT^*}{dx^*} \right)_{x^*=1}}{\lambda \left(1 - T_{sp}^{*4} \right)} \qquad (64)$$

The differential equation (58) could be solved numerically using local view factors F displayed in Figure (24) however the display of the results would be voluminous so it was assumed that the fin had a 180° look angle for space, i .e. F = 0 and equations (58) and (64) were solved on an IBM 650 computer by a double boundary value technique.

The radiation fin effectiveness is indicated in figures (26) and (27) as a function of the non-dimensional parameters λ and T^*_{sp} Figure (27) is a plot for a limited but important range of λ .

The rectangular fin geometry may be optimized by finding the λ for a fixed weight fin which gives the maximum Q_A. Combining (61) and (63) and solving for Q_A gives

$$Q_A = \eta_f \sigma \epsilon 2L T_R^4 \left(1 - T_{sp}^{*4} \right) \qquad (65)$$

for constant fin weight

$$bL = c' \tag{66}$$

With the definition of λ and equations (65) and (66) it can be demonstrated that

$$Q_A = \left[2T_R^3\left(1-T_{sp}^{*4}\right)\left(\sigma^2\epsilon^2 k c'\right)^{1/3}\right]\eta_f \lambda^{1/3} \tag{67}$$

where the bracketed term is a constant for a fixed weight fin in a given environment operating with a given root temperature. By using the relation defined by figure (27) the λ and corresponding η_f may be found that will maximize Q_A for a given T^*_{sp}. This maximizing λ is plotted in Figure (28) as a function of T^*_{sp}. Since the Q_A variation is not great in the area of the maximum, limiting λ's are also plotted corresponding to Q_A one percent less than the maximum. This permits a rather broad choice of nearly optimum λ values.

The longitudinal effectiveness of the radiator, η_L, is due to temperature drop of the fluid as it flows along the tubes of the radiator. The simplifying assumption is made that the drop occurs linearily. The temperature along the tube T_{ℓ} is related to the temperature at entrance $T_{\ell\, in}$ by

$$T_{\ell} = T_{\ell\, in} - \left(\frac{\Delta T_f}{L_r}\right) L \tag{68}$$

By series expansion and retention of the first two terms the radiation driving potential is given by

$$T_{\ell}^4 - T_{sp}^4 = T_{\ell in}^4 \left[1 - \frac{4}{T_{\ell in}}\left(\frac{\Delta T_{fl}}{L_r}\right)L\right] - T_{sp}^4 \qquad (69)$$

If

$$T_{sp}^{*4} = \frac{T_{sp}}{T_{\ell in}} \quad \text{and} \quad \Delta T_{fl}^{*} = \frac{\Delta T_{fl}}{T_{\ell in}} \quad \text{and} \quad L^{*} = \frac{L}{L_r}$$

then as in the case of the lateral efficiency the driving potential may be non-dimensionalized to

$$\left[1 - 4\,\Delta T_{fl}^{*} L^{*}\right] - T_{sp_{in}}^{*4} \qquad (70)$$

The ideal driving potential would be $1-T^*_{sp\ in}{}^4$. Integrating the driving potentials over the length L_r and solving for the longitudinal effectiveness yields

$$\eta_L = 1 - \frac{2\Delta T_{fl}^{*}}{1 - T_{sp_{in}}^{*4}} \qquad (71)$$

This function is plotted in Figure (29) as a function of $T^*_{sp\ in}$ with $\Delta\ T^*_{fl}$ as parameter. The total effectiveness of a fin-tube radiator is given as

$$\eta_{oa} = \eta_f \eta_L \qquad (72)$$

Inasmuch as the equivalent space temperature is important with respect to radiator calculations some indication of the variation of T_{sp} for certain conditions is necessary. Figure 30 shows the variation of T_{sp} with α/ϵ as a function of orientation of a two sided flat plate with respect to the sun for a mission in cis-lunar space. Figure 31 indicates the T_{sp} range that might be expected on a two sided flat plate radiator oriented edgewise to the sun and orbiting the earth in a plane containing the earth sun vector. Furthermore the normal to the plate remains in the plane of the orbit. Figure 32 shows the equivalent space temperature for a two sided flat plate orbiting the earth in a plane normal to the earth sun vector with the plate normal being parallel to the earth sun vector. To have an effective radiator, it is seen that the α/ϵ ratio must be as low as possible.

b. Endless Belt Radiator

A revolutionary radiator has been proposed in Reference 12 consisting of a thin travelling belt which absorbs heat in a contact or fluid heat exchanger and then radiates to space as it travels around a circuit. Several advantages are apparent for this type of radiator.

1. The meteoroid problem is minimized

2. For very high power levels weight may be only a fraction of the weight of the conventional fin-tube radiator

3. Packaging and deployment are simpler than for the fluid type radiators

Although this type radiator promises advantages for future vehicles, its revolutionary nature and development required may preclude its use except on future generation vehicles and will not be considered in detail here.

C. Mass Flow Heat Transfer Systems

As vehicles become physically larger and dissipation rates increase it is not possible to transfer thermal energy passively within the vehicle. Some type of active thermal transfer system relying on fluids is required. Mass transfer systems may be used for two major purposes. The first would be to increase the effective overall conductivity of the vehicle and the second to provide heat transfer to a radiator. In most cases the optimum situation from a thermal standpoint would be to ahcieve the maximum heat transfer with a minimum of pumping power. Therefore choice of fluid is an important consideration for a vehicle circulation system.

The heat transfer is given conventionally as

$$Q = hA\,\overline{\Delta T} \tag{73}$$

where h is given by Nusselt's equation for moderate ΔT as

$$h = 0.023 \frac{k}{D_h} (Re)^{0.8} (Pr)^{0.4} \tag{74}$$

The pressure drop is given conventionally by

$$\Delta p = f\left(\frac{L}{D_h}\right)\frac{\rho V^2}{2g} \tag{75}$$

The friction factor f may be computed from the following relations

$$f = 0.184\,(Re)^{-0.2} \quad \text{when } 5000 < Re < 200{,}000 \tag{76a}$$

$$f = \frac{64}{Re}, \quad 0 < Re < 2100 \tag{76b}$$

$$f \approx .036, \quad 2100 < Re < 5000 \tag{76c}$$

Pumping power is computed assuming incompressible flow as

$$P = \frac{\dot{m}}{\rho}\Delta p \tag{77}$$

Substituting equations (75) and (76a) in (77) and rearranging yields

$$P = \frac{0.184}{2g}\,\frac{L A_c}{D_h^{1.2}}\,\rho^{0.8} V^{2.8} \mu^{0.2} \tag{78}$$

Substituting equation (74) in (73) and rearranging yields

$$Q = 0.023\,\frac{A_s}{A_h^{0.2}}\,\frac{V^{0.8}\rho^{0.8} c_p^{0.4} k^{0.6}}{\mu^{0.4}}\,\overline{\Delta T} \tag{79}$$

$$A_c = \frac{D_h c}{4} \tag{80}$$

$$A_s = cL \tag{81}$$

Solving (79) for V gives

$$V = \left[\frac{D_h^{0.2}}{0.023 A_s} \frac{\mu^{0.4}}{\rho^{0.8} C_p^{0.4} k^{0.6}} \left(\frac{Q}{\Delta T}\right)\right]^{1.25} \tag{82}$$

Substituting in (78) gives

$$P = \frac{0.184}{2g} \left(\frac{1}{0.023}\right)^{3.5} \frac{1}{4} \frac{D_h^{0.5}}{L^{2.5} c^{2.5}} \left(\frac{\mu^{1.6}}{\rho^2 C_p^{1.4} k^{2.1}}\right) \left(\frac{Q}{\Delta T}\right)^{3.5} \tag{83}$$

This equation provides a comparison of fluids and geometries for a given heat transfer rate per degree temperature difference. For a given fluid the quantity $D_h^{0.5}/c^{2.5}$ should be minimized and still maintain the Reynolds Number at 5000 or above. This provides that in general passages should have high aspect ratios, i.e. be wider than they are deep.

For a given $Q/\Delta T$ the parameter $\frac{\mu^{1.6}}{\rho^2 C_p^{1.4} k^{2.1}}$ provides a comparison between various fluids flowing in a fixed geometry. Nitrogen gas at standard temperature and pressure (14.7 psia and 59°F) is chosen as the standard. The comparator is given by

$$P^* = \frac{P}{P_{N_2}} \propto \frac{\mu^{*1.6}}{\rho^{*2} C_p^{*1.4} k^{*2.1}} \tag{84}$$

This parameter has been computed for several gases at 1 atmosphere and 50 psia and for water and is shown in Table 3. The effect

of gas density is readily apparent from equation (84). The gas pressure should be as high as possible to provide efficient heat transfer. Gases are attractive as heat transfer mediums as no indeterminancy is introduced by two phase flow in a "zero-g" field.

The pressure drop in associated ducting of the cooling system for transferring fluid between exhangers is given as follows

$$\Delta p = \Sigma \left\{ C + f\left(\frac{L}{D_h}\right) \right\} \rho \frac{V^2}{2g} \qquad (85)$$

and the associated power loss is given from equation (5) as

$$P = \Sigma \left\{ C + f\left(\frac{L}{D_h}\right) \right\} \frac{\dot{m} V^2}{2g} \qquad (86)$$

Since the mass flow rate to be handled by the ducting is relatively fixed by the heat exchangers, the only way to reduce the ducting power loss is to reduce velocity, i.e. give the ducts the largest cross section and increase the hydraulic diameter as much as is possible. Since hydraulic diameter, $D_h = 4A_c/\mathcal{L}$ this implies that circular ducts are best i.e., the largest cross sectional area per wetted perimeter.

D. Refrigeration Systems

a. Vapor-Cycle Refrigeration

Most space vehicle and satellite components such as electronic equipment and personnel dissipate heat at or near room temperature. This places a maximum temperature limit on the ultimate heat dissipation surface unless a heat pump system such as vapor cycle refrigeration is used to increase the radiator temperature

above the temperature of the vehicle component releasing heat.

The effect of radiator temperature may be readily demonstrated. By an energy balance on a vehicle, the amount of internal dissipation per unit of primary surface radiator area that may be handled can be computed. The energy balance taking into consideration solar, albedo and earth thermal radiation can be approximated for the high noon position as

$$\frac{Q_G}{A_T} = \epsilon \left[\sigma T^4 - S \left\{ \frac{F A_{re}}{A_T} \left[\frac{1}{2} a \left(\frac{\alpha}{\epsilon} \right) + \frac{1}{4} (1-a) \right] + \frac{\alpha}{\epsilon} \frac{A_p}{A_T} \right\} \right] \quad (87)$$

where a is the albedo of the planet
and S is the solar constant of the planet given by Table (1), F is the geometric factor for earth thermal radiation to the vehicle, A_{re} is the reference area on which F is based, and A_p is the projected area in the direction of the sun.

The maximum internal thermal energy that may be dissipated per unit primary surface area of a spherical vehicle is shown in Figures 33 through 37 for the four planets nearest the sun and the moon as a function of altitude with radiator surface temperature as the parameter. A practical α/ϵ ratio of .25 is assumed. Figure 33 for Mercury, the planet nearest the sun, indicates that for near orbits radiator temperatures of at least 700°R are required to dissipate the energy to space. The condition at Venus is somewhat less severe and is shown in Figure 34. A radiator temperature of 550°R will accomplish appreciable heat dissipation.

Figures 35, 36 and 37 for the Earth, Moon & Mars, respectively indicate that it is possible to dissipate considerable vehicle heat

even with a radiator temperature as low as 500°R. For near planet missions further away from the sun than Mars, the heat dissipation possible is the same as for free space the same distance from the sun.

The alternate solution to increasing heat dissipation by raising radiator temperature is to use deployable radiators. Such an extended surface radiator may be oriented edgewise to the sun to eliminate direct solar heating on the radiator. Figure 38 shows the effect of orientation on such a radiator for a vehicle in the vicinity of the earth. The ratio of energy dissipation for a flat plate radiator normal to the suns rays to the energy dissipation from a flat plate radiator oriented edgewise to the suns rays with α/ϵ = .25, ϵ = .90 is plotted vs altitude with radiator temperature as parameter. This figure shows that orientation with respect to the sun has a major effect on dissipation at low radiator temperatures and low altitudes. As radiator temperature increases, the effect of orientation varies much less with altitude and orientation is not required when the radiator temperature is 800°R or above.

Figure 39 shows the relation between energy dissipation of flat plate radiators in free space as a function of the solar constant with radiator temperature as parameter. These curves are plotted for a radiator with α/ϵ = .25 and ϵ = .90 normal to the suns rays. Orientation with respect to the sun probably is unnecessary until the radiator dissipation decreases more than 10% from the maximum which would be the oriented edgewise condition. The 10% situation is indicated by the dotted line. This figure then shows that the higher the temperature of the radiator the higher the solar constant may be before orientation becomes desirable. For a 500°R radiator temperature, orientation is desirable outward from the sun to Mars orbit. Unless the radiator temperature is higher than 750°R, orientation is desirable in the vicinity of the earth.

From the above discussion it would appear desirable to use a vapor cycle refrigeration system so that thermal energy from electronic components could be dissipated to space at elevated temperatures thereby lightening the radiator by reducing the area required. One of the important parameters for the design of such a refrigeration system would be the head pressures required, as inordinantly high pressures would increase the weight of the system and increase leakage especially if deployable radiators and consequently flexible connections are required. It would seem inadvisable to use pressures higher than 100 psia. Sub-atmospheric refrigerant systems would not exhibit the terrestrial problem of reverse leakage since in a space vehicle the system would operate in a vacuum. Figure 40 shows the saturation pressure-temperature relations for common vapor refrigerants that might be applicable to space applications due to their moderate and low pressure characteristics and were extracted from Reference 13.

The vapor cycle refrigerating system may either be a direct system which would use the radiator as a condenser or a two fluid system where the condenser would be a heat exchanger transfering heat to a circulation fluid flowing in the radiator. A major disadvantage of a vapor cycle system for space applications is that it is a two phase system which presents severe problems in a zero-gravity field. It should also be remembered that the work that is used to drive the refrigeration cycle must also be removed by the system as heat. Therefore it is desirable to have a high coefficient of performance. The radiator area required per Btu/hr of internal heat dissipation may be computed from

$$\frac{A_r}{Q_G} = \left[1 + \frac{P_I \left(1 + \frac{P_I}{Q_G} \right)}{Q_G \eta_m \eta_{ac} \eta_d} \right] \frac{1}{\eta_f \epsilon \sigma \left(T_r^4 - T_{sp}^4 \right)} \qquad (88)$$

or in terms of ideal cycle coefficient of performance

$$\frac{A_r}{Q_G} = \left[1 + \frac{\left(1+\frac{1}{COP_I}\right)}{COP_I \eta_m \eta_{ac} \eta_d}\right] \frac{1}{\eta_f \epsilon \sigma \left(T_r^4 - T_{sp}^4\right)} \qquad (89)$$

For electronic equipment cooling, 40°F is a realistic temperature for the cold plate or evaporator. The A_r/Q_G for three common low and moderate pressure refrigerants have been calculated as a function of radiator and/or condenser temperature with T_{sp} as parameter and are shown in Figure (41). Realistic values were assumed for the cycle parameters, $\eta_m = .90$, $\eta_{ac} = .75$, $\eta_d = .80$, $\eta_f = .70$, $\epsilon = .90$, $COP_I = 4.0$ The refrigerants considered were Methyl Chloride, Freon 113 and Freon 11 as these are relatively non-toxic. The A_r/Q_G was essentially independent of refrigerant for these three refrigerants. Ordinarily a 100-150°F rise across a single stage refrigeration system is the maximum that may be expected.

A major consideration is the type of cycle drive. The lower pressure refrigerants require centrifugal compressors because of the high specific volumes. Freon 11 and 113 are of these types. A higher pressure refrigerant like Methyl Chloride could utilise a reciprocating compressor.

b. Expendable Refrigeration

An important method of cooling (Reference 18) for very high peak heat dissipations and/or short missions is to utilize an expendable refrigerant boiling and vented to space. To minimize weight such a refrigerant should have a high latent heat of vaporization. Water is one of the more common expendable refrigerants.

For water boiling at .25 psi (60°F) the latent heat is 1060 Btu/lb. The water requirement would then be 11.35 #/hr/ton of refrigeration.

c. Peltier Refrigerators

Peltier cooling (Reference 14) has become of interest for the cooling of electronic components with the advent of semi-conductors having suitable thermoelectric properties. The Peltier refrigerator is essentially a thermocouple in reverse i.e. by passing a current through positive and negative electrical carriers one junction can be driven warmer than the other and thermal energy is transformed to and transferred by electrical energy.

Peltier cooling is practical only in very special applications as such a system requires both a high energy input and heavy electrical conduits and, in addition, requires large equipment radiation areas, efficient internal heat transfer, and special locations with in the vehicle. Temperature differentials across the system cannot be greater than 30-40°F for efficient operation. Peltier cooling offers promise for heat transfer within electronic packages but many advances would be required for general application to space vehicles.

III APPLICATION OF THERMAL CONTROL SYSTEMS TO PARTICULAR VEHICLES AND MISSIONS

A. Estimates for Present and Predicted Missions

Types of missions that have been attempted or that may be attempted in the future are listed in Table 4 including an estimate or ranges in internal dissipation that may be expected or is predicted for these vehicles. The internal dissipation estimates were published in Reference 1. Also indicated is the estimated equivalent sphere size and total surface area of each of these vehicles and is at best only very rough. With these predictions it is possible to categorize the vehicles and missions with respect to the overall thermal control system. It is further assumed that since these vehicles contain electronic components comprising a large portion, if not the majority of the heat dissipation, the heat must be removed internally at 40-80°F. Unless a heat pump system is utilized the heat must then ultimately be radiated to space at about 500°R.

Table (5) shows the maximum internal dissipation density that may be dissipated from a spherical vehicle with an isothermal 500°R surface with α/ϵ = .25 for a near planet orbit (H/R = .087) and for free space mission in the vicinity of a given planet. Using these values the maximum required heat dissipation area for a given mission and vehicle were computed and are shown in Table 4. The available primary surface heat dissipation area for each vehicle was estimated as 75% of the total area for relatively passive vehicles such as satellites and probes, and as 50% of the total area for maneuverable or powered vehicles and is shown in Table 4.

In those cases where the required area with a 500°R surface is larger than the available area, two things may be done to increase the dissipation. Either the surface temperature may be increased

by using a heat pump such as vapor cycle refrigeration, or extended surface or deployable radiators may be used.

Use of vapor cycle refrigeration may practically be expected to raise the radiator temperature to a maximum of 600°R. Table 5 also shows the maximum dissipation density that can be radiated at this temperature from a spherical vehicle for a near planet orbit (H/R = .087) and for free space missions in the vicinity of a given planet. Using these values the maximum required primary heat dissipation area for a given mission and vehicle were computed and are shown in Table 4. The higher radiator temperature is seen to greatly improve the heat dissipation properties of the vehicle but at the cost of weight for a refrigeration system.

Table (6) shows the maximum internal dissipation density that may be radiated from a flat radiator with an isothermal (η_f = 1.0) 500°R surface with α/ϵ = .25 for a near planet mission and for a free space mission. Figures are shown for a radiator non-oriented, normal to suns rays, and for a radiator oriented edgewise to the sun. Using these figures for an oriented radiator, Table 4 shows the deployable radiator area required for those vehicles where primary surface radiators at 500°R will not suffice.

An attempt will be made to compare weight increase due to refrigeration system with weight saving of radiator due to increased dissipation temperature. Figure (41) has already shown the area of radiator required per Btu/hr of vehicle equipment heat removal as a function of deployable radiator temperature and equivalent space temperature.

Therefore vapor cycle refrigeration does not appear to offer any weight advantages. However, in spite of being heavy, refrigeration may be desirable in two situations. The first is that by using refrigeration, radiator temperatures may be increased possibly eliminating the need for deployable radiators and the attendent reliability and leakage problems in flexible connections. The second is that as missions approach the sun it becomes increasingly important to raise radiator temperature. This is seen in Tables 5 and 6. Missions in the vicinity of Mercury's orbit will undoubtedly require special precautions such as radiation shielding and increased radiator temperatures. From Table 5 it is seen that a low altitude mission to Mercury can not dissipate internal heat from the vehicle surface even at 600°R nor can an oriented radiator dissipate heat at 500°R as seen from Table 6. Missions in free space near Mercury's orbit will definitely require radiator orientation.

B. Conclusions on Application of Thermal Control Systems

Some general conclusions may be drawn with respect to the application of particular thermal control systems to particular missions.

1. For small earth satellites (less than 3' equivalent sphere diam.) with internal dissipation densities less than 48 Btu/hr-ft^2 passive surface thermal control may be used if the allowable operating temperature range is greater than 60°F. Active mechanical surface control is generally necessary if allowable operating temperature ranges are less than 50°F.

2. For small and large earth satellites with internal dissipation densities exceeding 48 Btu/hr-ft^2 and mission lengths less than 10 hrs. expendable water refrigeration is desirable from a weight standpoint.

3. For small earth satellites (less than 3' equivalent sphere diameter) with internal dissipation densities greater than 48 Btu/hr-ft^2 and missions longer than 10 hrs. extended or deployable surface radiators are required with an internal active transfer fluid, preferrably a gas such as nitrogen.

4. For large unmanned earth satellites (greater than 3' equivalent diameter) with internal dissipation densities less than 48 Btu/hr-ft^2 internal mass transfer is required to transfer the heat to surface radiators. Again a gas heat transfer medium is preferrable.

5. For large unmanned earth satellites (greater than 3' equivalent diameter) with internal dissipation densities greater than 48 Btu/hr-ft^2 and missions longer than 10 hrs. internal mass transfer is required as well as deployable radiators.

6. For all missions between Mercury and Mars where deployable radiators are required it is desirable to orient the radiator edgewise to the sun. Missions further from the sun than Mars do not need radiator orientation.

7. For vehicles requiring space storage of cryogenic propellants for periods longer than about 12 hrs. a combination of multiple radiation shield insulations and vehicle orientation is advisable. For missions less than about 12 hrs., orientation only may meet the thermal requirements.

8. Vapor cycle refrigeration although creating a severe weight penalty may be necessary for close satellite missions to Mercury as the only way to dissipate heat near this planet

is to raise radiator temperatures above the operating temperature of electronic equipment.

9. For vehicle missions into the vicinity of the Mercury orbit and closer to the sun, deployable flat radiators oriented edgewise to the sun's rays appear adequate for dissipating heat. A gas transfer system is required internally. The vehicle body should be protected from solar heating by insulation. Metallic radiation shields are desirable because of high equilibrium temperatures encountered.

10. Unmanned close missions to Venus will require deployable sun oriented radiators with an internal gas transfer system for vehicles with dissipation densities greater than 14 Btu/hr-ft^2. For small low dissipation density vehicles active mechanical surface control may be adequate.

11. Close Lunar vehicles less than 3' equivalent sphere diameter with dissipation densities less than 43 Btu/hr-ft^2 require active mechanical surface control primarily as a precaution to offset changes in radiation properties.

12. Large unmanned lunar vehicles with dissipation densities greater than 43 Btu/hr-ft^2 will require deployable radiators and internal mass transfer systems.

13. Small close Mars vehicles with dissipation densities less than 72 Btu/hr-ft^2 will best use active mechanical surface control.

14. Large unmanned Mars vehicles will require internal mass transfer systems and surface or deployable radiators depending on whether the dissipation density is less than or greater than 72 Btu/hr-ft^2.

15. Missions past Mars will undoubtedly require deployable radiators and internal mass transfer systems in view of the relatively small sizes and high dissipation rates necessary.

16. All manned missions will require internal mass transfer systems preferably of the gas type. Generally surface radiators will be adequate for Earth orbital missions. Lunar landing and circum-Mars or Venus missions will require deployable radiators.

17. Vehicles embracing high temperature thermodynamic processes in nearly every case will require deployable radiators and associated mass transfer systems. In these vehicles radiator orientation is relatively unimportant as the radiator will normally operate above 800°R.

The broad scope of this report has not permitted detailed design treatment of space thermal control systems, however, enough analytical treatment has been indicated to permit the general categorizing of vehicular thermal control systems with respect to missions to which they are applicable.

REFERENCES

1. "Environmental Control Study of Space Vehicles (Part II) Thermal Environment of Space" J. C. Ballinger, J. C. Elizalde, R. M. Garcia-Varela, and E. H. Christensen ERR-AN-004, Convair Astronautics, Nov. 1, 1960.

2. "Environmental Control Study of Space Vehicles (Part II) Supplement "A" Graphical Presentation of Solar, Planetary Thermal and Planetary Albedo Radiation Incident to Space Vehicles" J. C. Ballinger and E. H. Christensen, Convair Astronautics, Aerophysics, Dec. 31, 1960.

3. "Environmental Control Study of Space Vehicles (Part II) Supplement "B" Tabular Presentation of Planetary Thermal and Planetary Albedo Radiation Incident to Space Vehicles" J. C. Ballinger and E. H. Christensen, Convair Astronautics, Aerophysics, Dec. 31, 1960.

4. "Measurement of the Normal Solar Absorptivity and Total Hemispherical Emissivity of Engineering Surfaces and Coatings" by E. H. Christensen, R. M. Garcia-Varela and C. L. Crews, Convair Astronautics Report AE60-0713, August 23, 1960.

5. "The Design of Organic Coatings for Use in the Space Environment" by J. E. Cowling, Al Alexander and F. M. Noonan. Proceedings Coating for the Aerospace Environment Symposium WADD TR60-773, November 10, 1960, Wright Air Development Division.

6. "Effect of Ultraviolet Light on Thermal Radiation Parameters of Sherwin-Williams Flat White Acrylic Paint Subjected to Solar Radiation in Cis-Lunar Space", by E. H. Christensen, Convair Astronautics Internal Memorandum CA-HT-164, Sept. 15, 1960.

7. "Passive Thermal Control of the Centaur Electronic Packages" by E. H. Christensen, Convair Astronautics Report AE60-0484, May 31, 1960, Confidential.

8. "Thermal Insulation of Space Vehicles" by E. H. Christensen, Convair Astronautics Report AZJ-55-005, July 15, 1959.

9. "Temperature Control System for the Atlas Able-4 Lunar Satellite", by R. M. Acker, R. P. Lipkis, and J. E. Vehrencamp, ASME Paper 60-AV-46, June 5, 1960.

10. "Some Radiator Design Criteria for Space Vehicles" by J. P. Callinan and W. P. Berggren, ASME Journal of Heat Transfer, Vol. 81, Sec. C, Number 3, Aug. 1959, Par. 237-244.

11. "Radiation Fin Effectiveness" J. G. Bartas and W. H. Sellars, ASME Journal of Heat Transfer, Vol. 82, Sec. C, Number 1, Feb. 1960, Pages 73-75.

12. "A New Type of Thermal Radiator for Space Vehicles" by R. C. Weatherston and W. E. Smith, IAS Paper No. 60-78, June 28, 1960.

13. Air Conditioning and Refrigeration-3rd Ed. by B. H. Jennings and S. R. Lewis, International Textbook Company, Scranton, Pa. 1949, Pages 439-477.

14. "Application of Peltier Refrigerators to Space Vehicles" by M. E. Stelzriede, ASME paper 60-WA-238, Nov. 27, 1960.

15. "Effect of Surface Thermal Radiation Characteristics on the Temperature Control Problem in Satellites", W. G. Camack & D. K. Edwards, First Symposium Surface Effects on Spacecraft Materials, May 12, 13, 1959. ARDC and LMSD, Ad by F. J. Clauss

16. "Materials Effects in Spacecraft Thermal Control" by R. E. Gaumer, F. J. Clauss, M. E. Sibert, and C. C. Shaw, LMSD-704019, Nov. 1960, Lockheed Missiles and Space Division.

17. "A 20,000-Kilowatt Nuclear Turbo Electric Power Supply for Manned Space Vehicles" by R. E. English, H. O. Stone, D. T. Bernatowicz, E. H. Davison, and S. Lieblein. Nasa Memo 2-20-59E, March 1959.

18. "An Approach to Equipment Cooling Problems in an Orbital Space Vehicle" by J. S. Tupper SAE Preprint No. 87B, SAE Aero Meeting, Los Angeles, Oct. 2, 1958.

19. "Methods for Cooling Small Missile Components" by L. A. Jeffries, ERR-PO-007, Convair Pomona, Jan. 15, 1960.

20. "Thermal Environment of Electronic Equipment in Space Vehicles" by Neal E. Wood, Institute of Environmental Sciences Paper 887 April 6, 1960.

21. "Determination of Thermal Radiation Incident Upon the Surfaces of an Earth Satellite in an Elliptical Orbit, by A. J. Katz, IAS Paper No. 60-58, June 28, 1960.

22. "An Investigation of the Natural Environment of an Artificial Satellite" by M. Downing and R. M. Rhodes, Convair San Diego, Physics Section Report ZPH-039, Aug. 17, 1959.

23. "Proceedings Coatings for the Aerospace Environment Symposium" Wright Air Development Division Report TR-60-773, 9-10 Nov. 1960.

24. "First Symposium Surface Effects on Space Craft Materials" Edited by F. J. Clauss, May 12 & 13, 1959, ARDC and LMSD.

25. "Environmental Control Study of Space Vehicles Bibliography, (Part I) Convair Astronautics Aerophysics ERR-AN-004, March 9, 1960.

26. Heat and Mass Transfer by Eckert, E.R.G. and Drake, R. M. McGraw-Hill, 1959, Pages 395-402.

TABLE I PLANETARY DATA

Planet	Distance To the Sun (Astronomical Units)	Moon Radius (Nautical Miles) (R)	Solar Heat Flux (Btu/hr ft^2) (S)	Albedo (a)	Planetary Thermal Radiation (Btu/hr-ft^2) (I_t)	Altitude Correction Factor	Umbra Cone Apex Altitude (N. Miles)	Umbra Cone Angle (Degrees)
Mercury	0.387	1,308	2953.9	0.07	686.79	2.639	109,200	1.37
Venus	0.723	3,307	846.3	0.76	50.78	1.043	518,700	0.73
Earth	1.000	3,441	442.4	0.40	66.36	1.000	746,800	0.53
Mars	1.524	1,799	190.5	0.15	40.48	1.916	592,400	0.35
Jupiter	5.203	37,758	16.4	0.51	1.98	.091	46,974,000	0.09
Saturn	9.539	31,067	4.9	0.50	0.61	.111	69,477,000	0.05
Uranus	19.18	18,818	1.2	0.66	0.10	.269	54,739,000	0.03
Neptune	30.06	11,645	0.5	0.62	0.05	.296	77,686,000	0.02
Pluto	39.52	1,564	0.3	0.16	0.06	2.203	13,347,000	0.01
Moon	1.000	938	442.4	0.07	102.86	3.676	202,200	0.53

TABLE 2

REPRESENTATIVE THERMAL RADIATION PROPERTIES OF COMMON ENGINEERING SURFACES AT OR NEAR ROOM TEMPERATURE

Finish	Temperature Range °F	Normal Solar Absorptivity	Total Hemispherical Emissivity	$\frac{\alpha}{\epsilon}$
Sherwin Williams Flat White Acrylic Paint	70-100	0.27	0.895	.30
Andrew Brown Co. Hi-Heat Aluminized Enamel	70-120	0.24	0.27	.89
Fuller Paint Co. Dull Black Enamel	70-145	0.91	0.85	1.07
Speco, Inc. Extra High Heat Gold Paint	70-120	0.43	0.52	0.83
.010" Rokide "A" (Aluminum Oxide)	70-85	0.21	0.82	0.26
.010" Rokide "Z" (Zirconium Oxide)	70-100	0.39	0.86	0.45
.010" Sprayed Pure Aluminum	70-110	0.31	0.25	1.25
Electro Plated Gold	70-150	0.29	0.08	3.60
Vacuum Deposited Gold Vapor Plate	70-150	0.26	0.11	2.35
Vacuum Deposited Aluminum Vapor Plate	70-150	0.24	0.10	2.40
347 Stainless Steel	70-175	0.54	0.27	2.00
Clean 7075 Aluminum	70-250	0.55	0.11	5.00

TABLE 3

FLUID TRANSPORT PROPERTIES AND PUMPING POWER COMPARISONS FOR EQUIVALENT HEAT TRANSFER

	Viscosity lb/ft-hr	Density lb/ft^3	Specific Heat C_p Btu/lb-°F	Thermal Conductivity K Btu/hr-ft-°F	Power Ratio Relative to Nitrogen, P*
Nitrogen (1 atm)	.0411	.0743	.25	.0145	1.0
Carbon Dioxide (1 atm)	.0340	.1170	.21	.0091	.99
Ammonia (1 atm)	.0242	.0425	.52	.0136	.47
Helium (1 atm)	.0436	.0106	1.25	.0844	.142
Hydrogen (1 atm)	.0208	.0053	3.50	.1109	.025
Nitrogen (50 psia)	.0411	.253	.25	.0145	.087
Carbon Dioxide (50 psia)	.0340	.117	.21	.0091	.086
Ammonia (50 psia)	.0242	.0425	.52	.0136	.041
Helium (50 psia)	.0436	.036	1.25	.0844	.0124
Hydrogen (50 psia)	.0208	.018	3.50	.1109	.0022
Water	2.66	62.4	1.0	.353	1.9×10^{-7}

TABLE 4

VEHICLE ESTIMATES AND RADIATOR AREAS FOR FUTURE MISSIONS

	MISSION	Max. Load Btu/hr	Predicted Equiv. Sphere Diam. ft.	Total Surface Area ft^2	Avail Area for Internal Heat Diss. ft^2	Heat Dissipation From Spherical Surface: Unit Heat Diss. 500°R Btu/hr-ft^2	Heat Dissipation From Spherical Surface: Area Req'd 500°R ft^2	Heat Dissipation From Spherical Surface: Unit Heat Diss. 600°R Btu/hr-ft^2	Heat Dissipation From Spherical Surface: Area Req'd 600°R ft^2	Heat Dissipation From an Oriented Radiator @500°R: Unit Heat Diss. Btu/ft^2	Heat Dissipation From an Oriented Radiator @500°R: Rad. Area Req. ft^2
Unmanned Earth Satellites Min. Load-5 Watts	Navigation	85	3	28	21	48.6	1.75				
	Scientific	280	3	28	21	48.6	5.75				
	Orbit-Recovery	550	3	28	21	48.6	11.30				
	Weather & Recon	800	3	28	21	48.6	16.50				
	Logistic Supply	920	10	310	155	48.6	18.90				
	Satellite Interception	1200	5	80	40	48.6	24.70				
	Communication	6200	5	80	40	48.6	127.5	158	39	76	82
Unmanned Space Vehicles Min. Load 10 Watts	Circum-Lunar & Return	200	5	80	40	43.5	4.6				
	Lunar Satellite	550	3	28	21	43.5	12.6				
	Mercury Probe	820	3	28	21	0		36	22	0	
	Mars Satellite	1200	3	28	21	72.3	16.6				
	Lunar Soft Landing	1900	5	80	40	43.5	43.6	150	12.7	73	26
	Circum-Mars & Return	2800	5	80	40	72.3	38.7				
	Venus Satellite or Soft Landing	5700	10	310	155	14.0	406.0	120	48	67.5	85
	Jupiter Saturn Probe	8700	5	80	60	72.3	120.0	175	50	76	115
	Soft Mars Landing	16000	10	310	155	72.3	221.0	175	92	76	210
	Neptune-Pluto Probe	62000	10	310	232	72.3	860.0	175	355	76	815

TABLE 4 (CONT.)

MISSION		Max. Load Btu/hr	Predicted Equiv. Sphere Diam. ft	Total Surface Area ft^2	Avail Area for Internal Heat Diss. ft^2	Heat Dissipation From Spherical Surface: Unit Heat Diss. 500°R Btu/hr-ft^2	Heat Dissipation From Spherical Surface: Area Req'd 500°R ft^2	Heat Dissipation From Spherical Surface: Unit Heat Diss. 600°R Btu/hr-ft^2	Heat Dissipation From Spherical Surface: Area Req'd 600°R ft^2	Heat Dissipation From an Oriented Radiator @500°R: Unit Heat Diss. Btu/ft^2	Heat Dissipation From an Oriented Radiator @500°R: Rad. Area Req. ft^2
Orbit Re-entry	Manned Satellites & Space Vehicles Min. Load 40 Watts	1000	5	80	40	48.6	20.5				
Reconnaissance		2000	10	310	232	48.6	41.1				
Sat. Interception		3100	10	310	155	48.6	63.8				
Circum-Lunar & Return		11000	2-10'	620	310	43.5	253.0				
Space Station		22000	4-10'	1240	930	48.6	452.0				
Lunar Landing		38000	4-10'	1240	620	43.5	870.0	150	250	73	520
Circum-Mars		≈100000	4-10'	1240	620	72.3	1380.0	175	570	76	1320
Circum-Venus		≈100000	4-10'	1240	620	14.0	7150.0	120	834	67.5	1480

TABLE 5

MAXIMUM ALLOWABLE INTERNAL DISSIPATION DENSITY Q_G/A_T THAT CAN BE RADIATED FROM A SPHERICAL VEHICLE

Planet	500°R Radiator Temperature		600°R Radiator Temperature	
	Near Planet H/R=.087	In Vicinity of Planet H > 6R	Near Planet H/R=.087	In Vicinity of Planet H > 6R
Mercury	0 Btu/hr-ft^2	0 Btu/hr-ft^2	0 Btu/hr-ft^2	36 Btu/hr-ft^2
Venus	14	49.5	120	155
Earth	48.6	72.3	158	175
Moon	43.5	72.3	150	178
Mars	75	85	180	191
Jupiter	95	96	197	200
Saturn-Pluto	97	97	201	201

TABLE 6

MAXIMUM ALLOWABLE INTERNAL DISSIPATION DENSITY Q_G/A_T THAT CAN BE RADIATED FROM A DEPLOYABLE FLAT PLATE RADIATOR AT 500°R

	Normal to Sun's Rays		Edgewise to Sun's Rays	
Planet	Near Planet H/R = .087	In Vicinity of Planet H > 6R	Near Planet H/R = .087	In Vicinity of Planet H > 6R
Mercury	0 Btu/hr-ft^2	0 Btu/hr-ft^2	0 Btu/hr-ft^2	97 Btu/hr-ft^2
Venus	0	2	67.5	97
Earth	17.9	46.7	76.0	97
Moon	6.	47.4	73.	97
Mars	59.	76.0	87.	97
Jupiter	96	97	96.5	97
Saturn-Pluto	97	97	97	97

Fig. I
Adiabatic Plate Equilibrium
Temperature as a function of α/ϵ
Ratios and Distance from the Sun

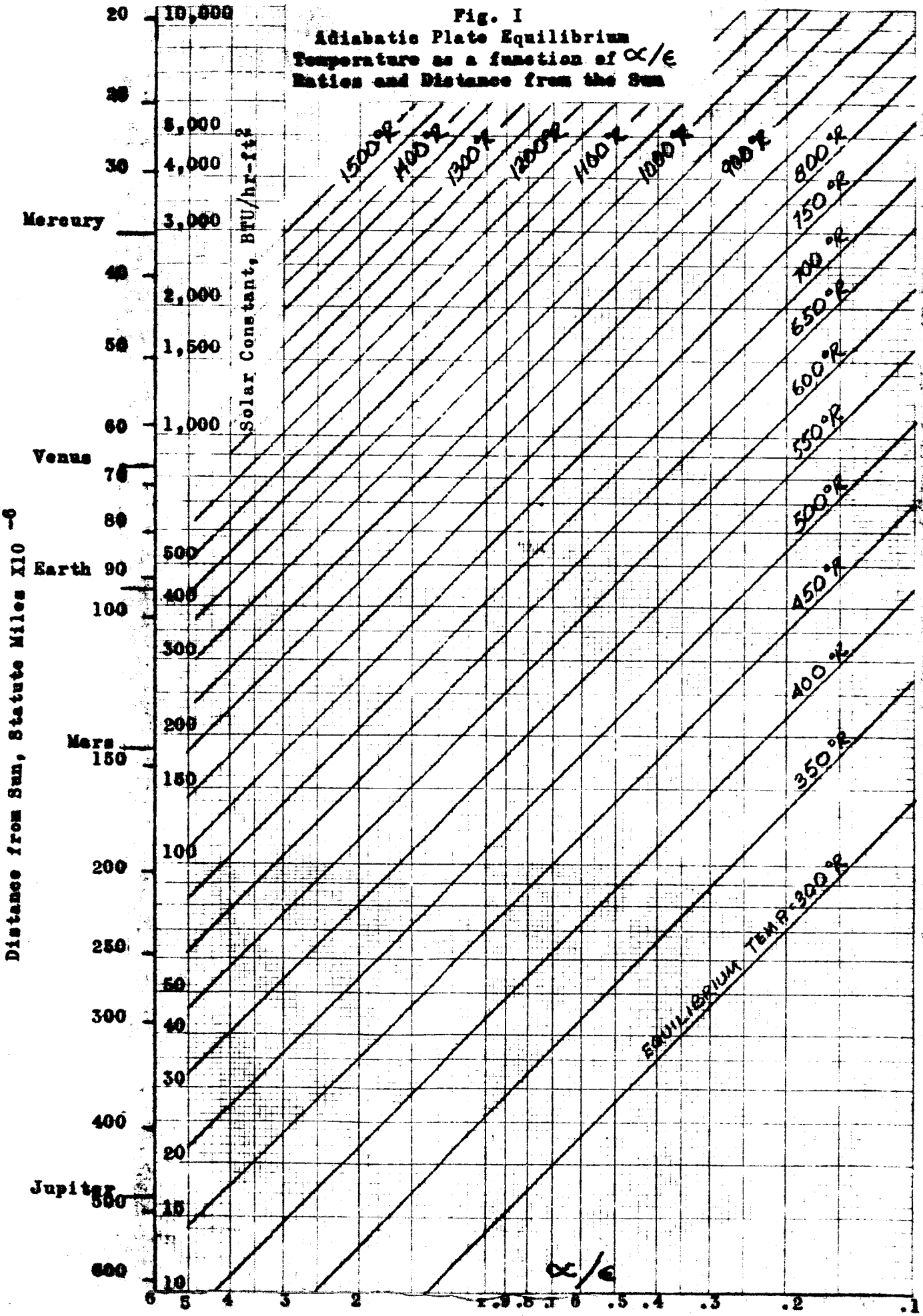

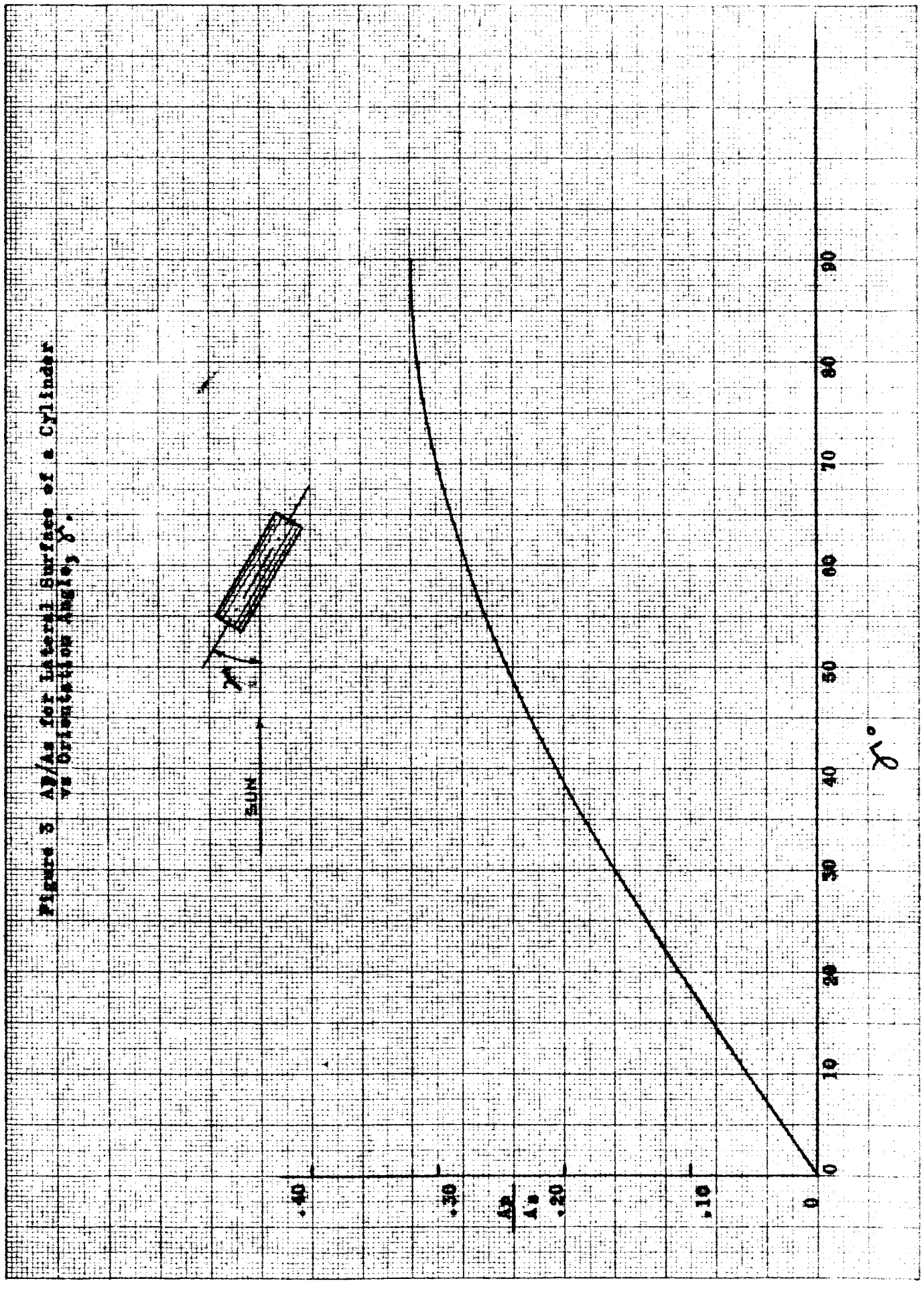

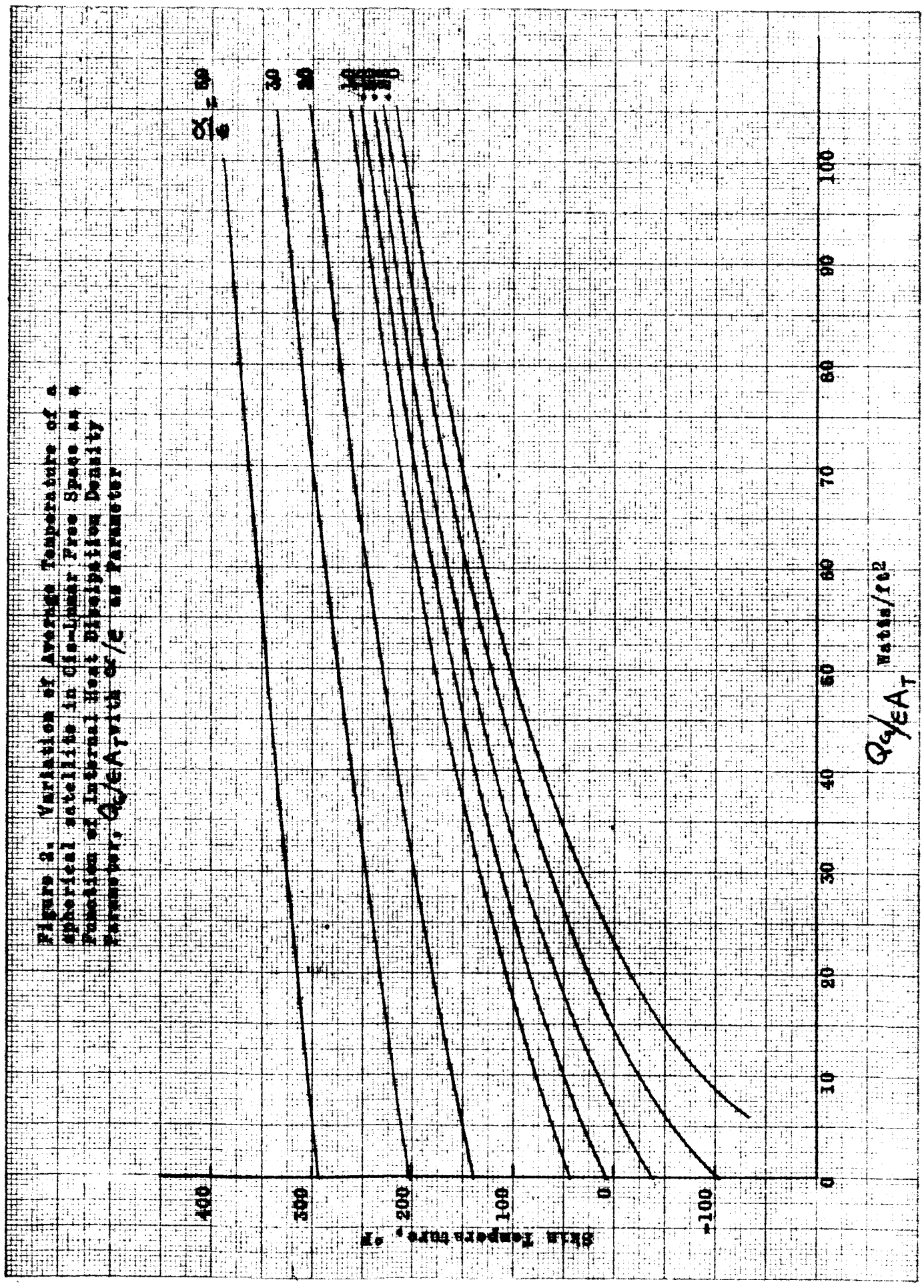

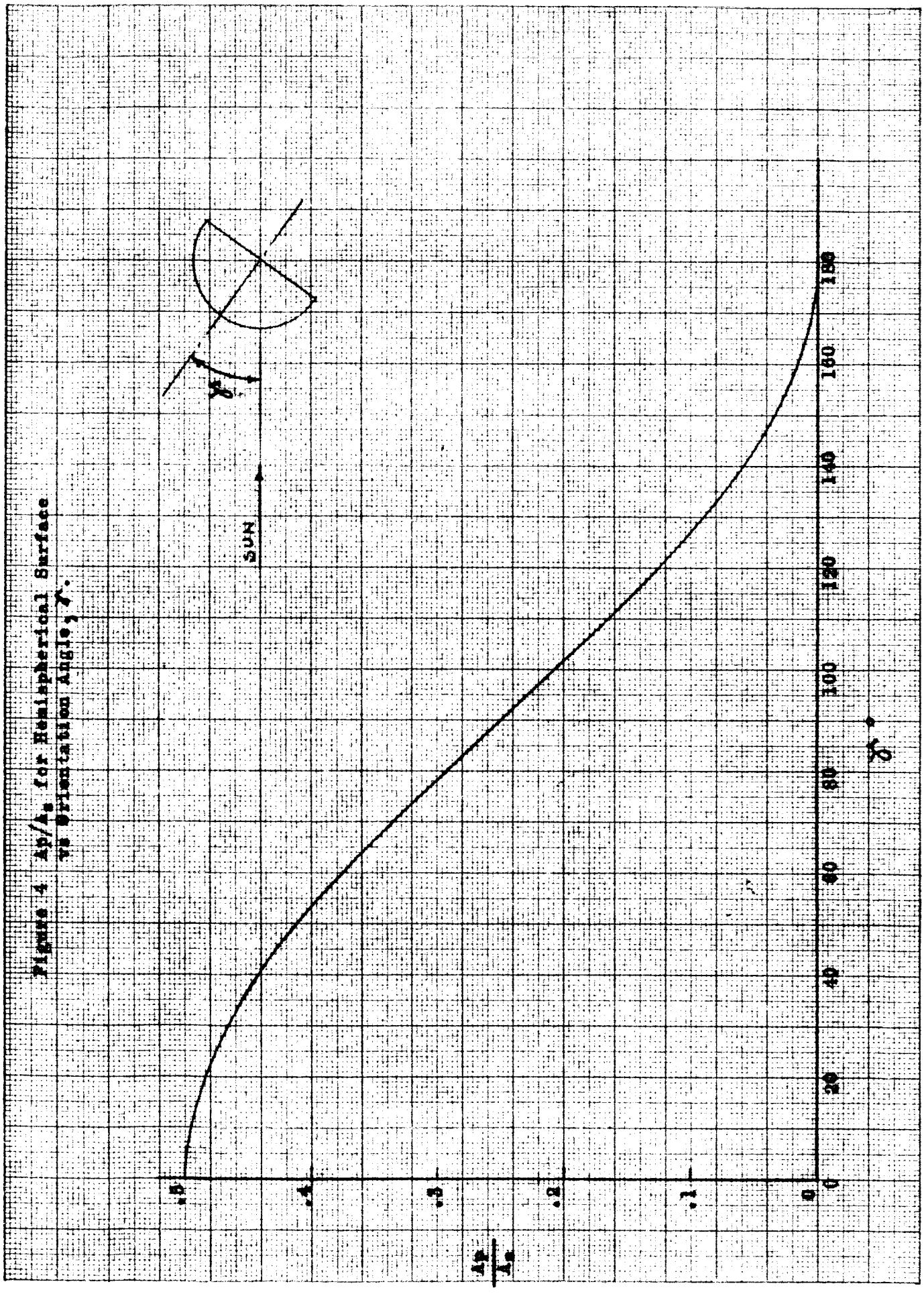

Figure 4 A_p/A_s for Hemispherical Surface vs Orientation Angle, γ.

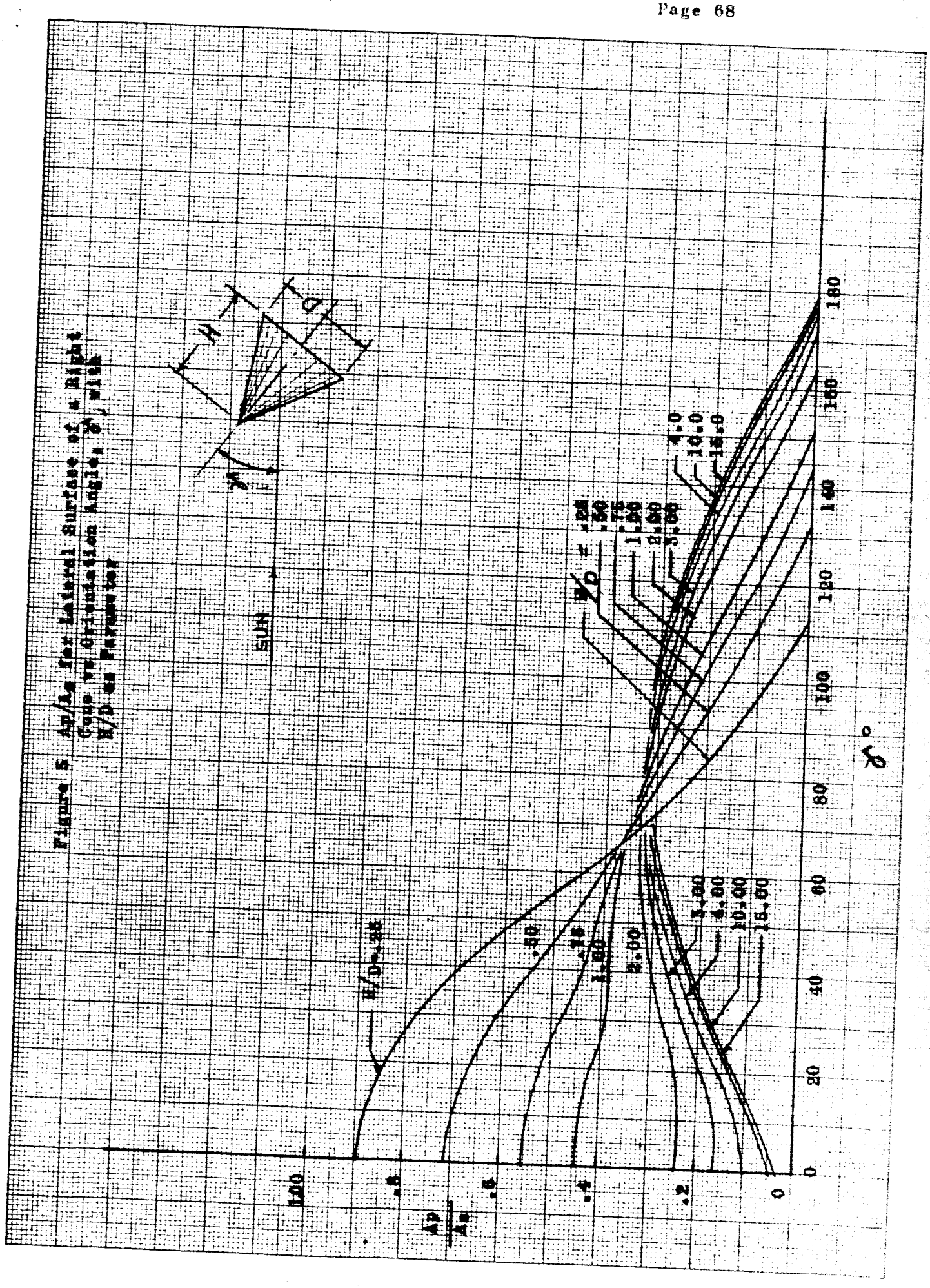

Figure 5 Ap/As for Lateral Surface of a Right Cone vs Orientation Angle, γ, with H/D as Parameter

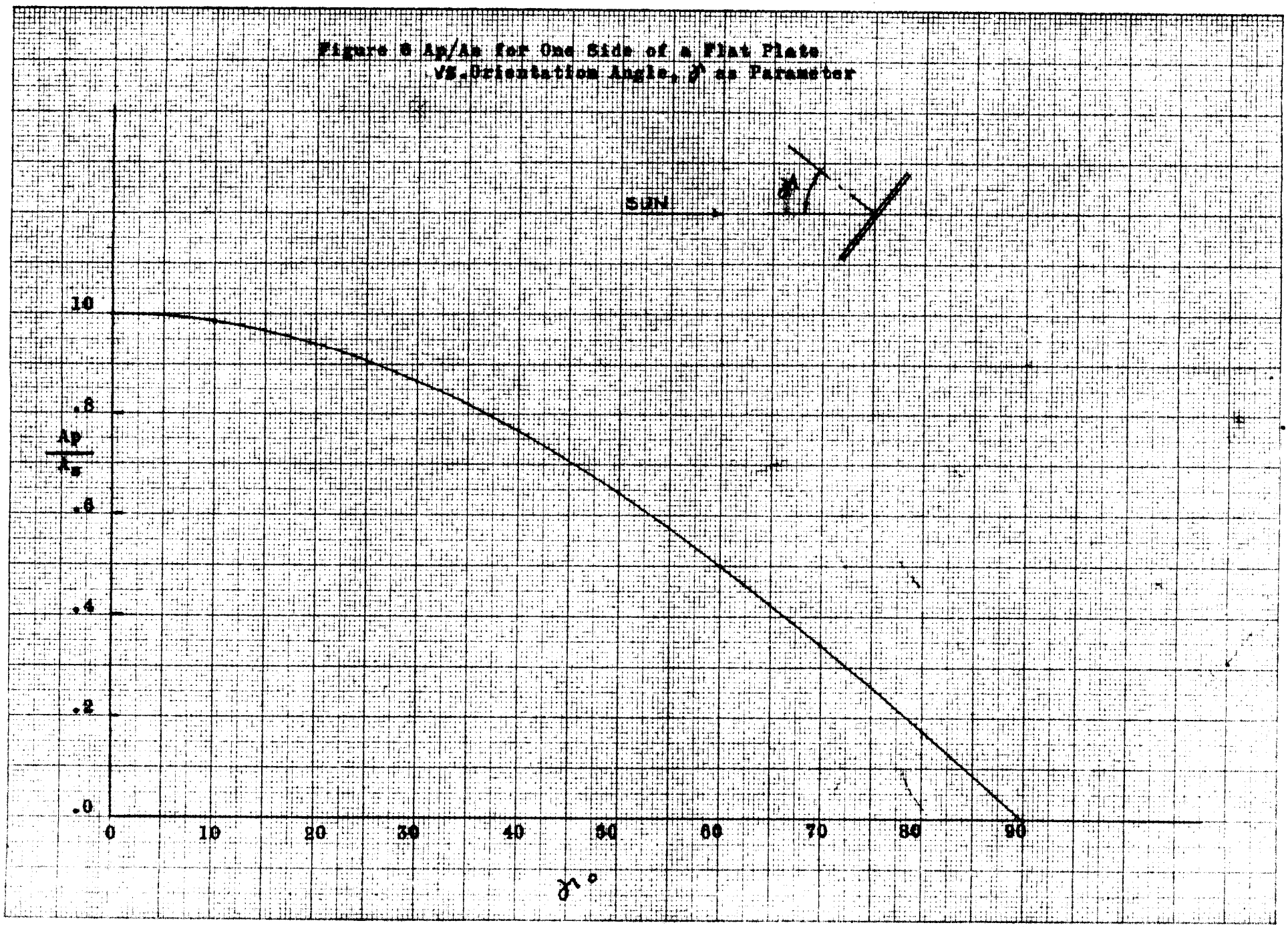

Figure 7 Ap/At for Cylinder with Flat Plate Ends vs Orientation Angle, δ, with L/D as Parameter

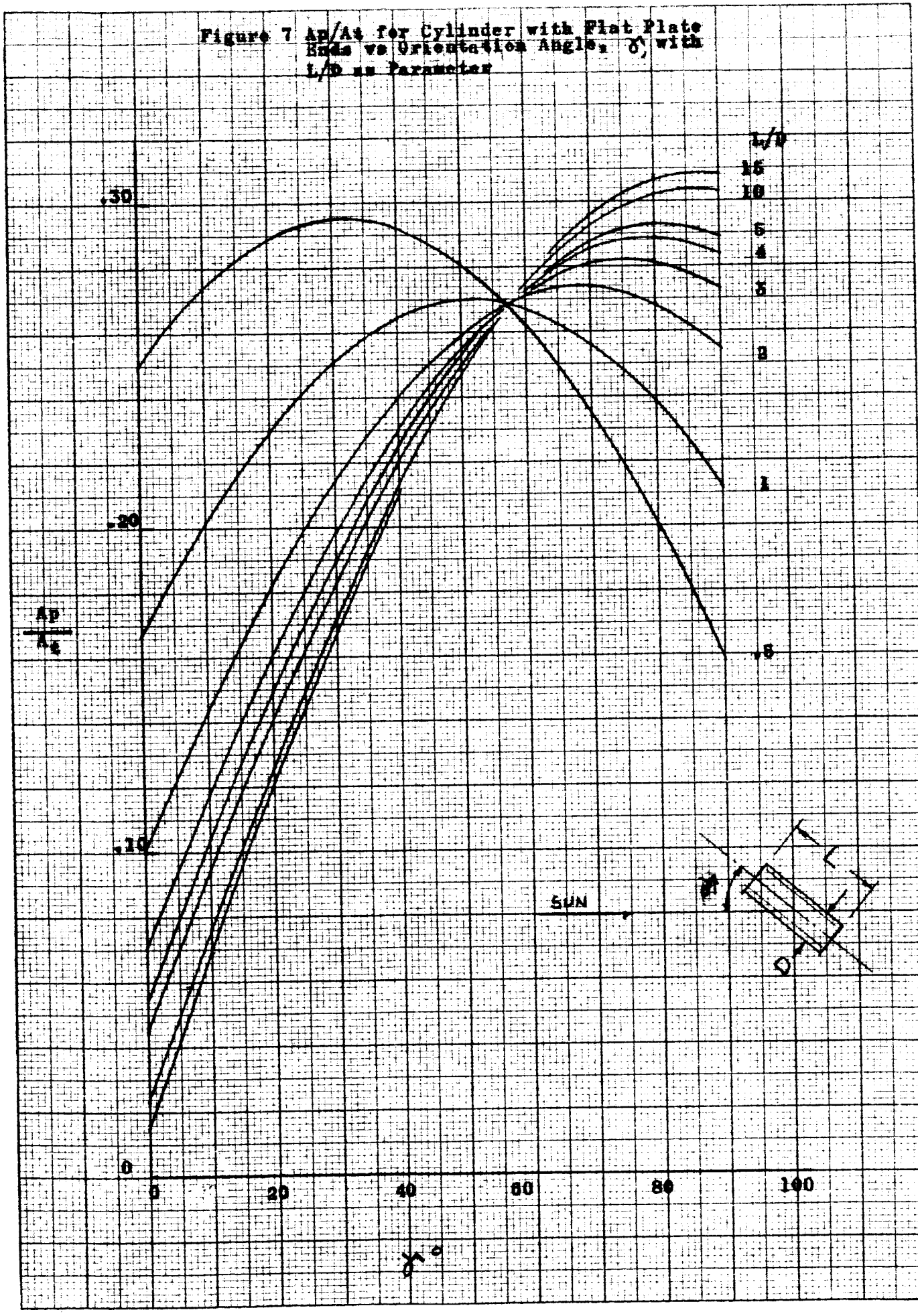

Figure 8 Ap/At for Cylinder with Hemispherical Ends vs Orientation Angle, γ , with L/D as Parameter

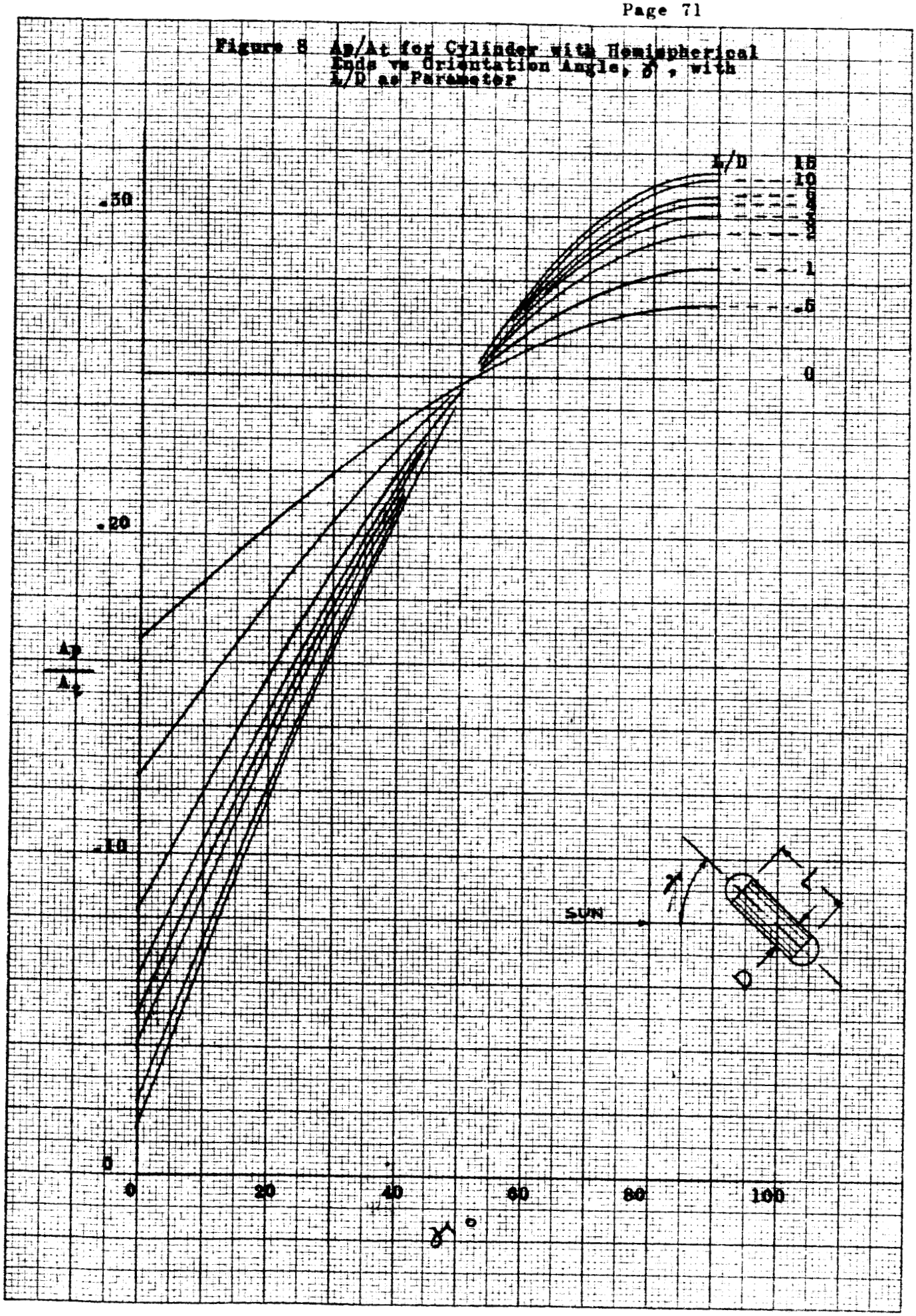

Figure 9 A_p/A_t for Hemisphere with Flat Plate Base vs Orientation Angle, γ.

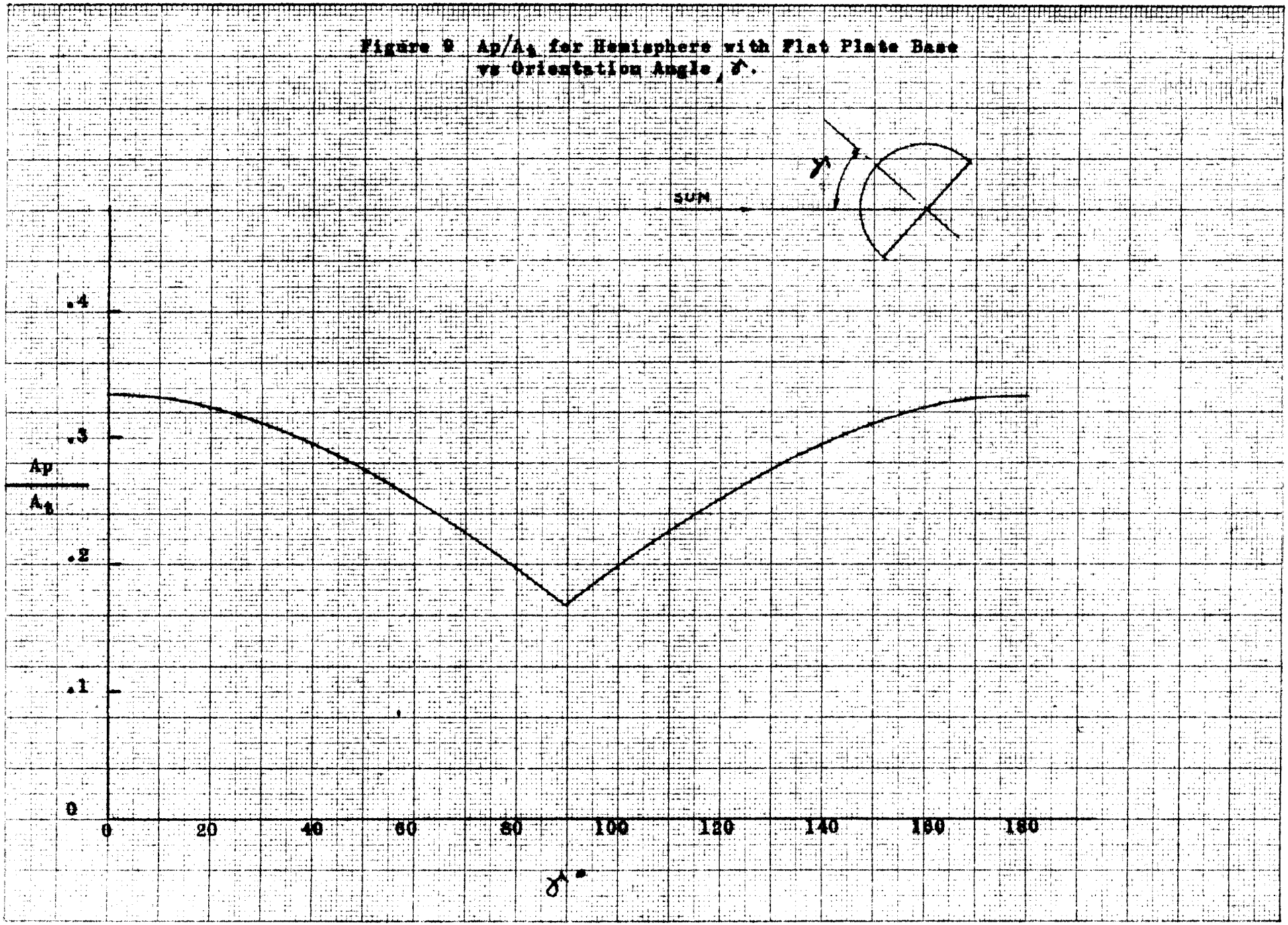

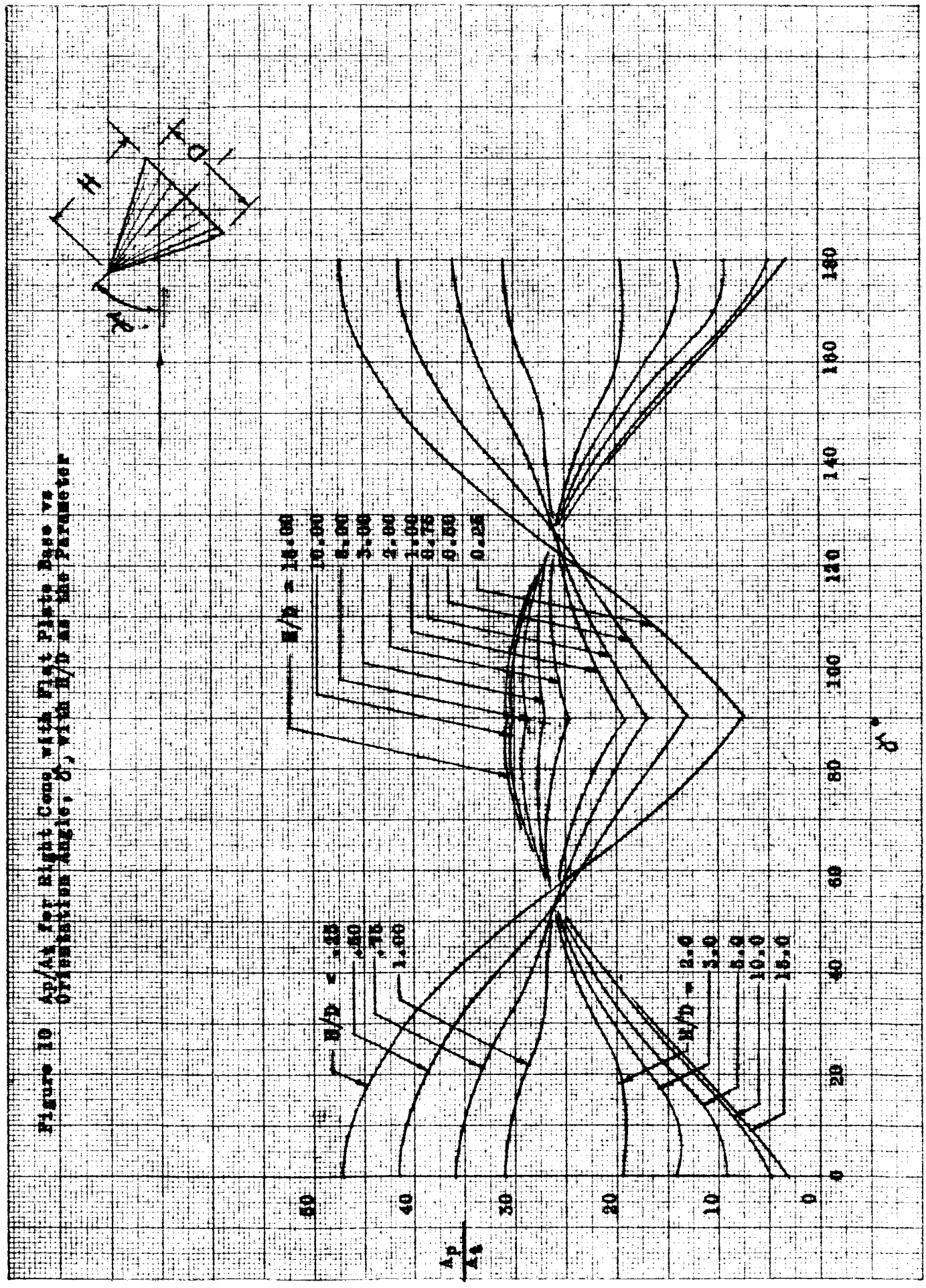

Figure 11 A_p/A_t for a Cone-Cylinder with flat plate end vs orientation angle, δ°, with L/D of cylinder as Parameter (H/D of cone = .5)

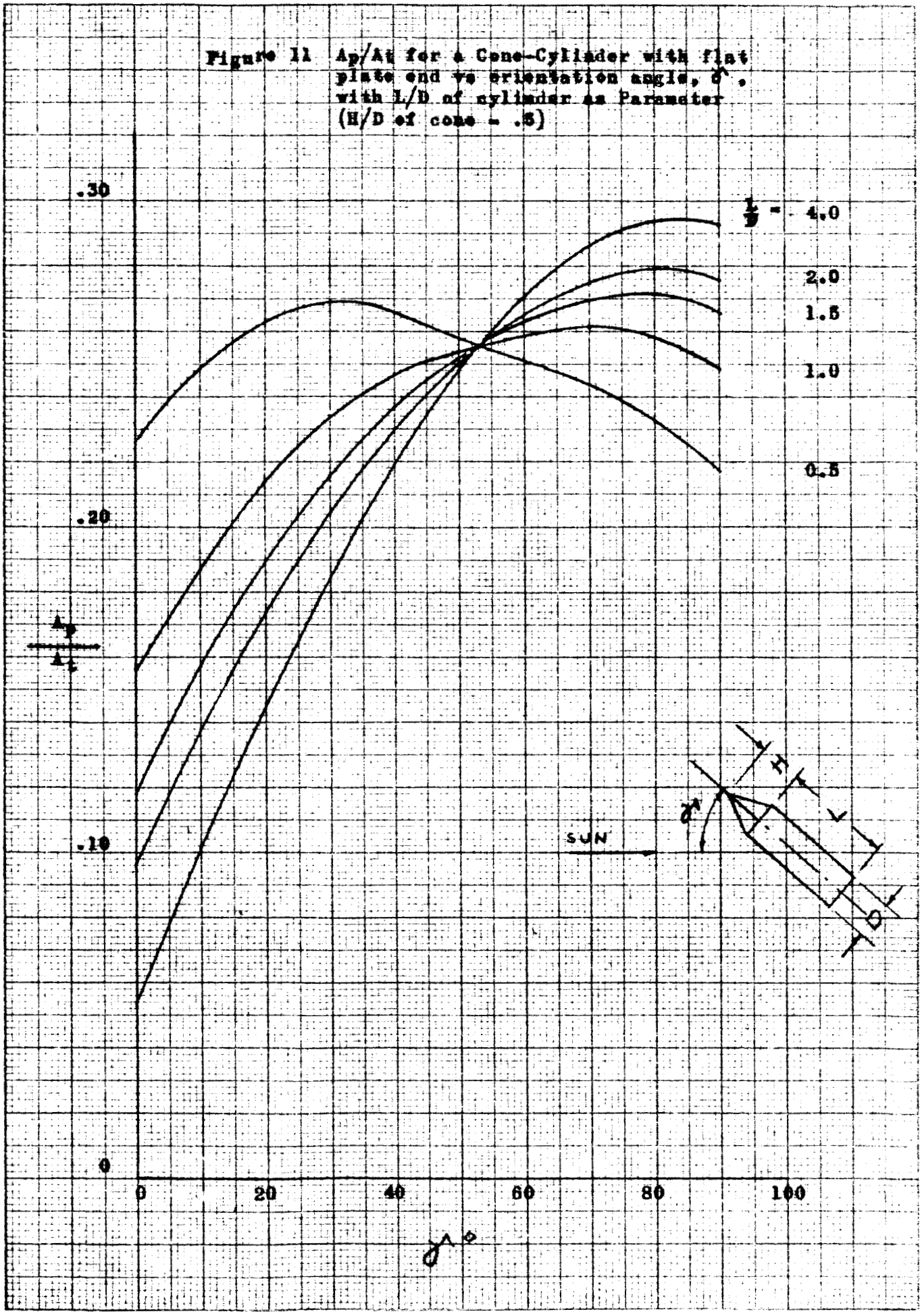

Figure 12 A_p/A_t for a Cone-Cylinder with Flat Plate End vs orientation Angle, δ°, with L/D of Cylinder as Parameter (H/D of cone = 1.0)

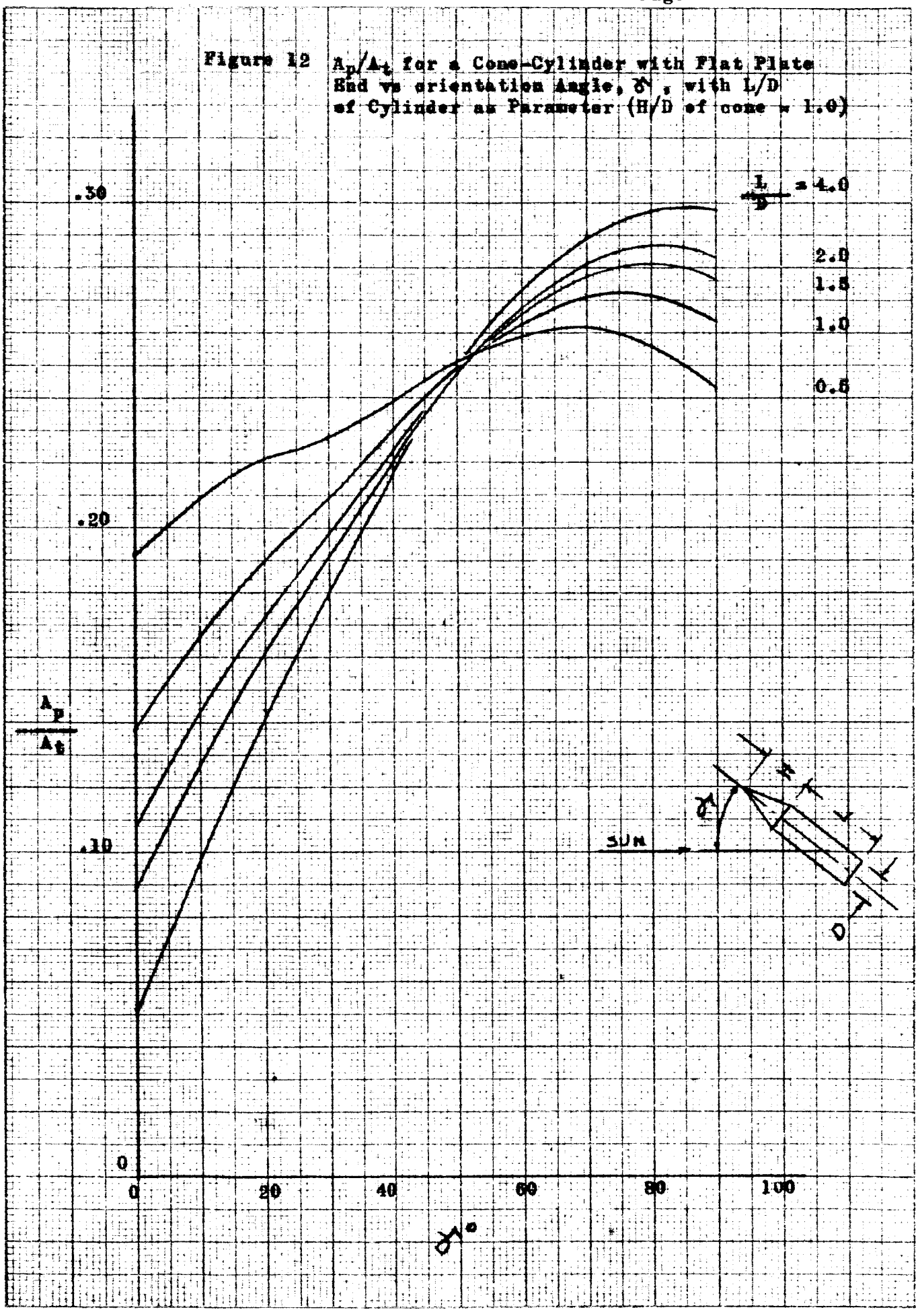

Figure 13, A_p/A_t for a cone-cylinder with Flat Plate End vs orientation angle, γ, with L/D of Cylinder as Parameter (H/D of cone = 2.0)

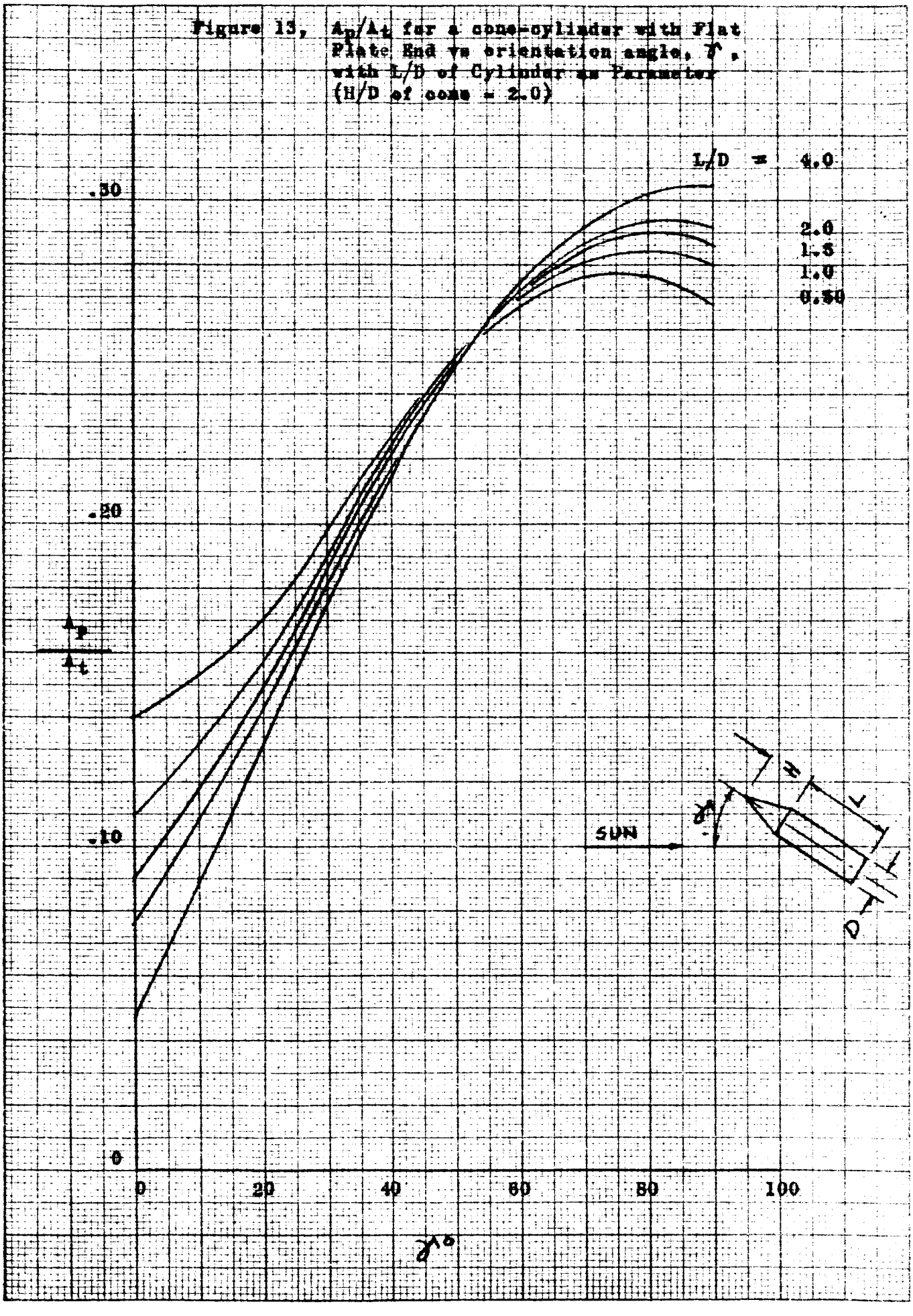

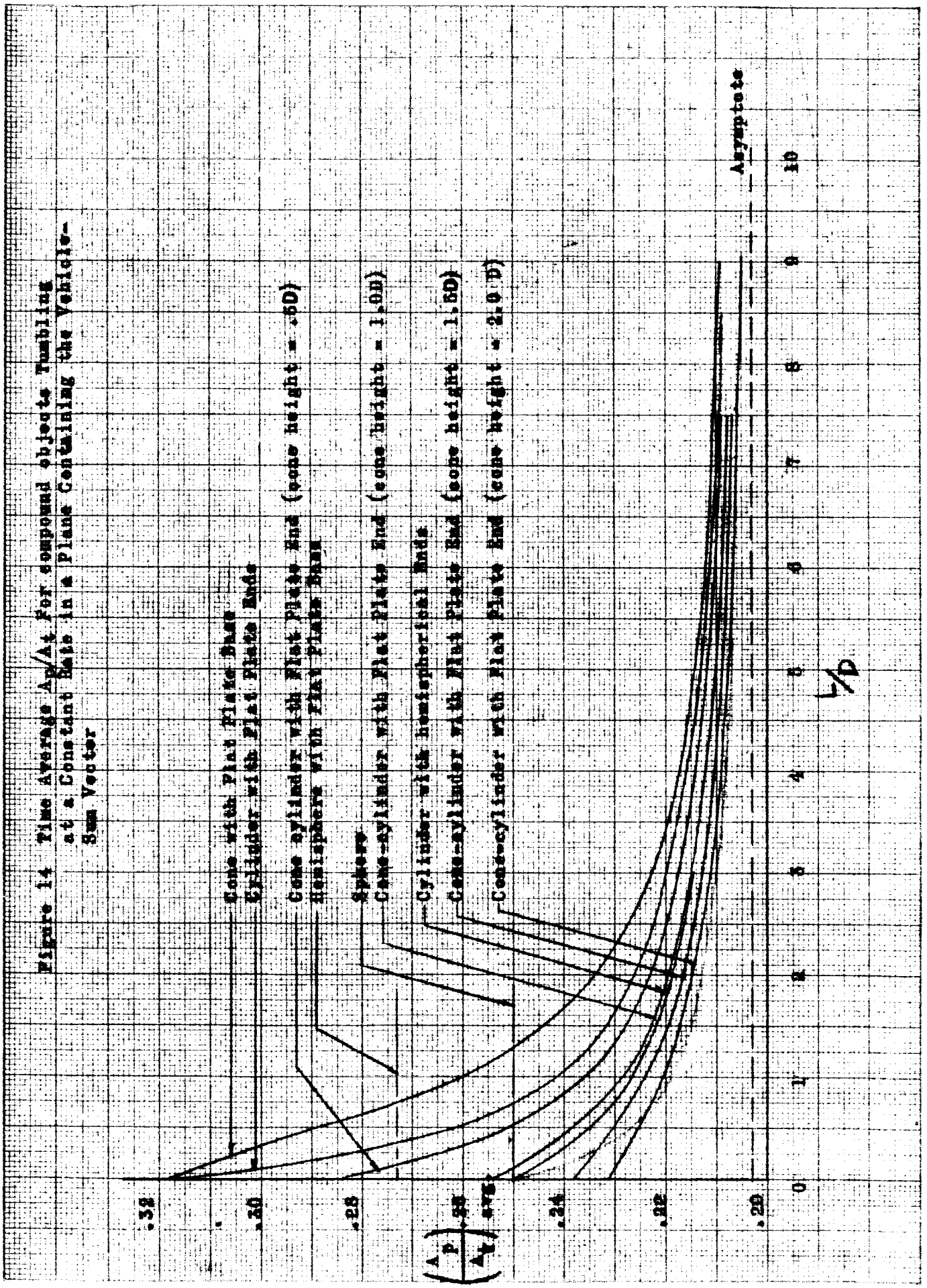

Figure 15 Local View Factor on Land of Rectangular Fin

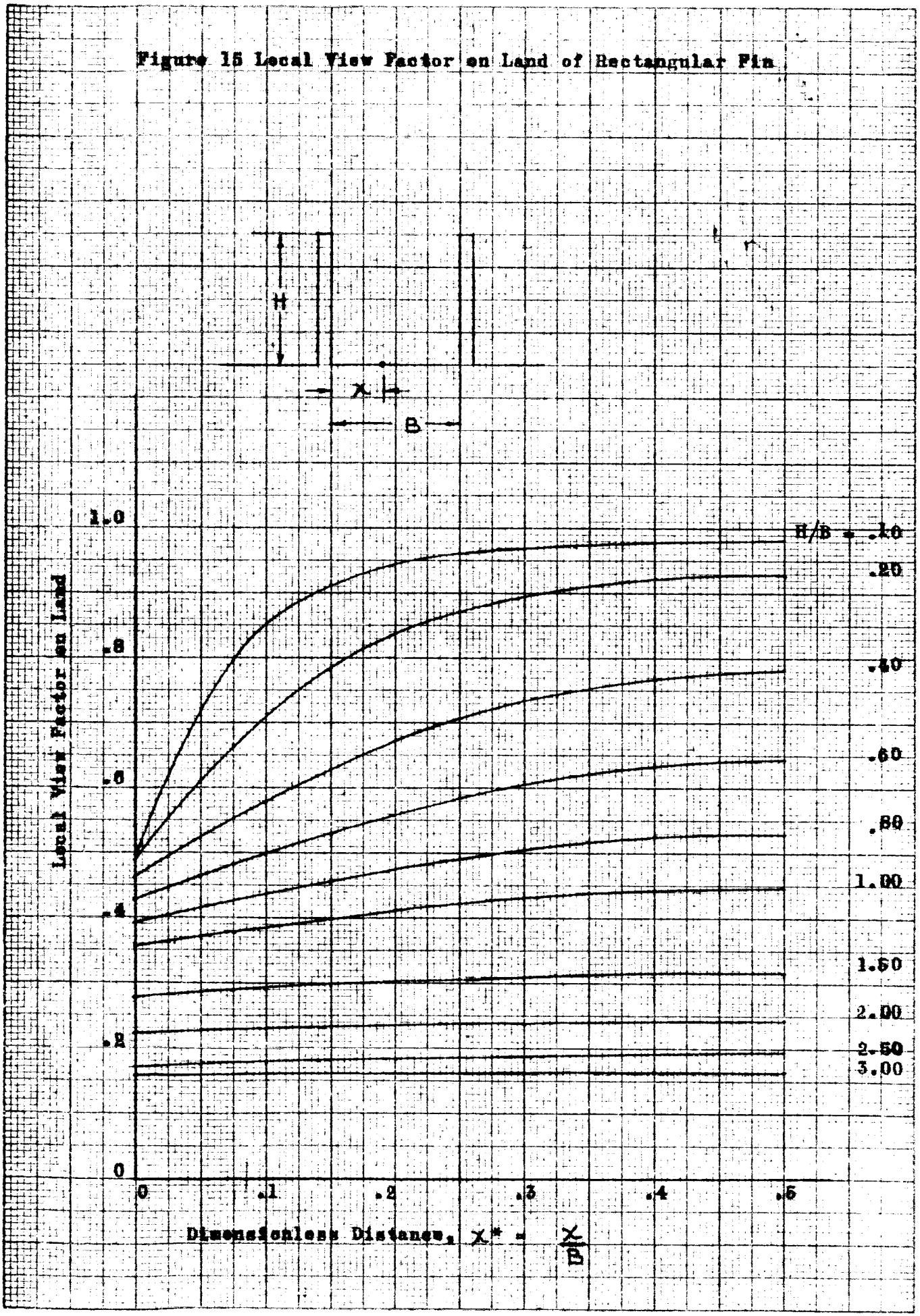

Figure 16 Local View Factor on Fin

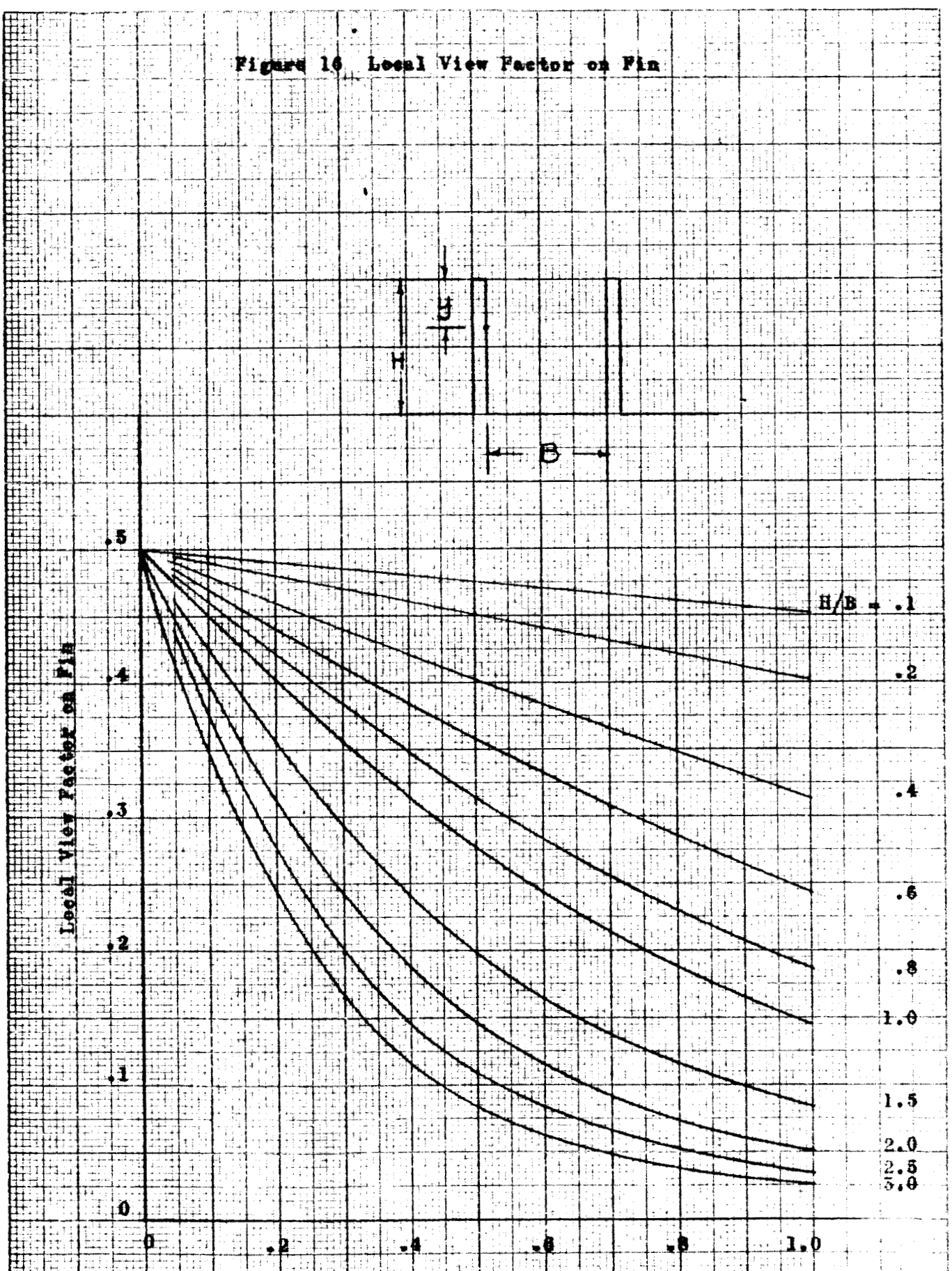

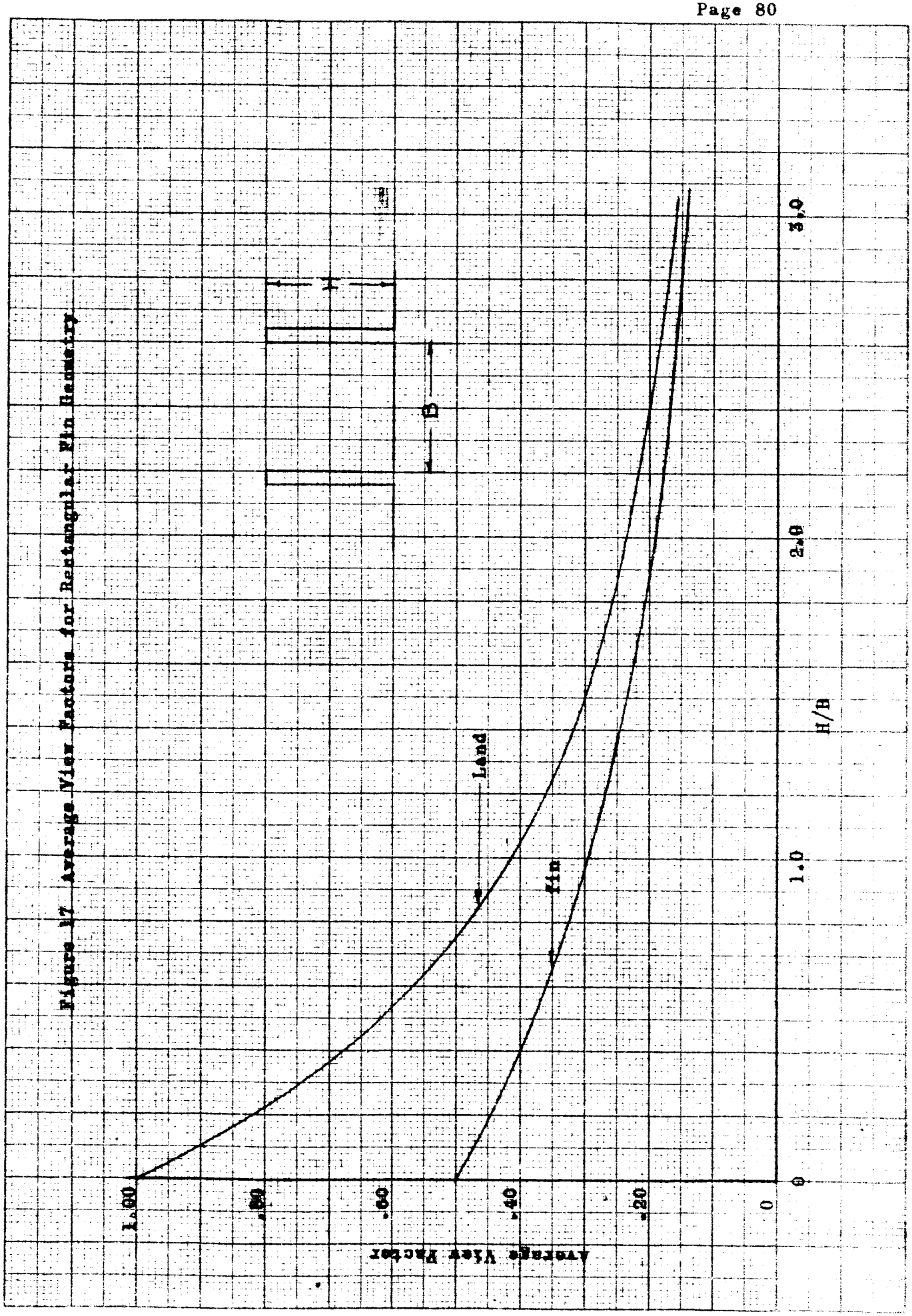

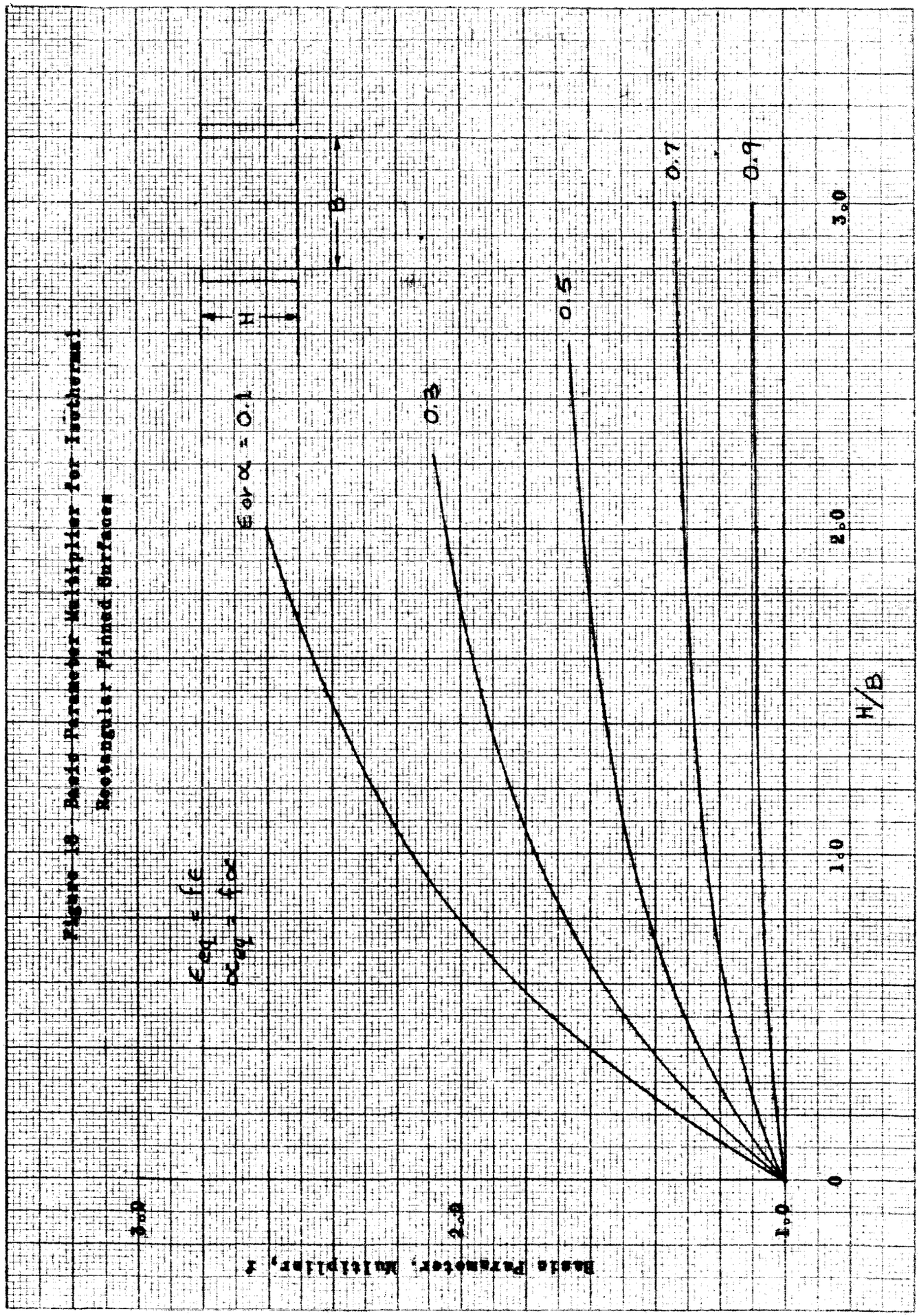

Figure 19 Alignment Chart for Solution of Conventional Insulation Equation.

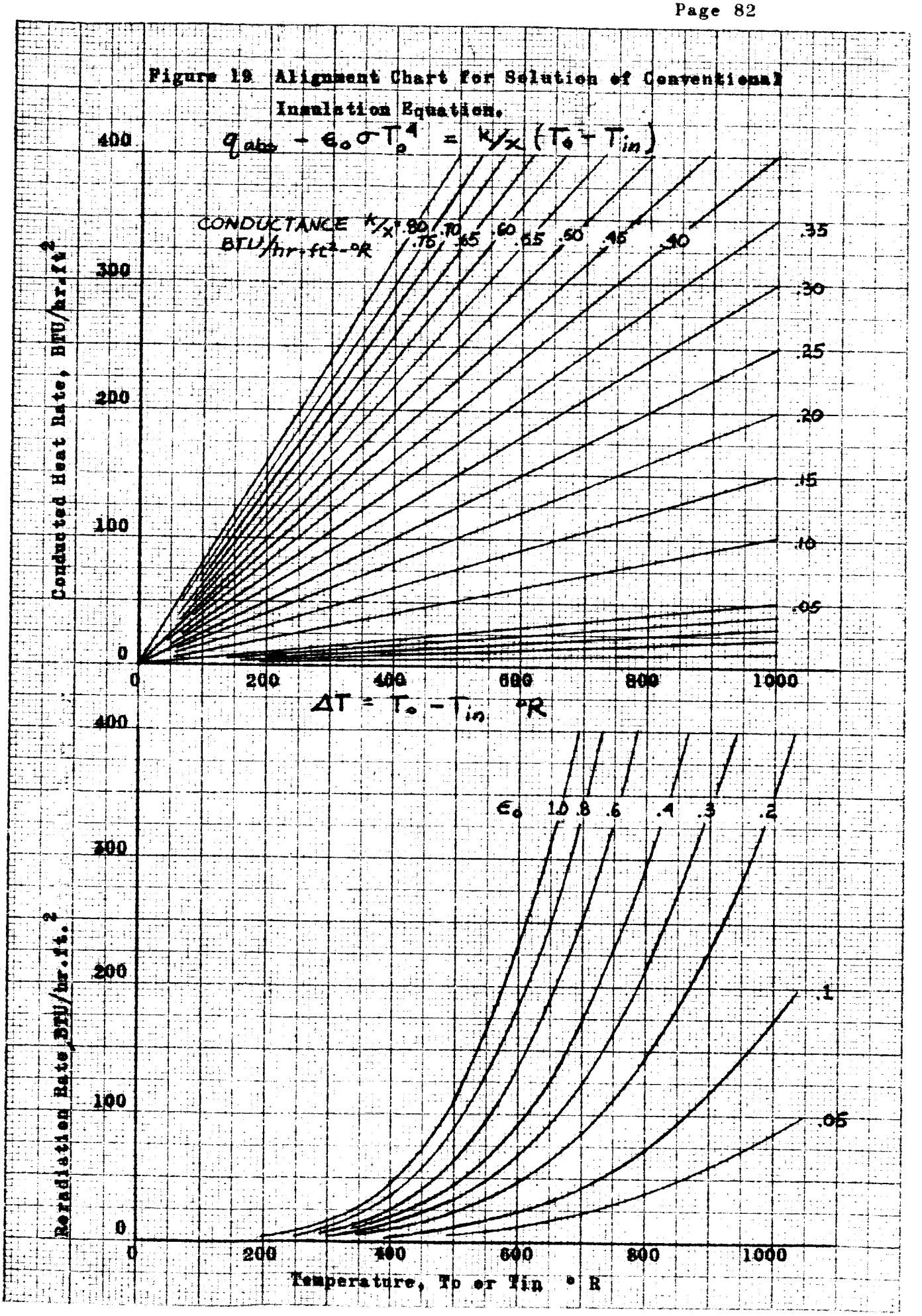

Figure 20 Alignment Chart for Solution of Radiation Shielding Equation.

$$q_{abs} = \epsilon_o \sigma T_o^4 = J\sigma (T_o^4 - T_{in}^4)$$

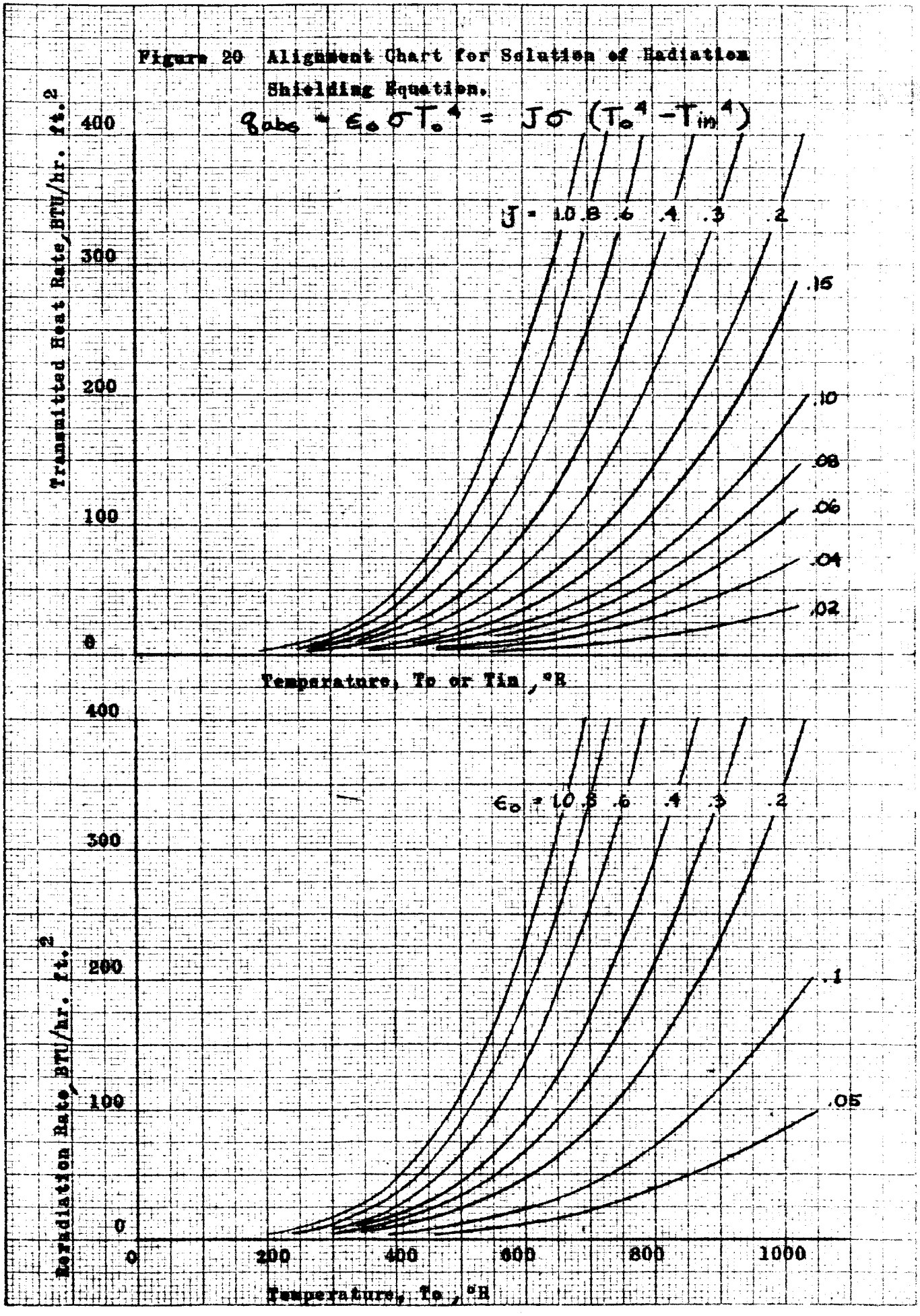

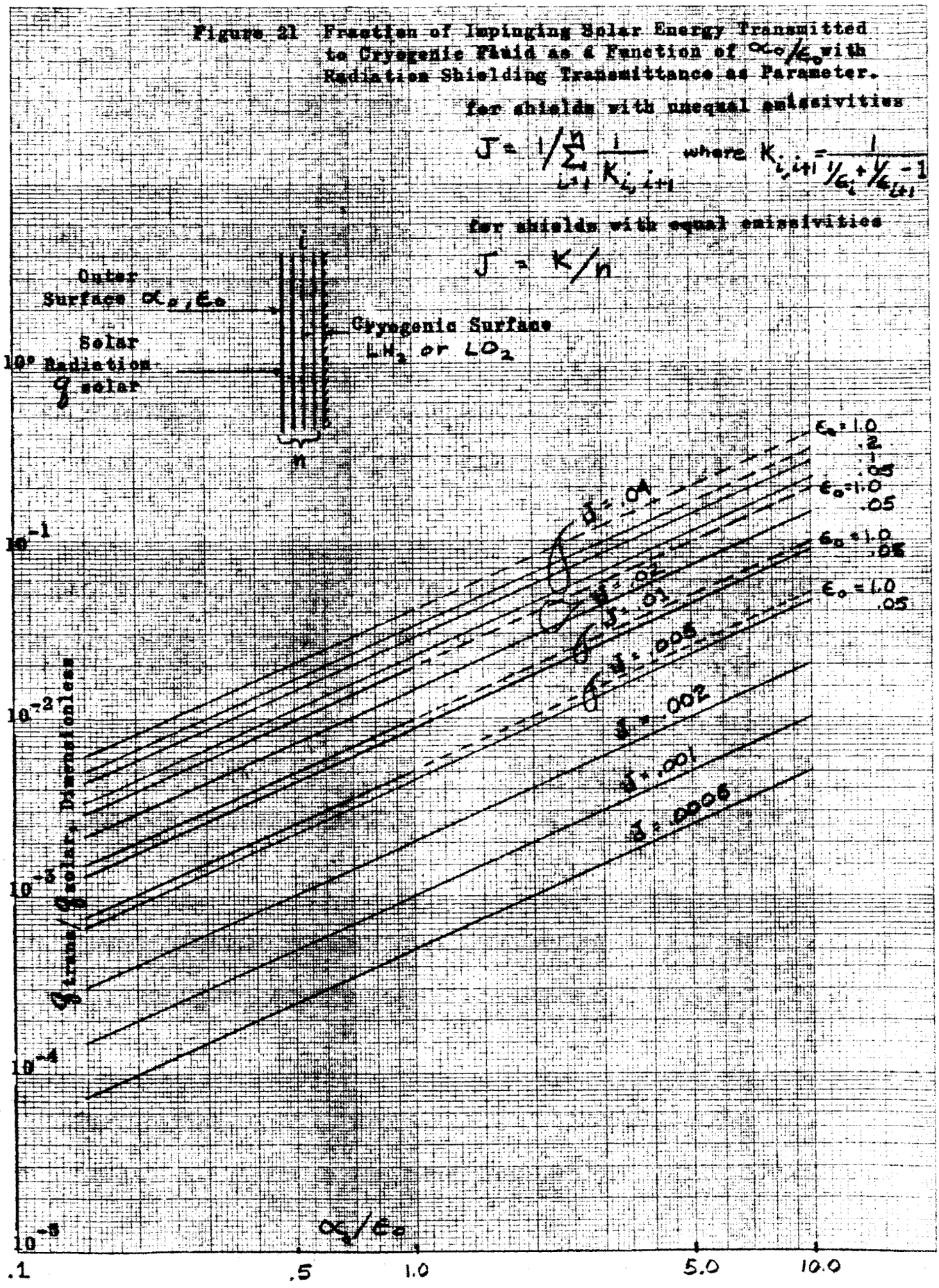

Figure 21 Fraction of Impinging Solar Energy Transmitted to Cryogenic Fluid as a Function of α_o/ϵ_o with Radiation Shielding Transmittance as Parameter.

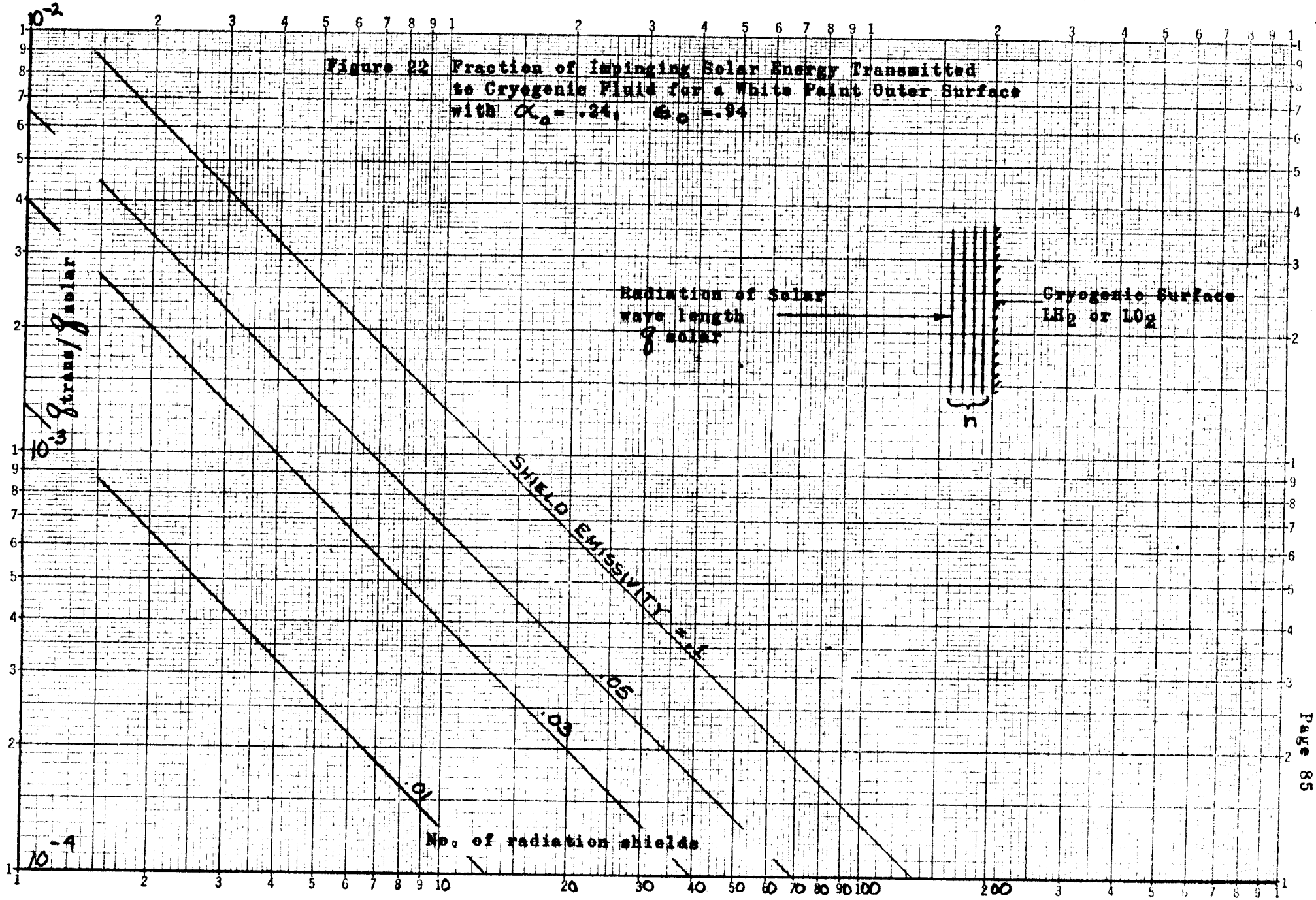

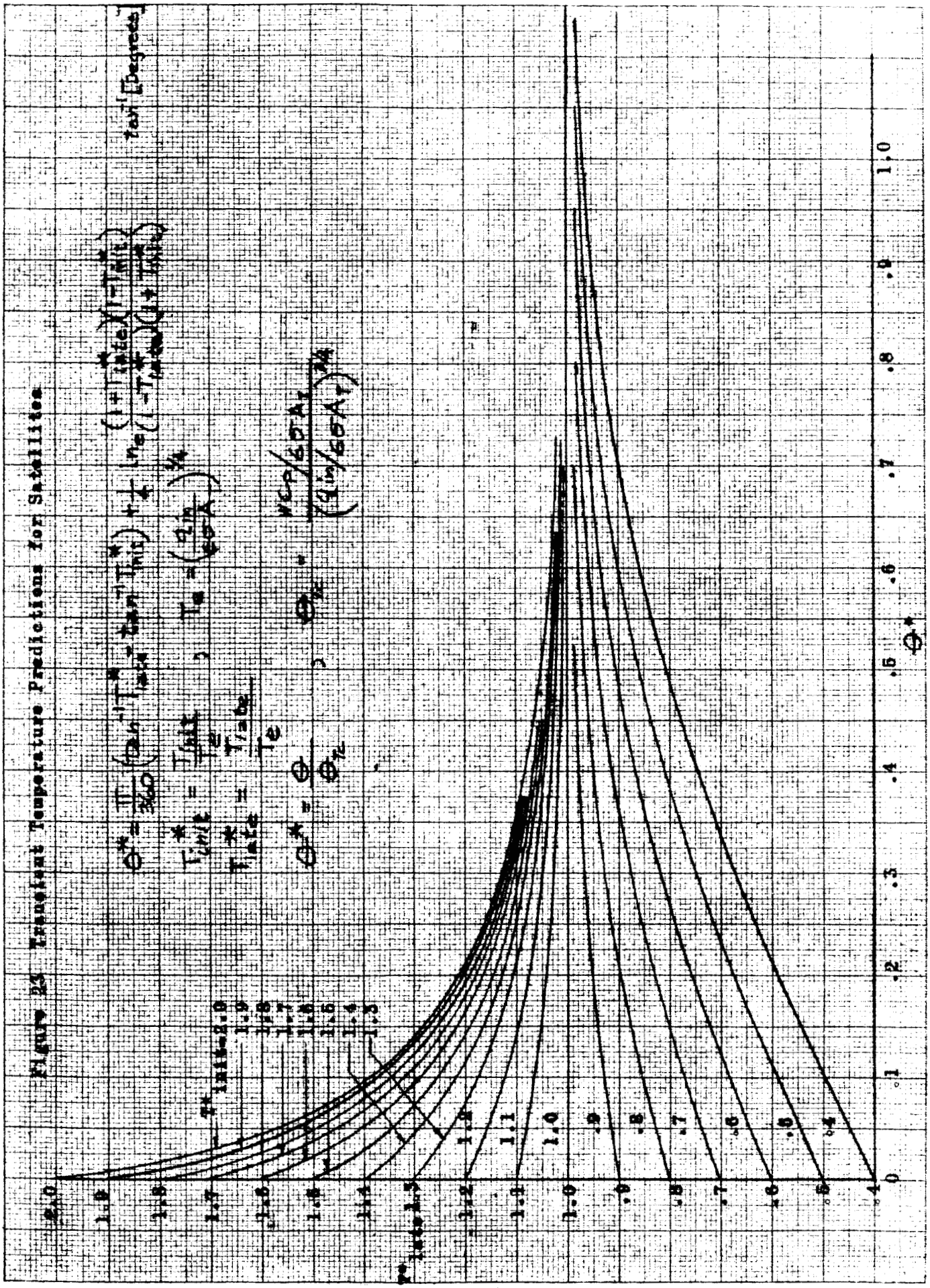

Figure 24 Local View Factors on Fin of Fin-Tube Radiator

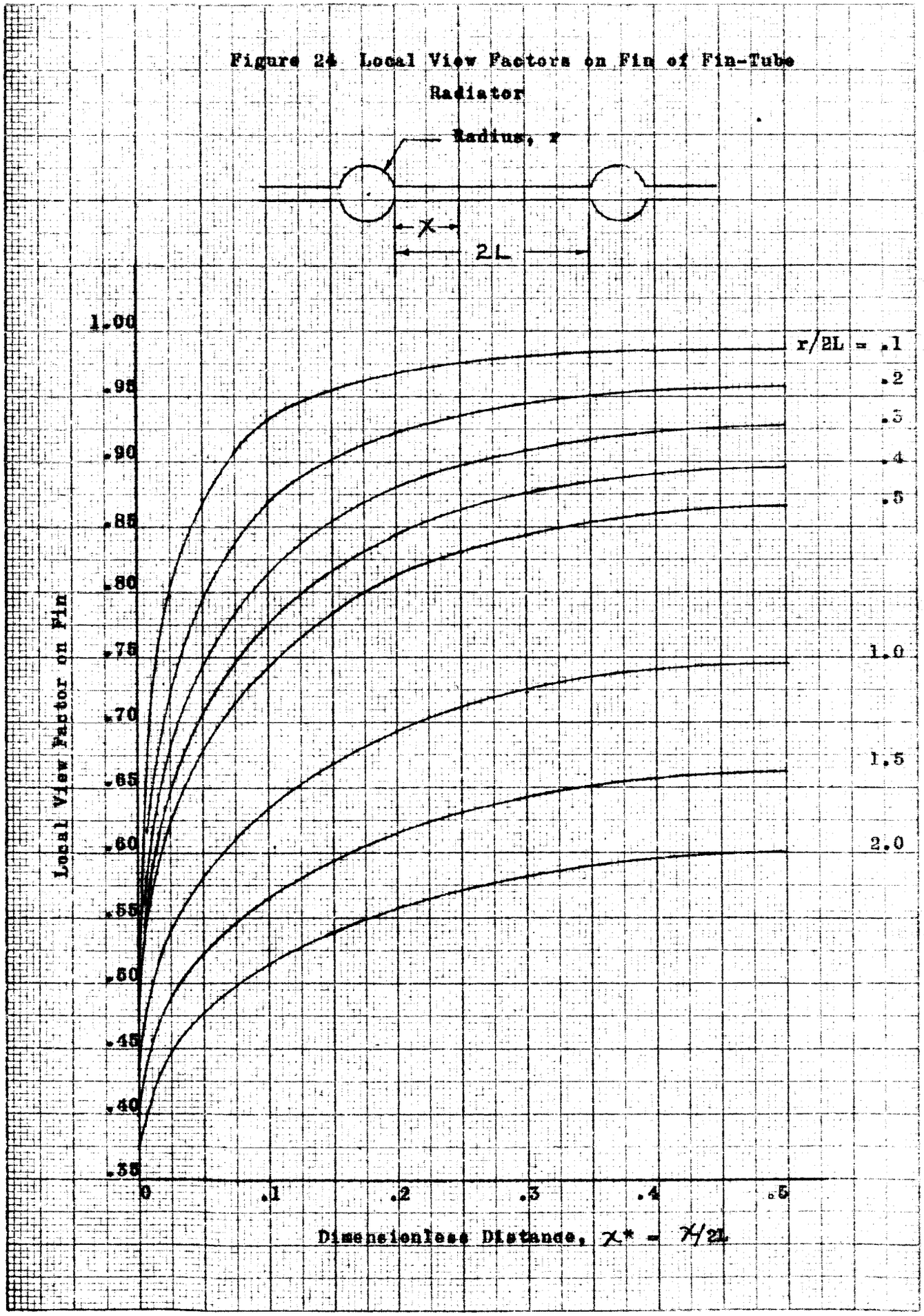

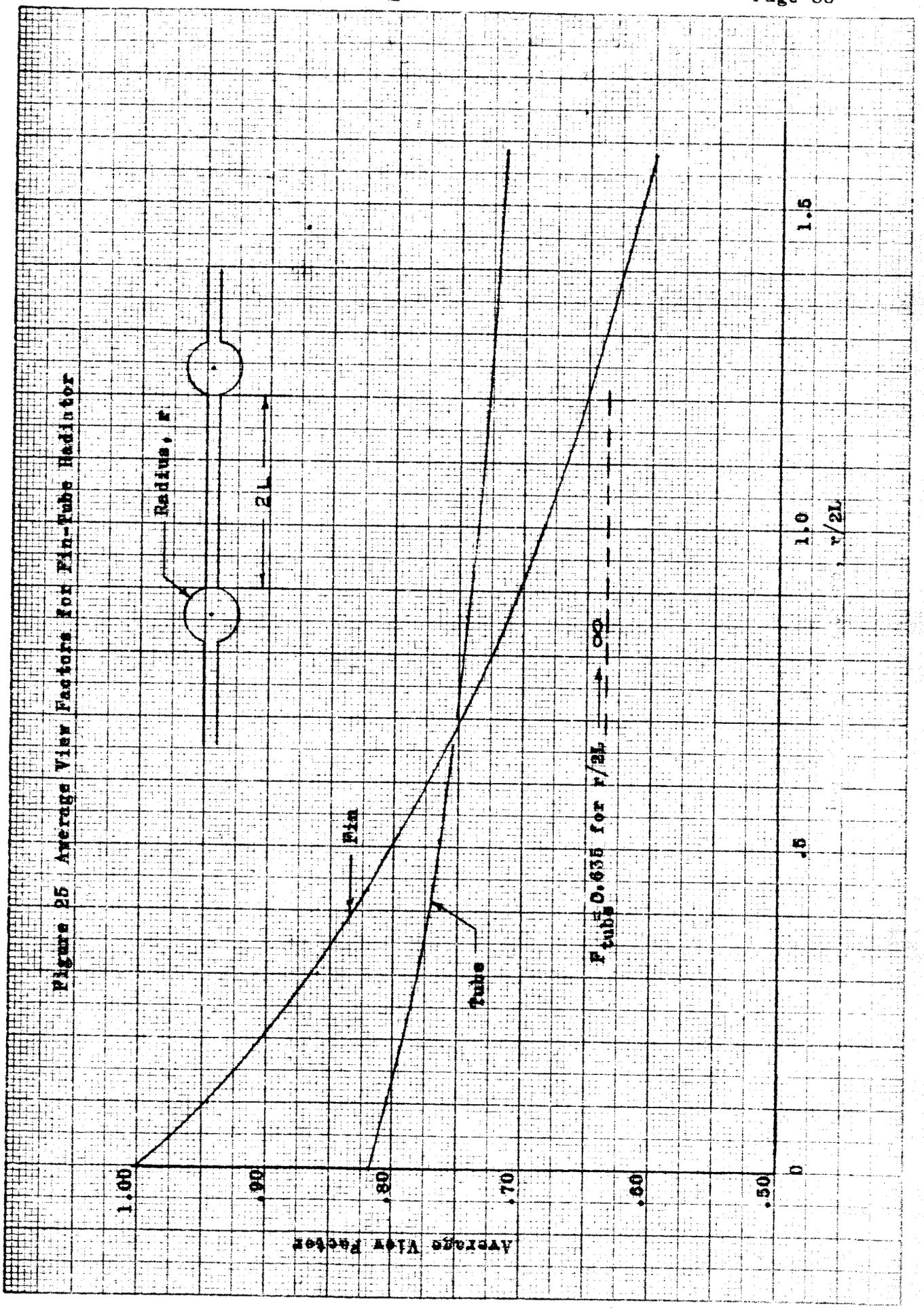

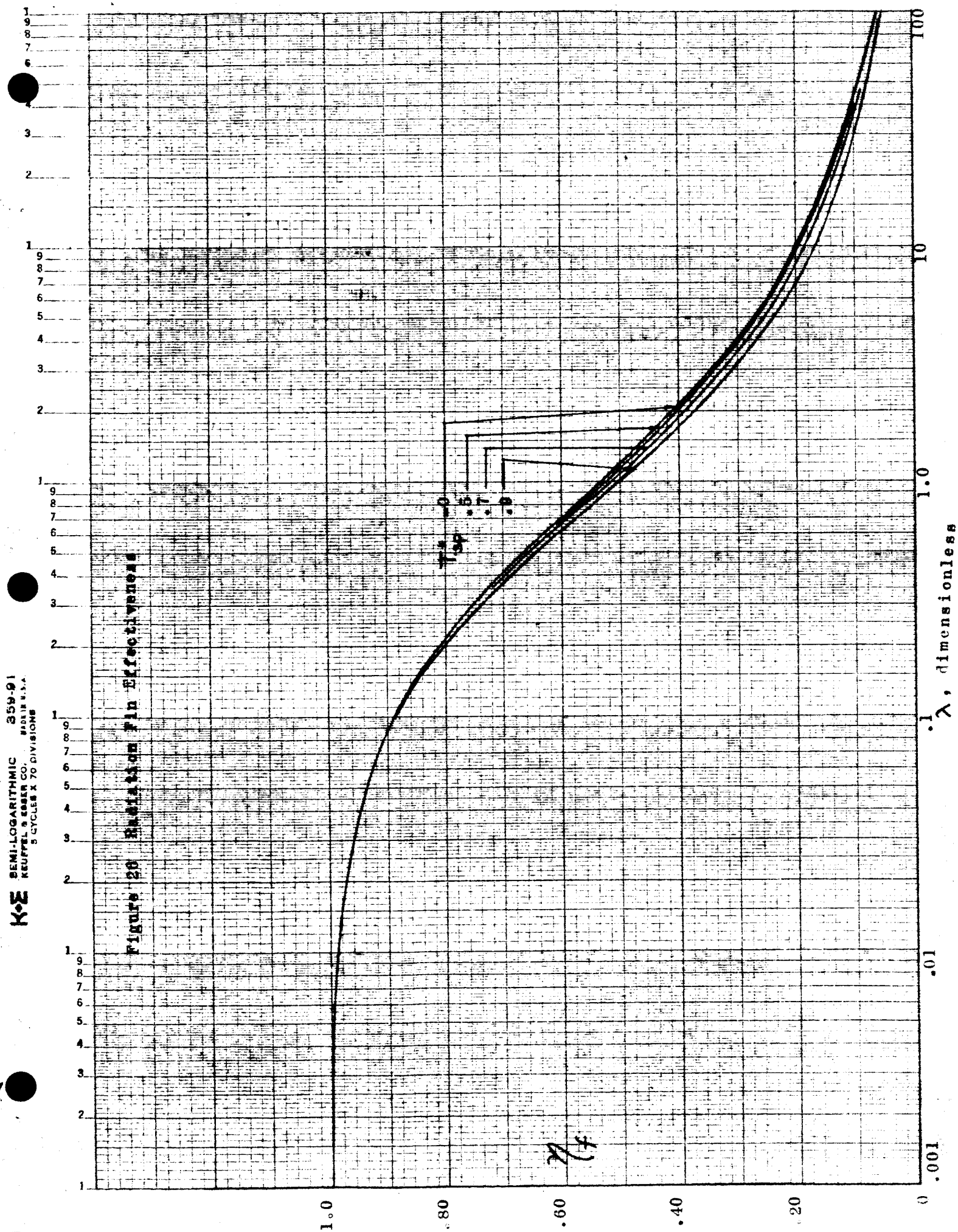

Figure 20 Radiation Fin Effectiveness

SEMI-LOGARITHMIC 359-91
KEUFFEL & ESSER CO. MADE IN U.S.A.
5 CYCLES X 70 DIVISIONS
K&E

Figure 27 Radiation Fin Effectiveness in Optimum Range of λ.

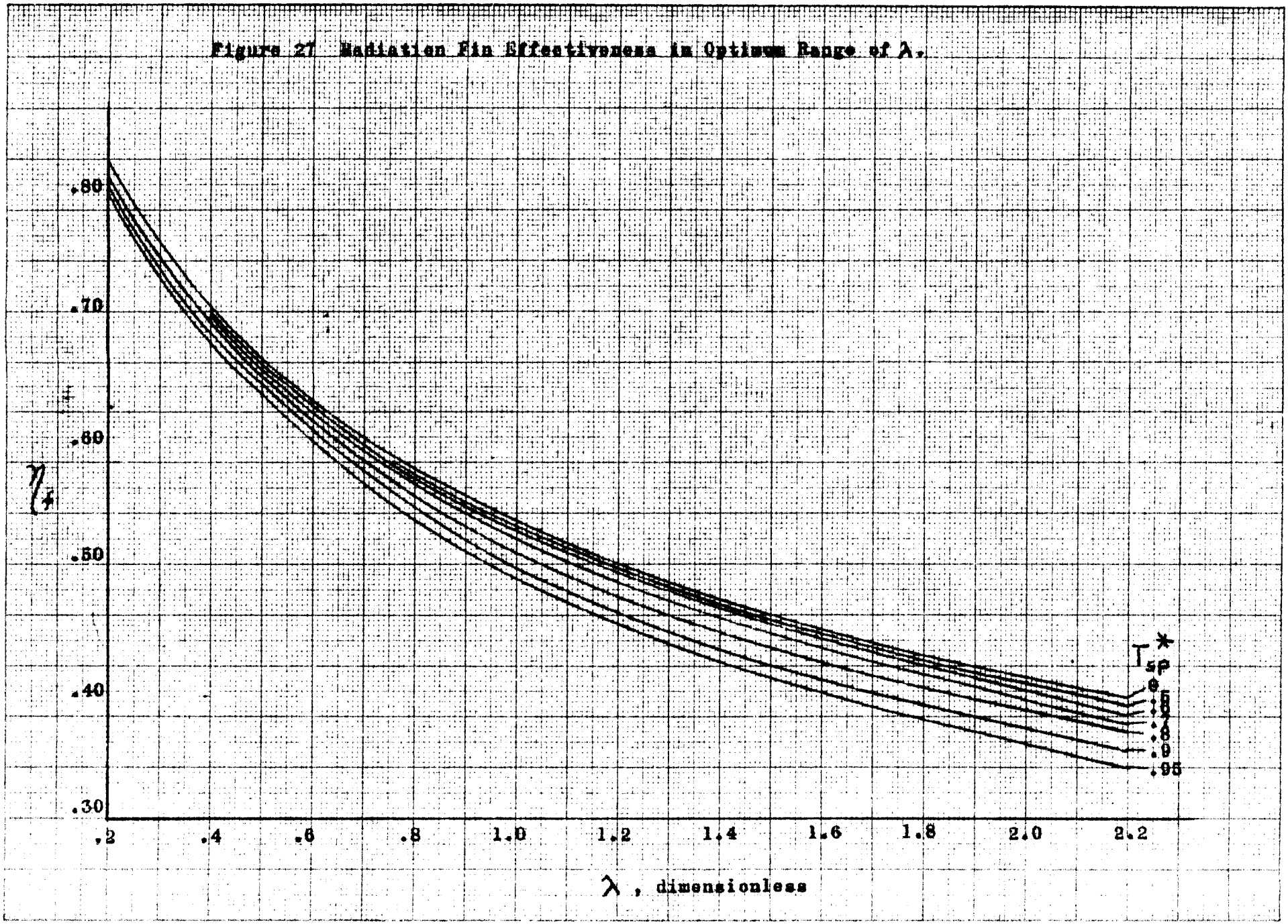

Figure 28 Optimum λ for Maximum Heat Dissipation From Constant Weight Rectangular Fin

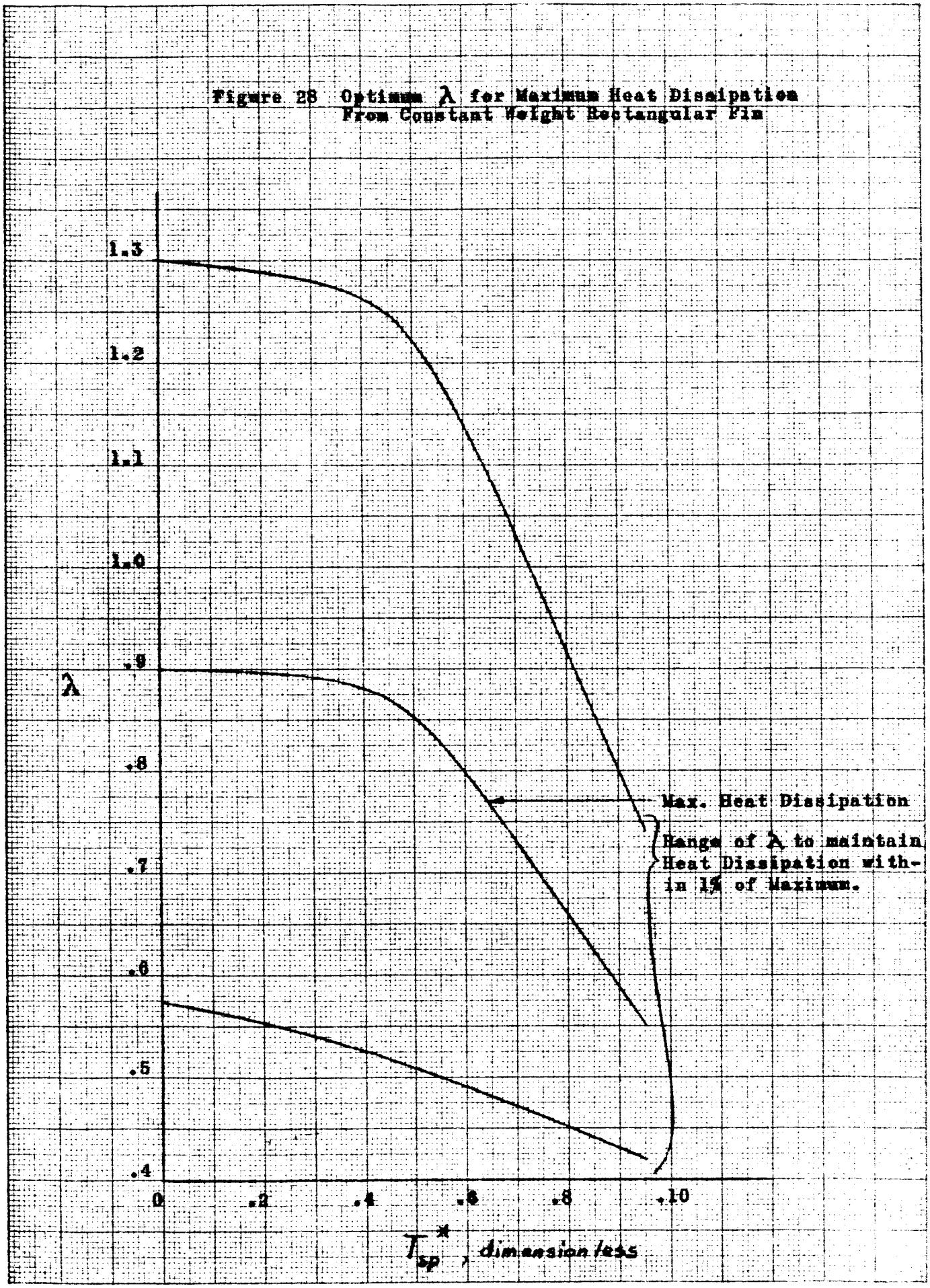

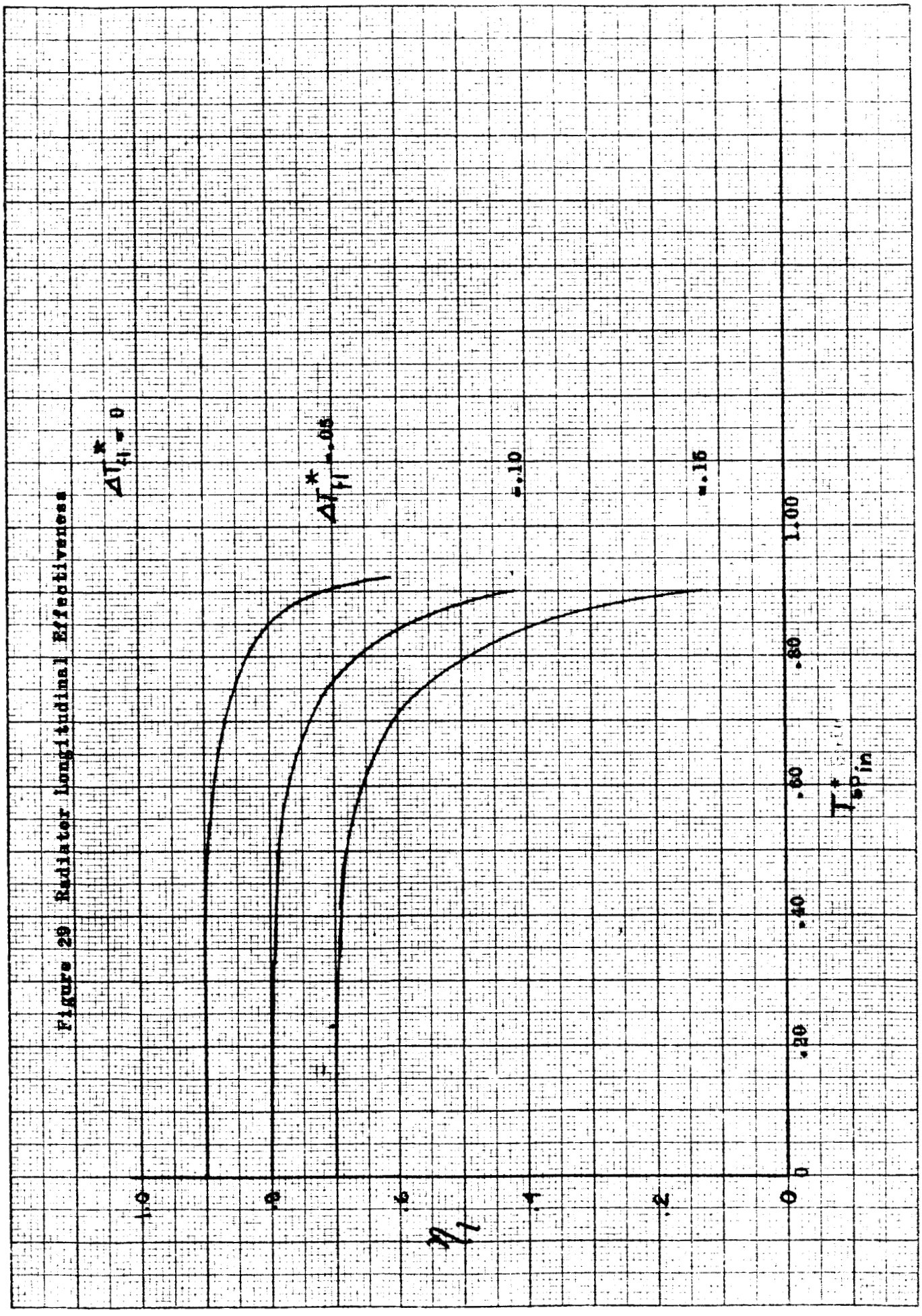

Figure 29 Radiator Longitudinal Effectiveness

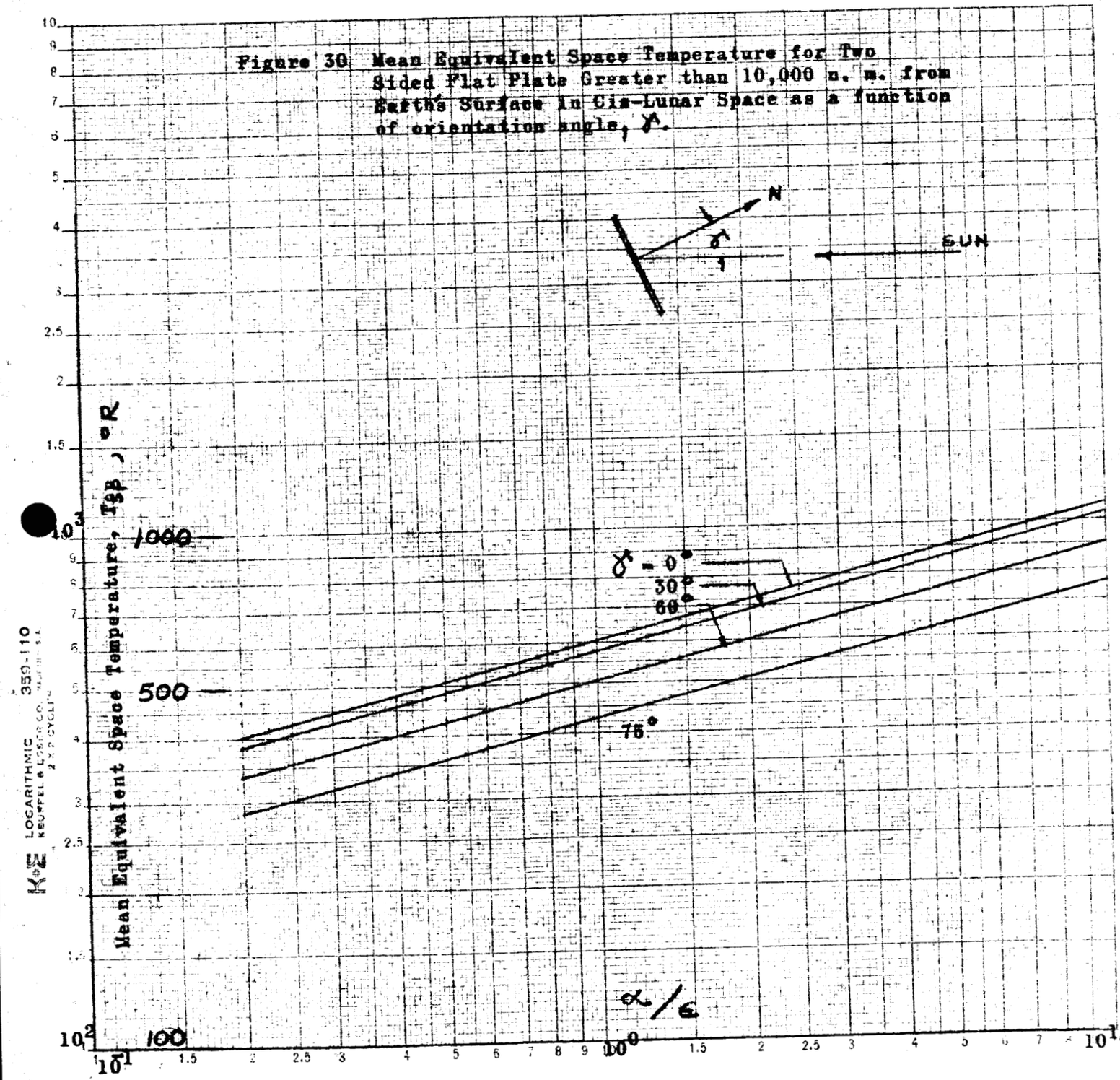

Figure 30 Mean Equivalent Space Temperature for Two Sided Flat Plate Greater than 10,000 n. m. from Earth's Surface in Cis-Lunar Space as a function of orientation angle, γ.

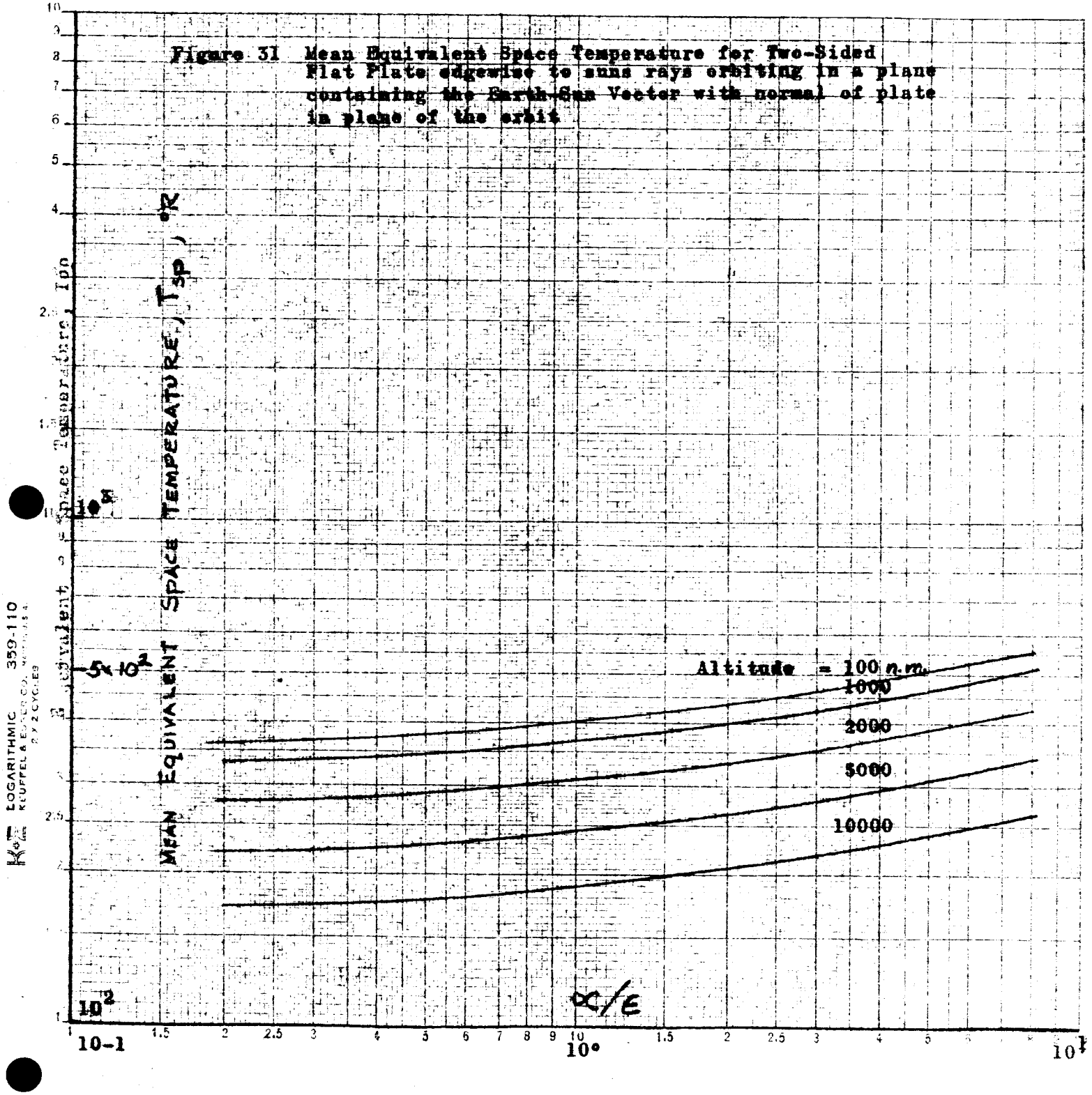

Figure 31 Mean Equivalent Space Temperature for Two-Sided Flat Plate edgewise to suns rays orbiting in a plane containing the Earth-Sun Vector with normal of plate in plane of the orbit

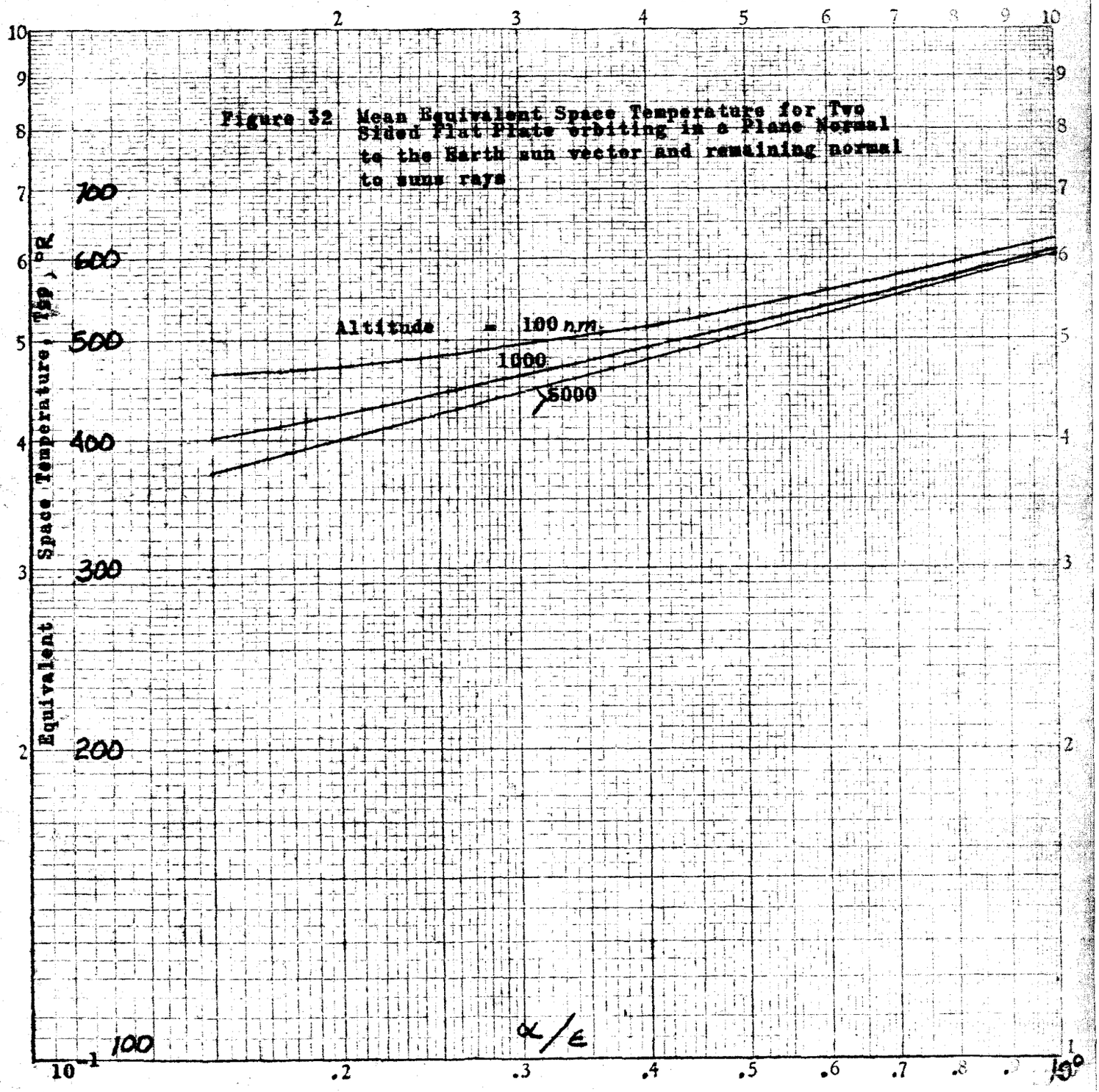

Figure 32 Mean Equivalent Space Temperature for Two Sided Flat Plate orbiting in a Plane Normal to the Earth sun vector and remaining normal to suns rays

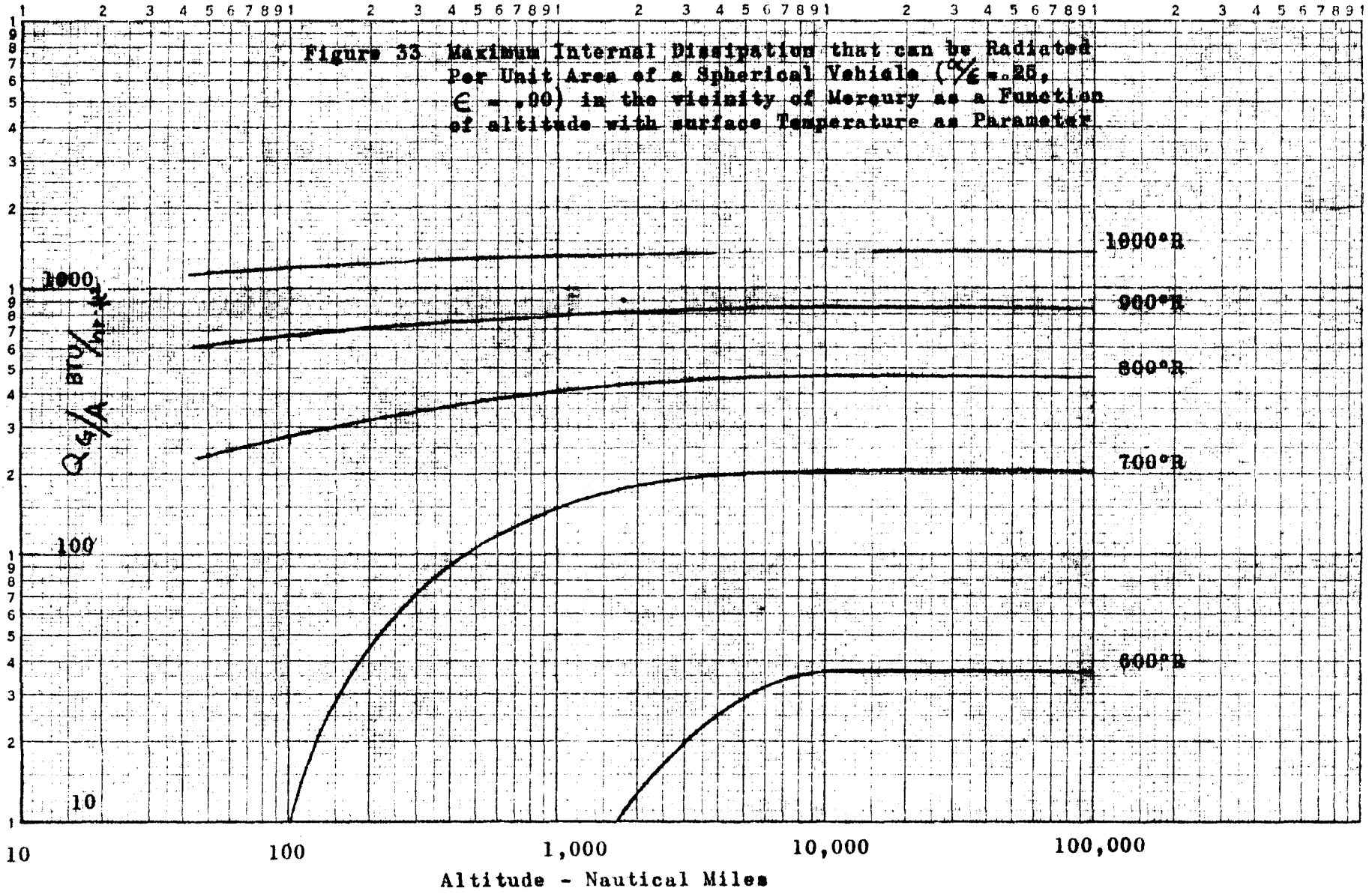

Figure 33 Maximum Internal Dissipation that can be Radiated Per Unit Area of a Spherical Vehicle (α/ϵ=.25, ϵ = .00) in the vicinity of Mercury as a Function of altitude with surface Temperature as Parameter

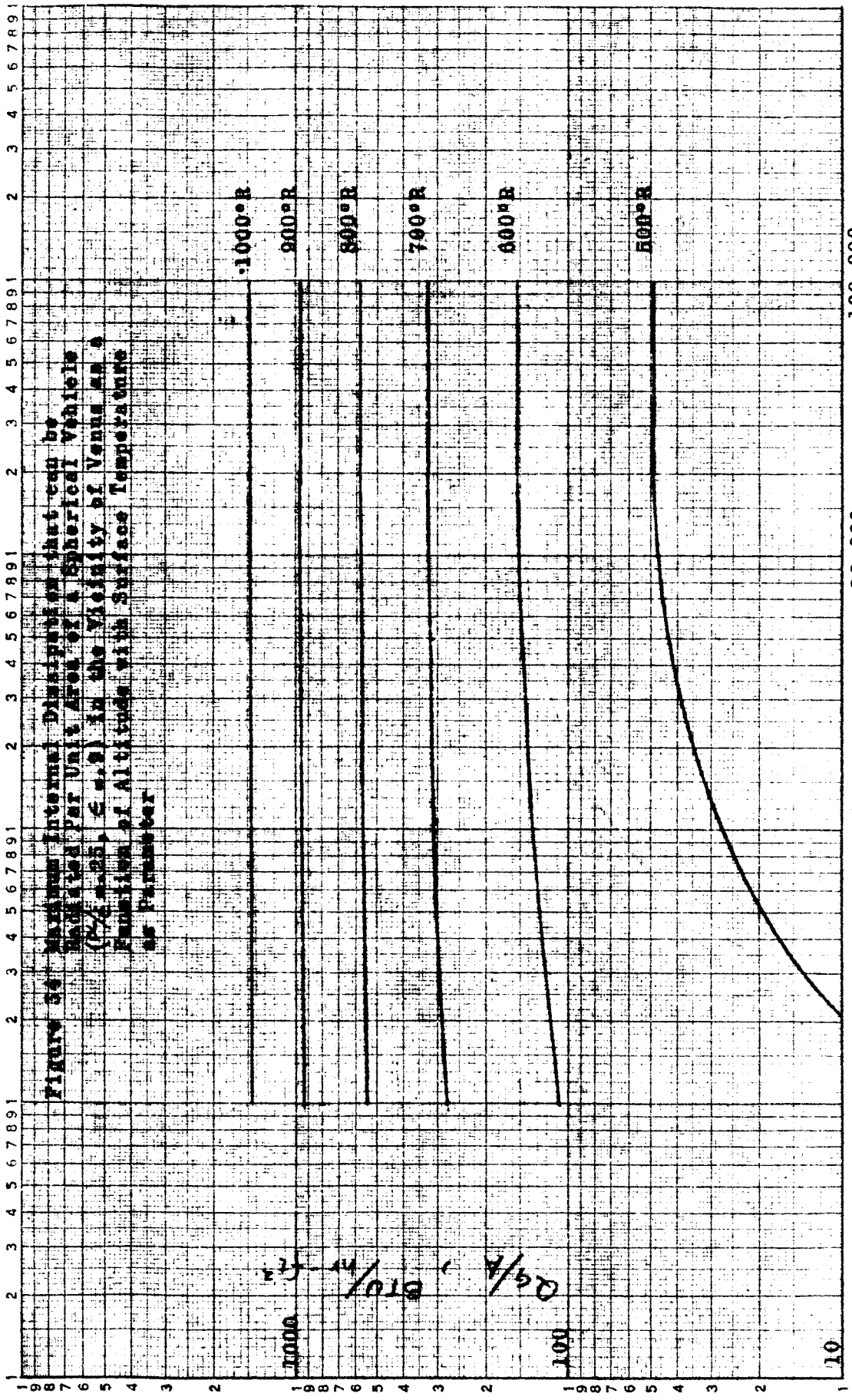

Figure 44 Maximum Internal Dissipation that can be Radiated Per Unit Area of a Spherical Vehicle (ϵ_w = 0.25, ϵ_g = 0.8) in the Vicinity of Venus as a Function of Altitude with Surface Temperature as Parameter

LOGARITHMIC 359-125G
KEUFFEL & ESSER CO.

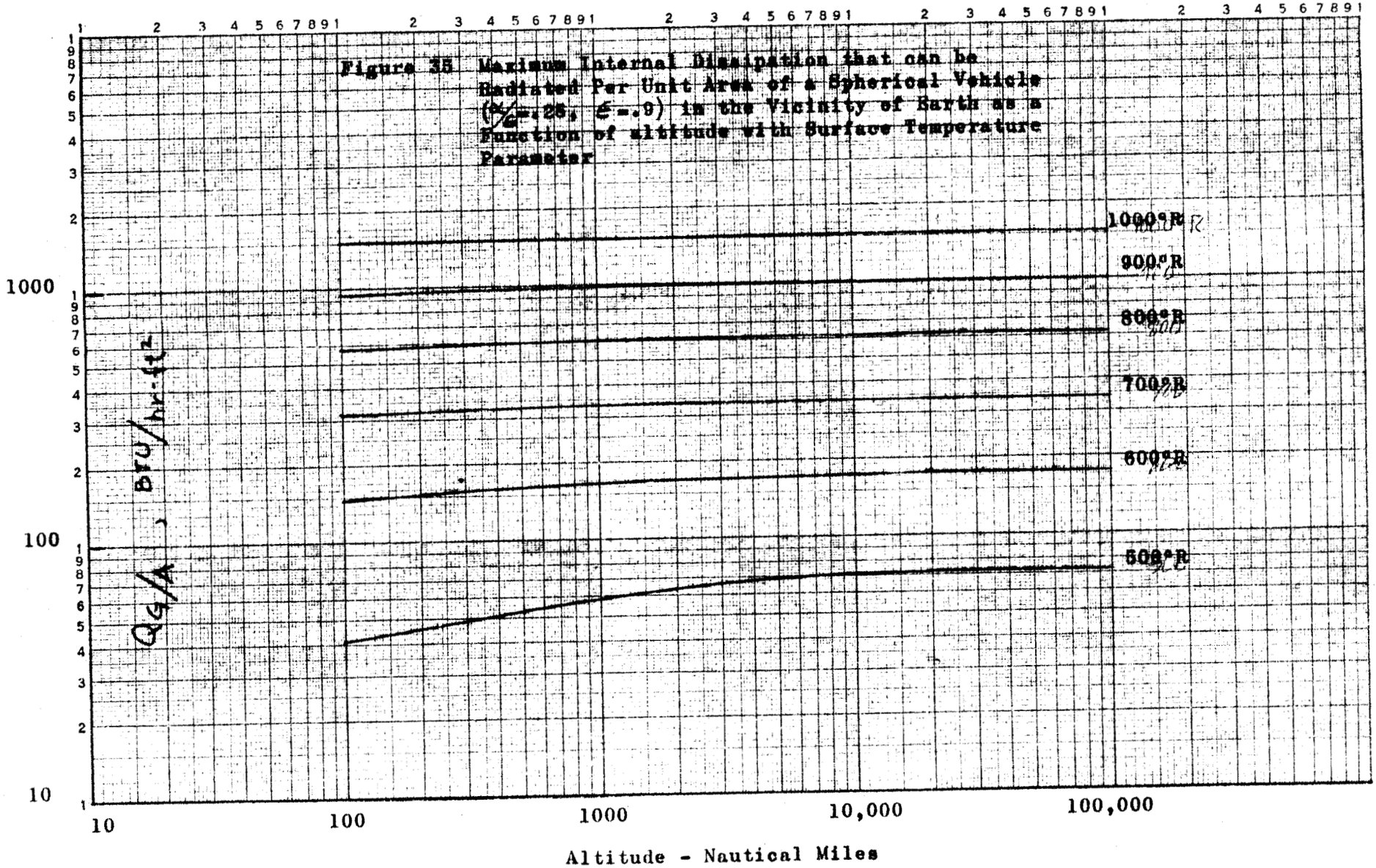

Figure 35 Maximum Internal Dissipation that can be Radiated Per Unit Area of a Spherical Vehicle (α_s=.25, ϵ=.9) in the Vicinity of Earth as a Function of altitude with Surface Temperature Parameter

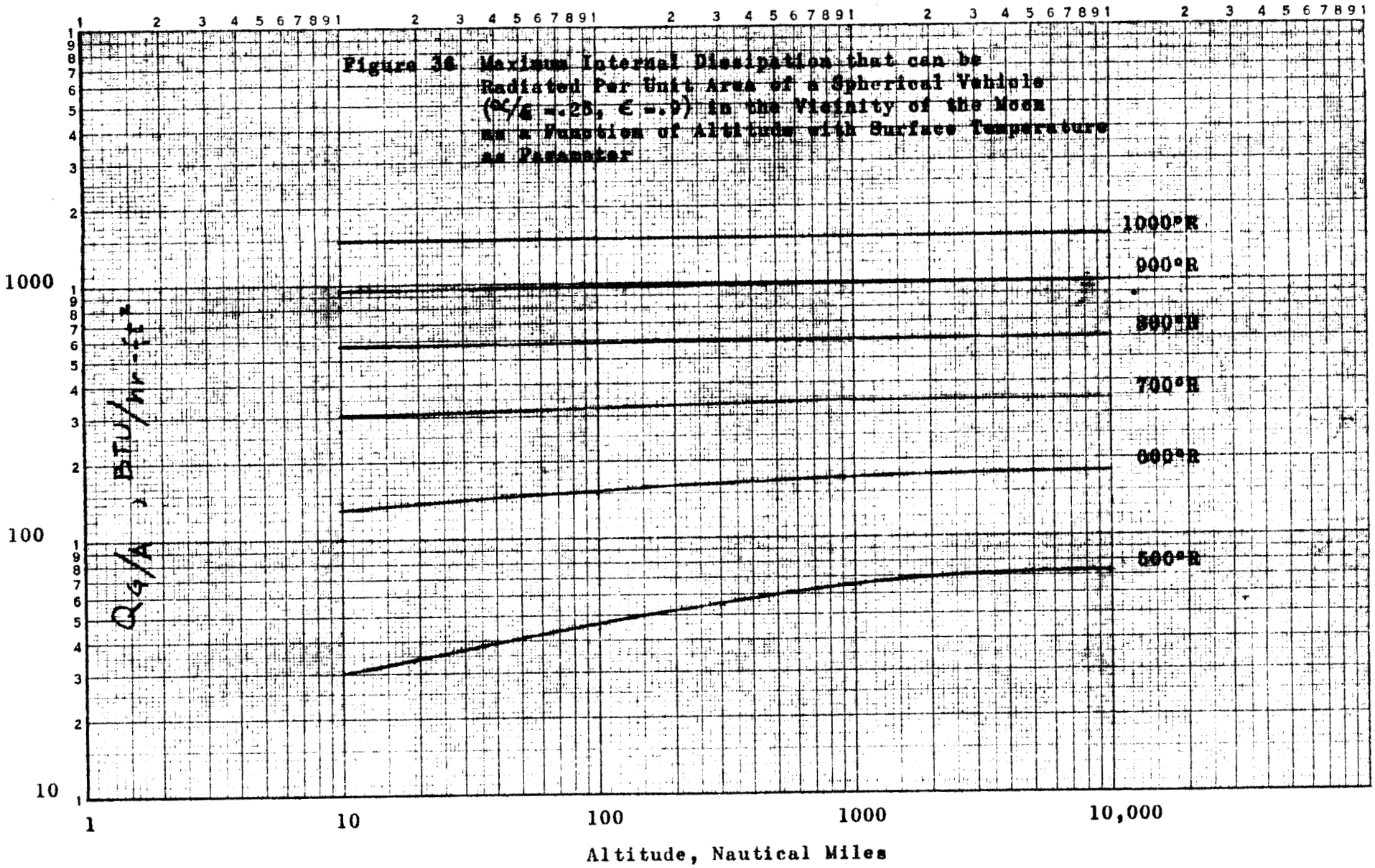

Figure 36. Maximum Internal Dissipation that can be Radiated Per Unit Area of a Spherical Vehicle (α/ϵ = .25, ϵ = .9) in the Vicinity of the Moon as a Function of Altitude with Surface Temperature as Parameter

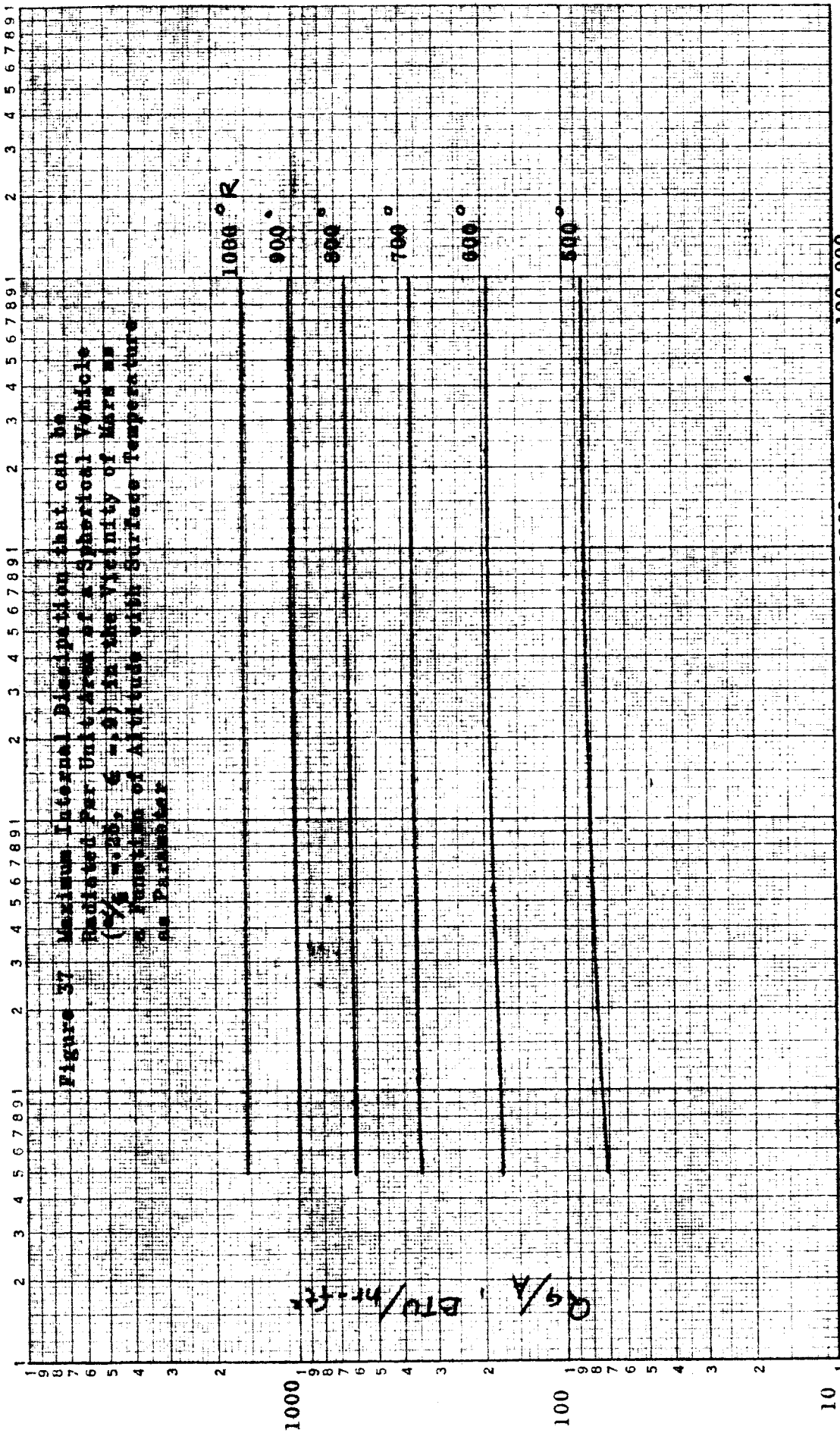

Figure 37 Maximum Lateral Discipation that can be Radiated Per Unit Area of a Spherical Vehicle ($\epsilon_w = .85$, $\epsilon = .8$) in the Vicinity of Mars as a Function of Altitude with Surface Temperature as Parameter

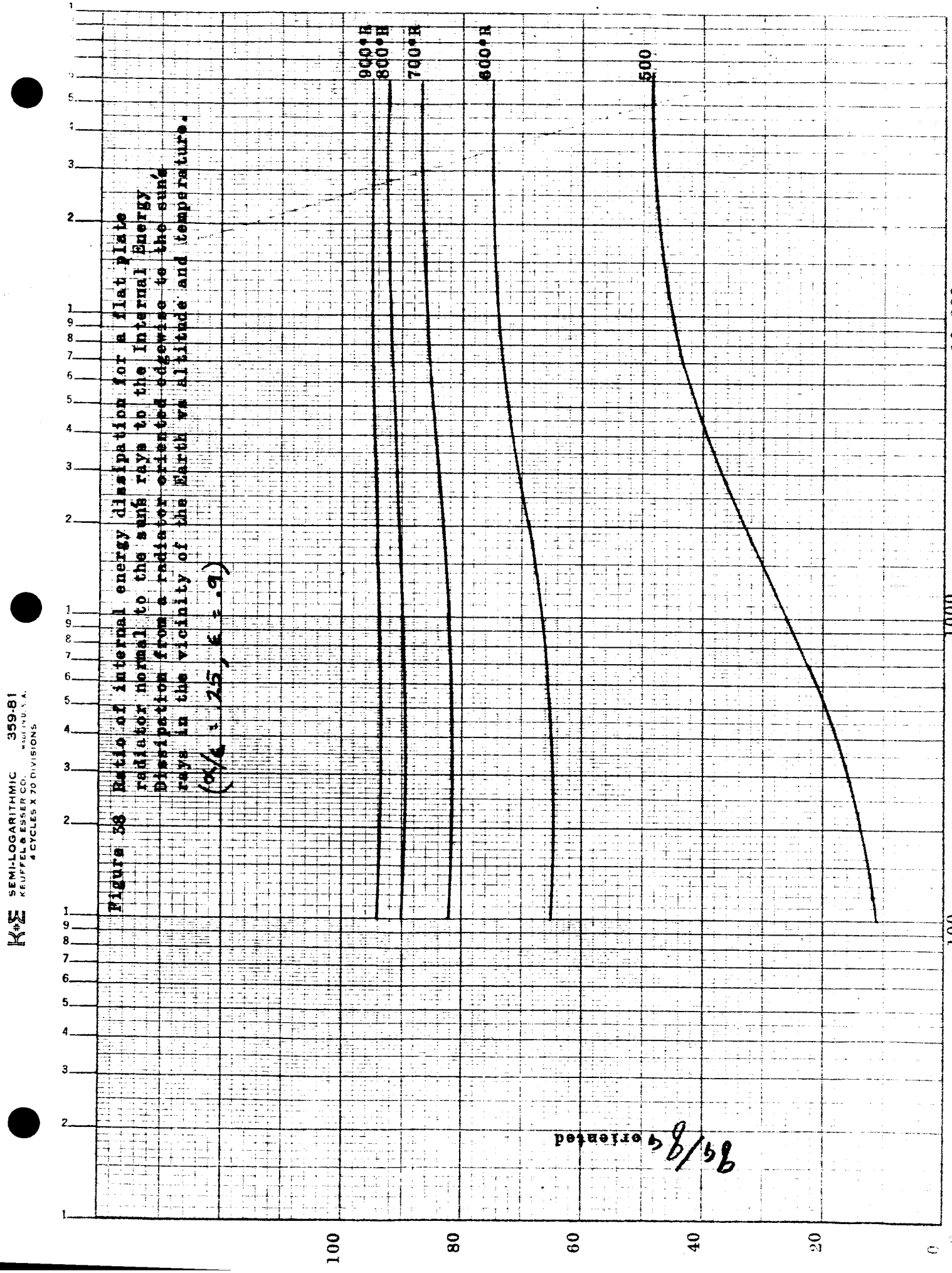

Figure 38 Ratio of internal energy dissipation for a flat plate radiator normal to the sun's rays to the Internal Energy Dissipation from a radiator oriented edgewise to the sun's rays in the vicinity of the Earth vs altitude and temperature.

$\left(\frac{\alpha}{\varepsilon} = .25, \frac{\varepsilon}{\varepsilon} = 1\right)$

SEMI-LOGARITHMIC 359-81
KEUFFEL & ESSER CO.
4 CYCLES X 70 DIVISIONS

Figure 39 Maximum Vehicle Internal Energy Dissipation per unit area of flat plate radiator in free space normal to sun's ray as a function of solar constant and radiator temperature.

$(\alpha/\epsilon = .25 \;,\; \epsilon = .9)$

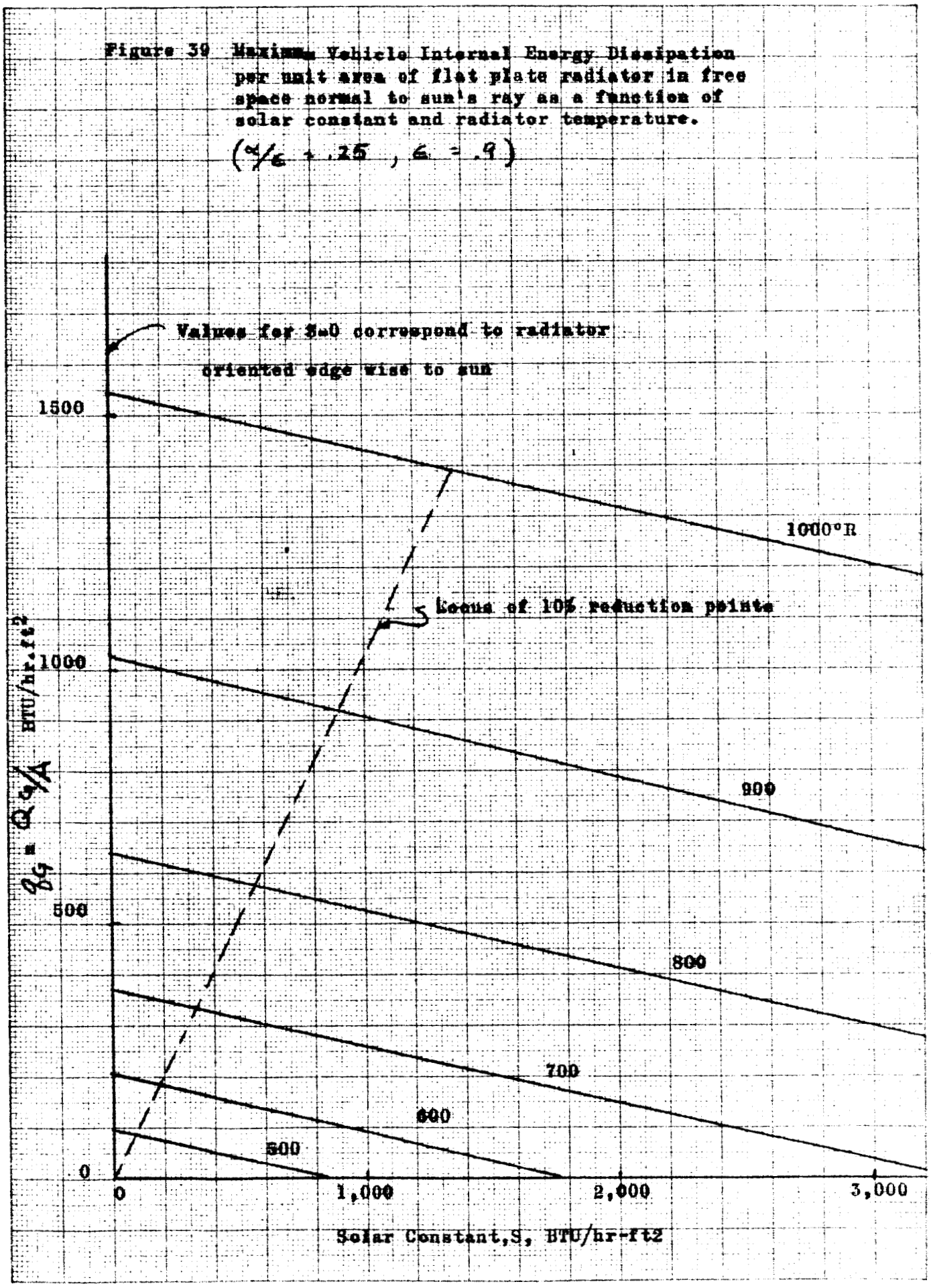

Figure 40 Saturation pressure-temperature relations for common Vapor Refrigerants.

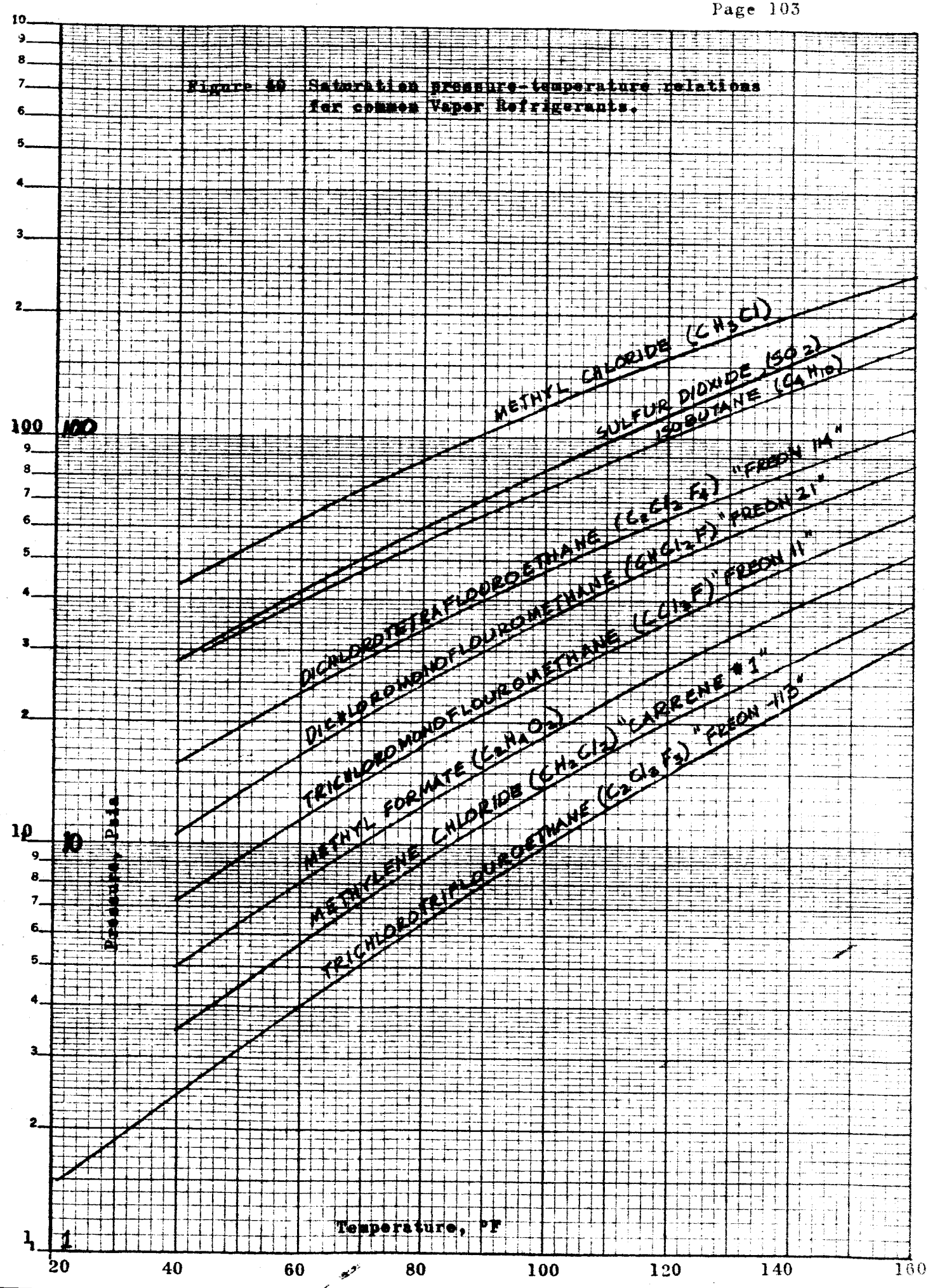

Figure 41 Radiator Surface Area Required per unit, internal dissipation as a function of radiatpr temperature for a Methyl Chloride, "Freon, 113" or "Freon 11" Refrigeration system absorbing energy at 40°F.

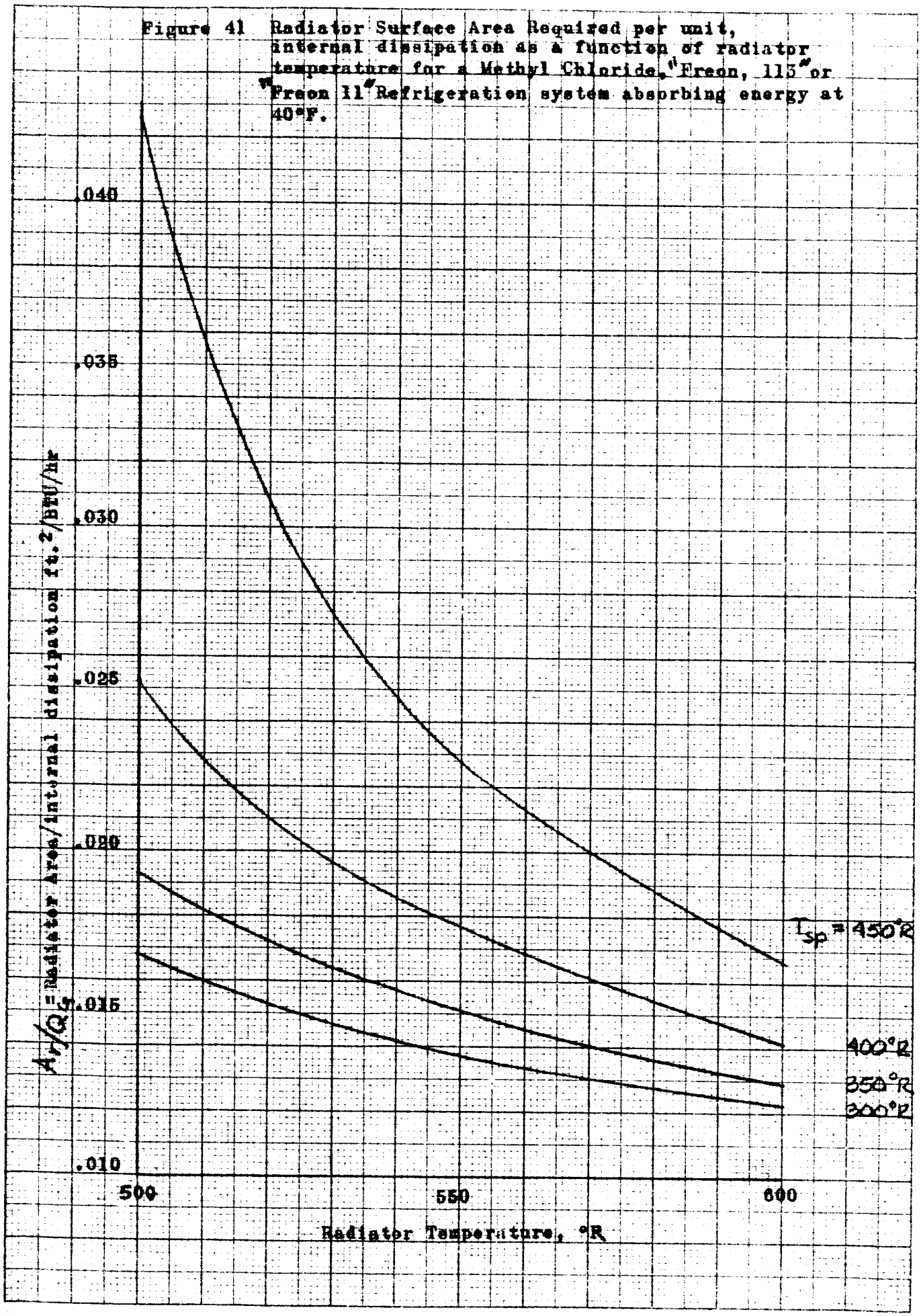

Figure 42 Comparison of Vapor cycle Refrigeration System and Associated Solar Cell Power Source Weight with Estimated Savings in Radiator Weight vs Radiator and/or Condenser Temperature

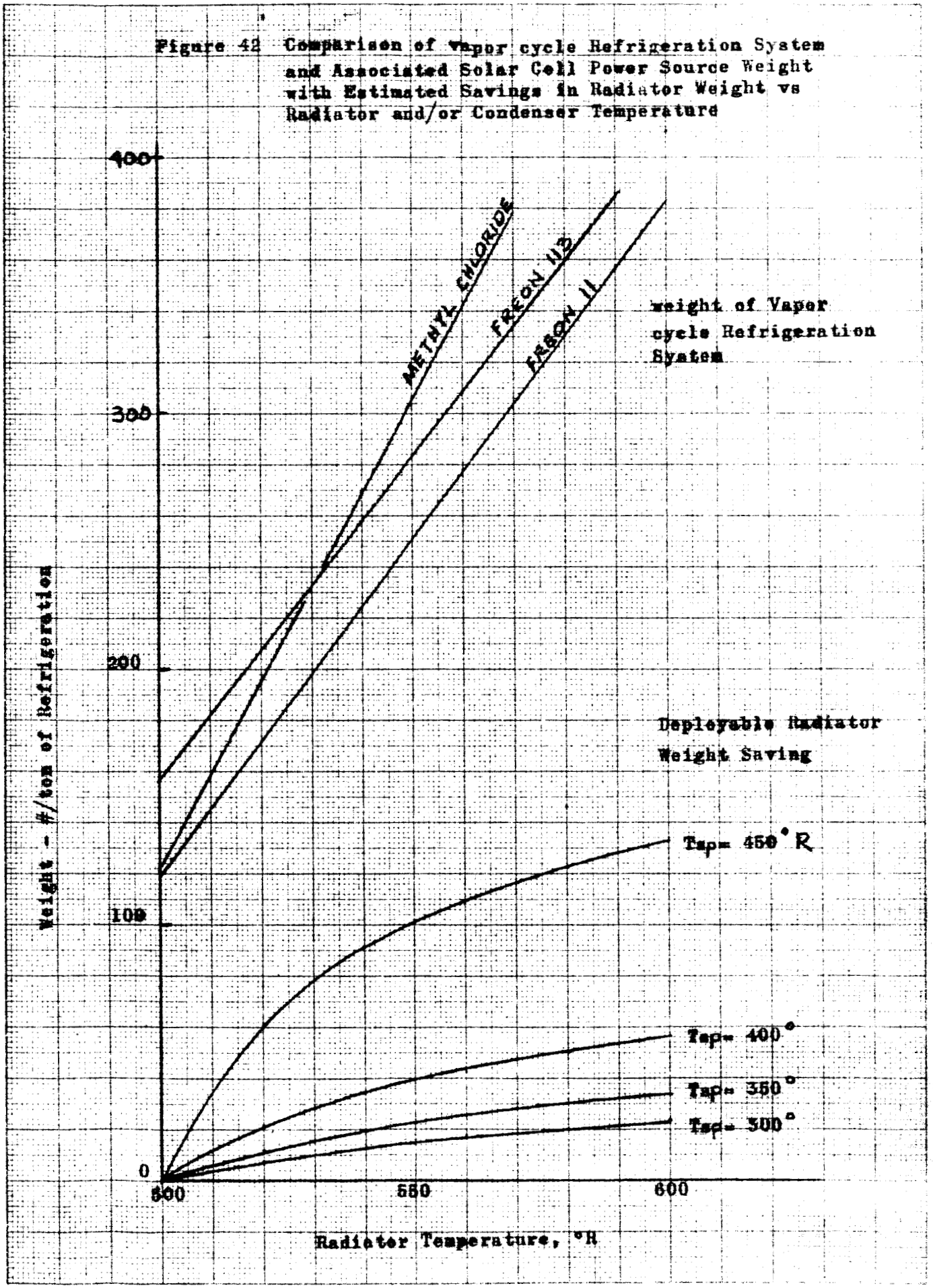

DISTRIBUTION

	No. of Copies
General Office	
R. C. Sebold	1
I. M. Nestingen	1
R. J. Lutz	1
San Diego Division	
C. W. Frick	3
F. Haas	1
R. E. Honer	1
E. Oertel/W. Boyce	1
Division Library	1
J. M. Boyer, Jr.	1
E. J. Steeger	1
C. Jackson	1
J. Peterson	1
Fort Worth Division	
E. L. Secrest	3
Division Library	1
L. H. Schreiber	2
R. N. Oliver	2
J. Fernandes	2
Pomona Division	
G. E. Burkheimer	3
J. M. Guthrie	1
Division Library	1

DISTRIBUTION (CONTINUED)

		No. of Copies
Astronautics Division		
H. F. Dunholter	[illegible]	1
F. J. Dore	[illegible]	1
W. F. Radcliffe	[illegible]	1
Division Library	[illegible]	2
C. C. Love	[illegible]	1
J. Guill	[illegible]	1
H. B. Steele	[illegible]	1
N. O'Rourke	[illegible]	1
F. A. Ford	[illegible]	1
W. B. Mitchell	[illegible]	1
J. C. Ballinger	[illegible]	20